Development and Evaluation of an In-Situ Forming Chitosan-Chondroitin Sulfate-Based Multifunctional Scaffold for the Management of Wound

THESIS

Submitted in partial fulfillment
of the requirements for the degree of

DOCTOR OF PHILOSOPHY

by

Sharma Swati Shivdayal

ID. No. 2017PHXF0421P

Under the Supervision of

Dr. Aniruddha Roy

BITS Pilani
Pilani | Dubai | Goa | Hyderabad

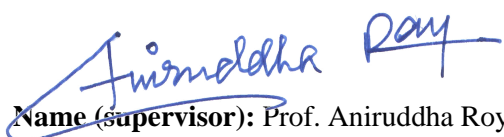## BIRLA INSTITUTE OF TECHNOLOGY AND SCIENCE, PILANI

2023

BIRLA INSTITUTE OF TECHNOLOGY AND SCIENCE, PILANI

CERTIFICATE

This is to certify that the thesis entitled **Development and Evaluation of an In-Situ Forming Chitosan-Chondroitin Sulfate Based Multifunctional Scaffold for the Management of Wound** submitted by **Sharma Swati Shivdayal** ID No **2017PHXF0421P** for award of Ph.D. of the Institute embodies original work done by her under my supervision.

Signature of the Supervisor

Name (supervisor): Prof. Aniruddha Roy

Designation   : Associate Professor

Date   : 12th April 2023

Acknowledgement

Abstract

Skin repair or wound healing is a complex process involving multiple cell types. It is an array of overlapping biological events spanning inflammation, proliferation, and matrix remodeling. However, prolonged infections or pathological conditions like diabetes hamper the healing synchrony, leading to chronic wounds. Across the globe, one out of four people with diabetes experiences diabetes-associated foot ulcers, with at least 10 percent of the cases needing amputations. Different wound dressings have been developed and used clinically, including polymeric scaffolds, hydrogels, films, gauges, foams, and membranes. These dressings primarily facilitate hemostasis, while a selected few have been shown to impart antimicrobial properties. However, most of these do not focus on the overall effect on the healing synchrony. Advancements in the wound dressings included decellularized dressings that act as ECM-mimetic dressings. These dressings enhance cellular proliferation and tissue remodeling (skin allografts); however, their limitations on poor mechanical strength and complex fabrication process make them undesirable. Also, these do not possess antibacterial properties and are prone to bacterial infections. Therefore, a considerable gap exists that needs all-around healing through developing a state-of-the-art dressing.

Polymeric scaffolds fabricated by combining natural and synthetic polymers tender high surface area to volume ratio and assist cellular adhesion, proliferation, migration, and differentiation, all of which are desirable features for wound healing. Despite their good wound healing potential, polymeric scaffolds have limited clinical use owing to high production costs, intricate handling, and packaging requirements. In addition, all such scaffolds are prefabricated by design, limiting the cell-polymer contact and thereby exhibiting reduced efficacy. On the contrary, *in-situ* hydrogels form 3D scaffolds at the wound site filling the deep and irregular wound crevices while showing direct gel-to-cell contact, improving healing. Hence, the present study aimed to design and fabricate one such *in-situ* polymeric scaffold for effective wound management.

It was hypothesized that a polyelectrolyte complex (PEC)-based scaffold could be highly beneficial for treating acute and chronic wounds. In this approach, two oppositely charged poly-electrolyte polymers interact to form a scaffold almost instantaneously, without using chemical cross-linking agents, making the process straightforward and free from any toxic chemicals. Owing to its *in-situ* fabrication, the scaffold can come in direct contact with the cells at the wound bed, supporting their proliferation and functionality. The proposed process includes simple

fabrication steps making the polymeric scaffold scalable. The study focuses on using natural poly-electrolyte polymers to fabricate an *in-situ* scaffold, which could mimic the extracellular matrix (ECM) and support cell migration and proliferation, improving their functional efficacy. Amongst the various screened polymers, chitosan (CH) and chondroitin sulfate (CS) was found to make an *in-situ* forming scaffold with the best physicochemical properties, including porosity and water absorption. CH is a well-established polymer used in the field of wound healing. CS is a glycosaminoglycan, an important constituent of the ECM with anti-inflammatory and cell proliferative activity. Upon mixing (1:1 v/v), these polymers with opposite charges form ionic bonds and give rise to a CH and CS-based PEC (CH-CS PEC).

Our study used high molecular weight CH and low molecular weight CS to develop the CH-CS PEC. Due to low molecular weight, the CS solution's viscosity is less, allowing it to spontaneously mix with the viscous CH solution, making electrostatic cross-linking, leading to instant scaffold formation. Various physicochemical characterizations like FTIR, thermal degradation studies, solid-state NMR, and X-ray diffraction were performed to confirm the formation of the CH-CS PEC. The results demonstrated change in the original pattern of peaks compared to CH-CS PEC in FTIR and other studies. Therefore the characterization data confirms crosslinking and ionic interaction of CH-CS, resulting in the formation of CH-CS PEC. The fabrication of CH-CS PEC was optimized using Quality-By-Design (QbD) approach. The polymeric complex further demonstrated good water absorption capacity (914±15.47%) and porosity (95.97±1.89), making it an ideal dressing for wound healing. The biochemical estimation depicted effective hemocompatibility and high blood cell adhesion and clotting ability. Also, the evaluated rheological parameters of CH-CS PEC demonstrated good viscoelasticity and self-healing property that could mimic the dermal ECM.

The major players involved in wound healing are the dermal fibroblasts, keratinocytes, macrophages, and endothelial cells. Fibroblasts are involved in the synthesis of ECM constituents which support keratinocytes in the re-epithelialization and wound closure. To evaluate the behavior of the major skin cells in the presence of the CH-CS PEC, we studied the functional efficacy of fibroblasts and keratinocytes treated with CH-CS PEC in an *in-vitro* cell culture-based system. Both keratinocyte (HaCaT) and fibroblast (HDF) cells exhibited 1.4 and 1.7-times increased protein expression of PCNA, a cell proliferation marker, respectively, when seeded on the CH-CS PEC, compared to the cells

seeded on the CH film. Significantly increased expression of different functional markers (involucrin, HGF, β1-integrin) was observed with the HaCaT cells seeded on the CH-CS PEC compared to others. With the HDF cells, significantly increased expression of α-SMA and collagen was observed. Notably, the expression of collagen I to collagen III was found to be in the ratio of 1.3:1, indicating scar-free wound healing. In the rat skin excisional wound model, treatment with the *in-situ* forming CH-CS PEC exhibited significantly enhanced wound healing efficacy (in terms of wound closure rate, collagen content, as well as α-SMA, and β1-integrin expression) compared to the same CH-CS PEC applied as a lyophilized scaffold, as well as a clinically available CH based preformed scaffold, indicating the superior activity of the *in-situ* forming scaffold.

After confirming the effective functional efficacy of the CH-CS PEC on fibroblasts and keratinocytes, we next evaluated the change in the macrophage behavior when treated with CH-CS PEC. Macrophages are well known for their microenvironment-dependent phenotypic transitions either to M1 or M2 types. Viscoelasticity is one of the physical properties reported to affect macrophage polarity and phagocytic activity. We found the CH-CS PEC scaffold to be moderately stiff, which could drive the macrophage M2 polarization. Hence, after confirming the cytocompatibility of the macrophages (RAW 264.7 murine macrophage cell line), we evaluated the change in the macrophage morphology by staining the f-actin of CH-CS PEC treated cells. The cells treated with CH-CS PEC showed elongated morphology with low circularity (0.34±0.07) compared to CH (0.74±0.02), depicting the non-circular elongated morphology, an initiation for the alteration of macrophage to M2 phenotype. The mRNA expression of TNF-α and IL-10 showed an increase in IL-10 expression and a decrease in TNF-α expression in the macrophages treated with CH-CS PEC, indicating M2 polarization. We then looked into the biophysical impact of CH-CS PEC on macrophages by β1-integrin immunoblotting. Increased β1-integrin expression depicted the activation of the biophysical cues associated with the increased phagocytic activity of the macrophages through an immunomodulatory M2 phenotype. After evaluating the effect of CH-CS PEC on macrophage behavior, we wanted to check its phagocytic potential in an infected state, as wound infections are one of the prime causes of chronicity development. Initially, the antibacterial efficacy of CH-CS PEC against *P. aeruginosa* was evaluated. The data represented the bacterial membrane de-stability and increase in ROS concentration as the cause of cell death

when treated with CH-CS PEC. Taking this finding and the effect of rheological properties of CH-CS PEC on the macrophage as a base, we studied the behavior of CH-CS PEC treated murine macrophages (RAW264.7) under *Pseudomonas aeruginosa* using an in-vitro infection model. Macrophages treated with CH-CS PEC in uninfected conditions showed elongated morphology and changes in the actin cytoskeleton, a mark of M2 phenotype. Further, bacteria exposed to CH-CS PEC treated macrophages showed enhanced phagocytic potential. The data exhibited bacterial clearance and an increase in the level of pro-inflammatory cytokine post 3h of infection. However, at 6h post-infection the inflammation was reduced (1.14 ± 0.26 fold), and a marked increase in IL-10 mRNA expression was observed. The results demonstrated a change in cytokine expression and phagocytic potential post 3h and 6h of infection, indicating the macrophage's ability to clear the bacterial load and then reduce the inflammation to its normal level. The immunoblotting study for NF-κB-p65 protein confirmed the inflammation changes. Furthermore, the antibacterial and anti-inflammatory property was confirmed in the *in-vivo* rat infection wound model. The *in-vivo* model corroborates with the findings of the *in-vitro*-infection model as we found a reduction in the bacterial count with reduced expression of NF-κB-p65 protein in the CH-CS PEC treated wound sections.

After studying the biological efficacy of CH-CS PEC on different cells involved in wound healing, we further wanted to understand the use of CH-CS PEC as a carrier for drug loading. Moldable self-healing scaffolds can be an effective carrier for drug loading for localized drug action. The scaffold's enhanced water absorption capacity and porous network increase the entrapment of drugs and can modulate their release kinetics from the scaffold. CH-CS PEC was found to have a highly beneficial effect on three key players of wound healing, namely keratinocytes, fibroblasts, and macrophages, as demonstrated by previous experiments. We targeted the fourth player involved in the wound healing process, namely angiogenesis, and chose a pro-angiogenic drug, simvastatin (SIM), to incorporate into CH-CS PEC to study its angiogenic potential. SIM is a well- known lipid-lowering drug; recent studies have reported it as a pro-angiogenic molecule that enhances VEGF expression. It is a BCS class-II drug having a logP of 3.8. Hence, we developed SIM-loaded Soluplus(Sol)-Vitamin E TPGS (TPGS) mixed micelles. Sol-TPGS micelles in the ratio of 4:1 showed enhanced entrapment efficiency and reduced PDI compared to the other ratios. When loaded into CH-CS PEC, the SIM micelles showed a controlled drug release for 48h

following the Korsmeyer-Peppas dissolution kinetics model. Further, the biological efficacy and angiogenic potential of drug-loaded CH-CS PEC were evaluated on *ex-vivo* rat aortic ring and chronic excision wound models. The *ex-vivo* rat aortic ring displayed enhanced sprouting of the endothelial cells in SIM-loaded CH-CS PEC. Surprisingly, the CH-CS PEC alone also showed elevated angiogenic potential. The *in-vivo* chronic wound healing data corroborated the *ex-vivo* data depicting the enhanced wound healing potential in both CH-CS PEC and SIM-loaded CH-CS PEC.

In summary, the present work demonstrated the effect of CH-CS PEC on the pivotal players in wound healing. This study illustrated the importance of physicochemical properties affecting the healing mechanism. The porous CH-CS PEC could mimic the ECM's biophysical cues, thereby enabling the cells to increase their proliferation and biofunction. On the other hand, the simplicity in the development of CH-CS PEC makes it scalable for translation. Also, CH-CS PEC could be further used as a carrier for cell encapsulation due to its ECM mimetic property. Overall the formulation was fabricated with minimum steps and a simple fabrication method and showed effective biological efficacy on the major cell types involved in the healing process.

List of Tables

List of Figures

Table of Contents

List of Abbreviations

CH	Chitosan
CS	Chondroitin sulfate
CH-CS PEC	Chitosan Chondroitin sulfate polyelectrolyte complex
PEC	polyelectrolyte complex
Col-I	Collagen-I
Col-III	Collagen-III
α-SMA	Alpha-smooth muscle actin
Sim	Simvastatin
HDF	Human dermal fibroblst
ACN	Acetonitrile
CDR	Cumulative drug release
DAPI	4'6'-Diamidine-2-phenylindole
qPCR	Quantitative real time polymerase chain reaction
TNF-α	Tumor necrosis factor-α
DCFDA	2',7'-dichlorofluorescein diacetate
DLS	Dynamic light scattering
DMF	Dimethylformamide
DMSO	Dimethyl sulfoxide
DMEM	Dulbecco's Modified Eagle medium
FBS	Fetal Bovine Serum
BSA	Bovine serum albumin
EDTA	Ethylenediaminetetracetic acid
EE	Entrapment efficiency
FESEM	Field emission scanning electron microscopy
EDS	Energy dispersive spectroscopy
HGF	Hepatocyte growth factor
NRG	Neurogilin growth factor
K5	Keratin 5
cDNA	Complementary DNA

K15	Keratin 15
FITC	Fluorescein isothiocyanate
MMP-2	Metalloproteinases-2
MTT	(3-(4,5-Dimethyl-2-thiazolyl)-2,5-diphenyl-2H-tetrazolium bromide)
PBS	Phosphate buffer saline
PDGFB	Platelet derived growth factor
PDI	Polydispersity index
TPGS	Tocopheryl polyethylene glycol succinate
VEGF	Vascular endothelial growth factor
NF-kB	Nuclear factor kappa-light-chain-enhancer of activated B cells
PI	Propidium Iodide
RIPA	Radioimmunoprecipitation assay
ROS	Reactive Oxygen Species
RT	Room temperature
IL-10	Interleukin-10
GFP	Green fluorescent protein
E. Coli	Escherechia Coli
TGF	Transforming growth factor
DSC	Differential scanning calorimetry
FTIR	Fourier transform infrared spectroscopy
SIM	Simvastatin

Chapter 1

Introduction

1. Background

Skin provides primary protection against the external environment, prevents infection, regulates body temperature, and maintains homeostasis. This multilayered organ comprises the epidermal, dermal, and hypodermal layers, with main keratinocyte, fibroblast, melanocyte, and endothelial cells. The spatiotemporal organization and biochemical function of individual cell types tightly regulate the cellular and molecular signals that govern skin function. Concerning its structure and function, skin impairment epitomizes a clinical burden affecting over seven billion patients [1]. Skin's regenerative capacity is lost in almost all wound types, disturbing its original function. The few Indian studies on the epidemiology of chronic wounds estimate their prevalence to be between 4.5 - 15.03/per 1000 population [2], significantly higher than in developed countries with a prevalence of around 1.8 per 1000 [3]. The high prevalence of nonhealing wounds observed here is probably due to the high frequency of diabetes mellitus, atherosclerosis, tuberculosis, and leprosy in the Indian population. Apart from chronic wounds, around 70 lakh people each year suffer from burn injuries in India, leading to 1.4 lakh deaths and 2.4 lakh disabilities (Indian National Health Portal). Normal wounds heal through the predefined stages of hemostasis, inflammation, proliferation, and ECM remodeling. However, pathologic conditions like diabetes mellitus, arterial perfusion, hypoxia, and poor nutrient supply impede wound healing [4]. Wounds that take more than 12 weeks to heal are termed chronic or nonhealing wounds [5]. These hard-to-heal chronic wounds mark around 8.2 million medical cases worldwide. The medical expenditure cost ranged from $28.1-$96.8 billion, covering the expenses of infectious wounds, surgical wounds, and diabetic ulcers [6]. The consequences of these difficult-to-heal wounds are amputations and sometimes death. With the rise in cases of diabetes, amputation because of diabetic foot ulcers has also elevated to 40-70% globally [7]. These clinical conditions demand long-term medical assistance at a high cost, depriving the quality of life and escalating the socio-economic burden [8].

Various wound care products, from conventional to modern, are available. Conventional wound dressings protect the damaged skin from external injury and opportunistic infections [9]; however, they have a marginal contribution to the cellular wound healing mechanism. Modern dressings such as hydrogels, fibers, foams, and sponges can help in the overall healing process. Adequate oxygen, a warm and moist environment, and, most importantly, structural support to

the surrounding cells are the primary trait of an ideal wound dressing [10]. In healthy skin, the extracellular matrix (ECM) provides a three-dimensional (3D) microenvironment to the cells controlling the cell behavior, migration, and proliferation [11]. ECM supplies nutrients and activates various biochemical and mechanical cell signaling to maintain cell homeostasis. Damage to the ECM is one of the causes of compromised wound healing. Modern wound dressings aspire to match the ECM properties of the skin to support the healing process. Making an ECM mimetic wound dressing that can support skin cell functions is gaining attention in the field of skin repair/regeneration. ECM mimetic dressings support the overall development of the tissue by providing the 3D structural support to the surrounding cells.

1.1 Skin wound healing process

Wound healing is categorized into three main stages: 1) Hemostasis and inflammation, 2) Cell proliferation, and 3) ECM remodeling. The primary response to skin damage is the cessation of blood flow. Skin injury triggers vasoconstriction and platelet activation at the wound site. It undergoes blood clotting by binding to the damaged collagen fibrils [12, 13]. Various proteins, namely fibronectin, vitronectin, and thrombospondin, are secreted during platelet aggregation. These develop into a supporting matrix for cell growth and further stimulate the endothelial cells to secrete adhesion molecules like P-selectins, ICAM-1, and growth factors like platelet-derived growth factor (PDGF) and transforming growth factor-β (TGF-β) [14]. This stimulates endothelial cells to migrate and perform neo-angiogenesis for new blood vessel formation [15]. Next, immune cell infiltration activates the inflammatory phase [16]. Mediators released by platelets allow movement of the primary immune cells, like neutrophils, leading to the activation of the inflammatory cascade [17]. Neutrophils are the primary activated immune cells against foreign invaders. Neutrophils produce antimicrobial substances which clear the microbes from the wound bed and produce inflammatory cytokines and growth factors [18, 19]. These also release various agents like reactive oxygen species, cationic peptides, and protease playing a key role in the host defense and foreign body clearance. Further, macrophages got activated to clear the bacteria and the apoptotic cells present in the wound bed. Macrophages are the critical players in the repair process, participating in inflammation and then resolving it, returning to their resting stage, and activating the fibroblasts for ECM synthesis and proliferation [20]. Based on their function, macrophages are classified as pro-

inflammatory (M1) and anti-inflammatory (M2) phenotypes. M1-macrophages secrete various chemokines and matrix metalloproteases which initiate the pro-inflammatory response. After the initial inflammation, the macrophages polarized to the M2-phenotype, which secrete various growth factors like TGF-β1, IGF-I, and others, supporting cellular growth and development of the microvasculature [21]. M2 macrophages also secrete various mediators that stimulate the fibroblasts for ECM formation and tissue remodeling. During the proliferative phase, granulation tissue is formed, consisting of fibroblasts, M2 macrophages, and blood vessels. The interaction of macrophages- fibroblasts plays a lead role in wound healing. Fibroblasts respond to the macrophages, growth factors and initiate the extracellular protein formation by synthesizing proteoglycans and ECM molecules [22].

After recruitment, fibroblasts undergo phenotypic differentiation. During the differentiation state, it secretes collagen-I and TGF-β1, which are essential in building tissue strength [23]. Collagen is one of the crucial fibrillary proteins in maintaining the tissue's structural integrity. There are many types of collagen, amongst which collagen Type-I (Col-I) and collagen Type-III (Col-III) are mainly involved in structural integrity and the development of scars. Expression of Col-III also supports wound contraction [24]. Reports demonstrate scar formation in Col-III deficient animals [25]. On the other hand, Col-I is mechanically stronger than Col-III and responsible for maintaining skin structure and tissue integrity [24]. During the granulation tissue maturation, Collagen-III gets degraded with Collagen-I synthesis. Hence the balance between Collagen-I and Collagen III is important to avoid fibrotic scar formation. Both collagens play a vital role in the wound-healing process. The ratio of Col-I to Col-III changes from 2.3:1 to 0.7:1 in fetal skin, compared to 9:1 to 4:1 in adults [26, 27].

During wound closure, fibroblasts secrete various growth factors like fibroblast growth factor (FGF) and keratinocyte growth factor (KGF), which stimulate the surrounding keratinocytes. Keratinocytes form the epidermal layer of the skin. The initial basal layer is the proliferative phase composed of keratins. This further gets differentiated to form the subsequent keratinocyte layers. In response to the disrupted epidermal layer, keratinocytes stimulate releases of IL-I, which activates its migration and proliferation [28]. During the proliferative stage, keratinocytes express K5 and K14, which develops the stratum basal layer of the epidermis. The keratinocytes proliferate at the basal layer while it undergoes terminal differentiation

expressing K1, K10, and other genes. Further, the activated keratinocyte signals the surrounding fibroblasts and endothelial cells to secrete the keratinocyte growth factor, supporting the keratinocyte migration and proliferation [29].

The crosstalk between the keratinocyte and the surrounding cells is essential for re-epithelialization. Activated keratinocytes from the surrounding tissue secrete matrix metalloproteases to make a path for the keratinocyte to enter the wound bed and undergo re-epithelialization [30]. These keratinocytes change their actin cytoskeleton and synthesize the components involved in the dermal-epidermal junction. Various adhesion proteins like laminin and integrin form the dermal-epidermal junction. Further, the keratinocytes secrete growth factors to activate the surrounding fibroblasts and endothelial cells for dermal layer formation and neovascularization.

In a nutshell, the wound healing mechanism demonstrates the participation and involvement of different cell types for efficient wound closure. The complex array of events between fibroblasts, keratinocytes, macrophages, and endothelial cells accomplishes the healing process. However, it can go off-center due to disease conditions like diabetes, aging, severe deep injury, or persistent infection [31]. Disturbance in the function of these cells will lead to impaired healing.

1.2 Problems associated with the nonhealing wounds

Chronic nonhealing ulcers vary with the etiological conditions. Large-scale infection, biofilm formation, ischemia, and low oxygen and nutrient supply deprive the cell migration and proliferation of the surrounding cells, causing a delay in the healing process [32]. Disturbed healing results from an abnormal change in the regulated biological process [33]. Repeated tissue injury, infections, or enhanced levels of platelet-derived factors and conditions like diabetes contribute to the recruitment of immune cells and lead to an immune dysregulated state, resulting in elevated inflammation [34]. Hyperglycemic conditions increase oxidative stress at the wound site and mark prolonged pro-inflammatory cytokine levels. The imbalance between the secretion of proteases and their inhibitors, inflammatory cytokines, results in depletion in the synthesis of growth factors which alter angiogenesis and promotes microvascular complications [35].

This imbalance results in proteolytic degradation of the ECM. The degradation in ECM not only prevents the healing process from progressing from inflammation to proliferation, but also leads to the activation of more inflammatory cells [36]. All of these cause the generation of ROS at the wound site preventing the surrounding cells from proliferating.
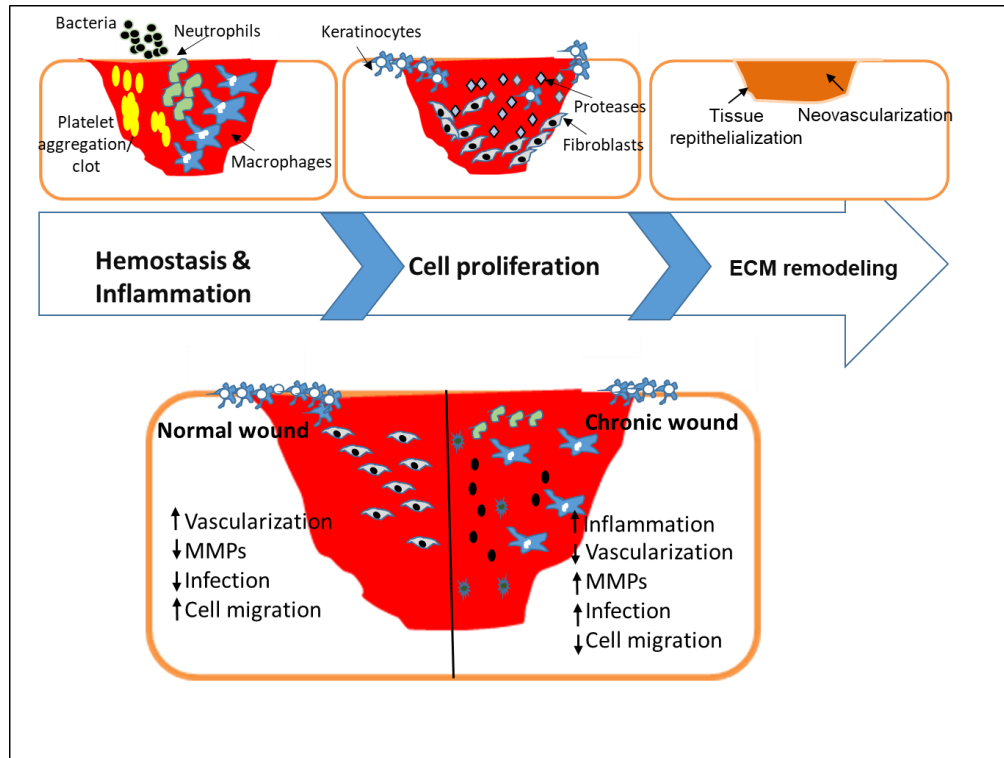
Fig. 1.1 The wound healing process. Comparison in physiological conditions between normal and chronic wounds

Wound infections are the other major contributors to the development of chronic wounds. Surface pathogens like *Pseudomonas aeruginosa* and *Staphylococcus aureus* are the prime bacteria found at the wound site. Neutrophils and macrophages are primarily activated in the presence of bacteria. Neutrophils get activated by the bacterial endotoxins and increase the ROS level triggering inflammation. They secrete excessive MMPs leading to a degraded ECM matrix, closing the platform for the other cells to migrate and proliferate at the wound bed [37]. These bacteria, when persisted long term, affect the bio-function of the fibroblasts and keratinocytes, causing impaired healing.

Henceforth, the major challenge associated with chronic wounds is transitioning from inflammation to a proliferation state and maintaining a balance between the proteases and their inhibitors to maintain ECM integrity. The ECM provides the 3D environment for the

surrounding cells to proliferate. The degradation in the ECM causes activation of immune cells and overall delays dermal repair.

1.3 Role of extracellular matrix in wound healing

The extracellular matrix is a 3D scaffold, composed of complex multi-domain proteins, polysaccharides, and water that comprise the acellular microenvironment in the tissue [38]. It controls cell fate by transferring biochemical and mechanical signals [11]. The biochemical signals are regulated by ECM's molecular networks, proteins, glycoprotein, and glycosaminoglycan (GAGs) [39]. These components provide structural support and mechanical stability to the surrounding cells. Fibroblasts are the cells involved in ECM synthesis. The fibroblasts-ECM interaction affects the healing process. ECM's fibrillar and non-fibrillar components include collagen, hyaluronan, fibronectin, elastin, and laminins. While these provide biochemical cues for the cells to grow and proliferate, increasing their secretion can cause scar formation or fibrosis [40]. The major proteins that maintain structural rigidity are collagen-I and collagen-III [41]. An imbalance in their ratio leads to the formation of hypertrophic scars. ECM plays a pivotal role in all the phases of wound healing, i.e., from the provisional matrix formation by platelets to the re-epithelialization performed by the migration of keratinocytes. Initially, the ECM proteins secreted by the fibroblasts form a granulation tissue for effective wound closure and to prevent infections. The granulation tissue facilitates the migration of surrounding cells involved in the healing process. The components of granulation tissues include collagen-I, which further interacts with the elastin and integrin $\alpha v\beta 1$ proteins for re-epithelialization. The ECM-cell interaction activates various signaling pathways, causing cell proliferation [42]. Besides cell migration and proliferation, ECM also supports the cells in secreting growth factors like TGF, PDGF, IGF, etc. The growth factors improve the cell function and maturation of the cell. Understanding their importance, various growth factors are being used as treatments for wound healing as these support faster-wound closure. Regranex was the first growth factor-based gel approved by the FDA for treatment of chronic wounds [43].

The biochemical role of ECM demonstrates the importance of ECM in cell-cell and cell-ECM signaling. The biochemical instructions can be tuned by altering the biophysical cues of the ECM. The fibroblasts, keratinocytes, and macrophages take the lead during the healing process

[44]. During skin injury, various transmembrane receptors get activated. Different mechanosensing pathways communicate these signals within and outside the cells. Focal adhesion kinases, integrin, and Rho/Rock are the most commonly known mechano-sensors [45]. The cell-ECM interaction affects cell behavior, adhesion, and migration. Integrin is the most common receptor interacting with the cell. The activation of integrin sensing changes the actin cytoskeleton modulating cell behavior [46].

Cells respond to the external microenvironment, such as topography, stiffness, and porosity, stimulating changes in the actin cytoskeleton with activation of the signaling pathways, as mentioned above. ECM surface topography regulates cell migration by controlling contact guidance to the cells [47]. The smooth topography supports cell migration; however, rough topography disturbs the migration rate. Cell-surface response to topographical changes is not known yet. However, mechanosensing studies described the relation between surface topography and stiffness of the microenvironment [48, 49]. Substrate property affects the cell-ECM interaction, thereby regulating cell behavior. Local stiffness and viscoelasticity of the ECM modulate cell function [50]. The high stiff scaffolds decrease the cell spreading and growth; however, they support cell differentiation, while soft hydrogel fails to build the matrix-cell interaction limiting cell growth. Hence, the optimum stiffness of the hydrogel is required for cell adhesion, spreading, and growth [51]. The substrate stiffness affects keratinocytes and fibroblasts as they show alteration in their actin filaments. When a mechanical injury occurs, fibroblasts are differentiated into myofibroblasts for wound closure, forming granulation tissue [52]. The substrate stiffness also modulates fibroblast function. The higher substrate stiffness leads to hypertrophic scar formation, while the low stiffness reduces proliferation. The stiffness has a direct effect on the actin cytoskeleton. This change in actin filaments activates the focal adhesion kinase and integrin signaling, which supports cell proliferation. The change in the substrate stiffness also affects macrophage immunomodulation by activating the mechano-transduction pathway [53, 54]. Therefore, studying the stiffness of the scaffold developed for wound treatment is necessary.

Emphasizing the biophysical cues of the extracellular matrix, the scaffold's viscoelasticity is another critical parameter to be considered for developing an advanced wound dressing (**Fig. 1.2**) [55]. Viscoelasticity regulates the cellular process via cell-substrate interactions [56].

Substantial literature has reported the effect of substrate stiffness on cell behavior [57, 58]. Viscoelasticity of the matrix determines the primary cellular responses like cell adhesion, cell spreading, and cell proliferation [59].

Porosity is another crucial parameter to consider when developing a wound dressing. Optimum porosity and interpenetrating networks are essential in the wound bed's gaseous exchange and nutrient supply. Regulating the pore size and covering the entire wound area could affect the scaffold performance. Very small pore sizes are required for the nutrient supply, while larger pores aid cell migration and angiogenesis. Porous interpenetration network dressings are mainly helpful in burn wounds as these help in vascularization and adequate nutrient supply [60]. Underwood *et al*. demonstrated the importance of pore size in epidermal cell migration. The study demonstrated higher keratinocyte migration with the 70-80 μm spherical rods [61]. The uniform pore size also reduces the scarring in the porcine model [62]. Therefore, tuning the biophysical aspects could also support the wound-healing process.

1.4 Existing ECM mimetic scaffold and its limitations

Achieving an overall skin repair similar to healthy and functional skin using a wound dressing remained a challenge in regenerative medicine. Prolonged inflammation and infections result in compromised healing. Considering these complications, the current treatment regimen shifted to faster wound closure instead of overall tissue remodeling. The existing solutions to wound healing include foams, hydrocolloids, gels, sponges, etc. These support faster wound closure preventing opportunistic infection [63]. The selection of these dressings depends on the complexity of the wound. Traditional dressings are mainly used as regular clinical dressings because of their low cost; however, these have limited wound healing efficacy as it only shields from the external environment. The contact of these dressings with the wound causes further damage to the skin at the time of removal [64].

These limitations led to the demand for the development of advanced wound dressing, which can actively support wound healing. Currently, the most advanced wound dressing for clinical use includes hydrogels and hydrocolloids, which support the surrounding cells to migrate at the wound site and participate in the healing process. These promote cell-matrix adhesion as a structural support for the cells to migrate and proliferate [65]. Hydrogels are a class of wound

dressing collectively suitable for all types of wounds. It promotes cell proliferation and faster wound closure, however, most commonly resulting in scar formation [63].

Therefore, an ideal wound dressing should provide structural support to the cells for growth and fast wound closure. ECM and its importance in the healing process are very well documented. Recent developments in wound dressings have focused on developing ECM mimetic wound dressing. These dressings support cellular growth and regulate the overlapping stages of wound healing. Substantial literature is available on designing polymeric ECM mimic matrices supporting the cells and providing nutrients and oxygen supply [66, 67]. Membranous extracellular matrices obtained from animal origin are promising for skin wound healing. These are decellularized membranes originated from human or animal tissue rich in bioactive substances like growth factors, collagen, and polysaccharide. Acellular dermal matrix and amniotic membrane are representative biomaterials that have been commercialized in the clinic [68, 69]. This benefits the healing process by simulating the biophysical and biochemical nature of the skin's ECM [69]. Apart from supporting the cells, it also supports the synthesis of growth factors and immunomodulation of macrophages [70, 71]. It turns macrophages into M2 phenotype, ceasing inflammation [72]. Various decellularized ECM mimetic scaffolds are listed in **Table 1.1**. Besides the immunomodulatory property, these scaffolds regulate cell adhesion and proliferation as they possess the Arg-Gly-Asp (RGD) motif [68]. This motif activates integrin-mediated signaling, supporting cell migration and proliferation [73].

Although decellularized membranes have shown excellent biological properties, their clinical use is limited. These scaffolds have poor mechanical strength and rapid biodegradation. They are derived from animal origin and are prone to immune reactions and opportunistic infection [74]. Also, the cost of developing these dressings is high.

Table1.1 Natural Decellularized matrices for wound healing.

	Type of scaffold	*In vivo* model	*In vivo* outcomes	**Ref**
Porcine dermis	Dermal matrix	Rabbit full-thickness wounds	Wound Contraction ↑ Collagen type I and III expression ↑ Vascularization ↑	[75]
Sheep dermis	Dermal matrix used	Rat burns	Inflammation ↓ Angiogenesis ↑	[76]

	as covering dressing		Granulation tissue formation ↑ Wound closure ↑	
Mouse dermis	Membrane	Murine full-thickness wounds	Angiogenesis ↑ Wound closure ↑ MSC retention ↑	[77]
Rat dermis	Hydrogel	Rat full-thickness wounds	Angiogenesis ↑ Collagen deposition ↓ Wound closure ↑ Re-epithelialization ↑ Epidermal junction formation ↑	[78]
Porcine skin	Hydrogel	Rat full-thickness wounds	Hair follicle growth ↑ Sweat gland formation ↑ Wound closure ↑ Collagen deposition ↑ Neovascularization ↑	[79]
Porcine skin	Porous crosslinked membrane	Rabbit full-thickness wounds	Wound closure ↑ Inflammation ↓ Fibroblast migration ↑ Epidermal thickness ↓ Collagen organization ↑ Cellular and vascular infiltration ↓ Time of regeneration ↑	[80]
Porcine dermis	Crosslinked Membrane	Rat full-thickness wounds	Wound closure ↑ Re-epithelialization ↑	[81]
Porcine urinary bladder	Membrane	Rat burns	ECM synthesis ↑ Inflammation ↓ Vascularization ↑ Wound contraction ↑ Granulation tissue ↑ Macrophage action ↑	[82]
Human placenta, umbilical cord and amniotic membrane	Hydrogel	Rat full-thickness wounds	Wound closure ↑ Skin appendages ↑ Inflammation ↓ Pro-angiogenesis↑ Keratinocyte growth ↑ Wound contraction ↑ Vascularization ↑ MMP1 deposition ↓ Scarring ↓	[83]
Human amniotic membrane	Membrane	Mouse burns	Granulation tissue formation ↑ Angiogenesis ↑ Collagen maturation ↑	[84]

Amniotic membrane	Membrane	Rabbit full-thickness burns	Epithelialization ↑ Angiogenesis ↑ Skin appendages ↑	[85]
Human Amniotic membrane	Membrane	Rat burns	Re-epithelialization ↑ Granulation tissue formation ↑ Inflammation ↓	[86]
Human amniotic membrane	Membrane	Rat full-thickness muscle and back defect	Foreign body reaction ↓ Inflammation ↓ Fibrosis ↓	[87]
Human amniotic membrane	Crosslinked Membrane	Not conducted	-	[88]
Bovine amniotic membrane	Sponge-like crosslinked membrane	Murine full-thickness wounds	Wound closure ↑ Granulation tissue formation ↑ Angiogenesis ↑ Fibroblast infiltration ↑ Sebaceous gland and hair follicle formation ↑	[89]

1.5 Development of polymer-based ECM-mimetic scaffolds

Understanding the limitations of the decellularized ECM matrix as a scaffold, research on developing an ECM mimetic synthetic dressing was fostered. These scaffolds are intended to have improved mechanical properties and similar biophysical and biochemical properties as that of the ECM. The polymers used for the development of these scaffolds include chitosan, collagen, polylactic acid (PLA), polyglycolic acid (PGA), polycaprolactone (PCL), polylactide-co-glycolide (PLGA), alginates, silk fibroin, chondroitin sulfate, cellulose, agar, etc. [90, 91]. These polymers are either used alone or in combination to develop wound dressings. These polymeric scaffolds were used because of their physicochemical properties, improved mechanical strength, and reduced fabrication cost compared to the decellularized matrices. Some of these polymers also have good antibacterial properties, which is an added advantage. Besides that, it protects the wounded skin, maintains optimum moisture level, and supports cell adhesion and proliferation [92].
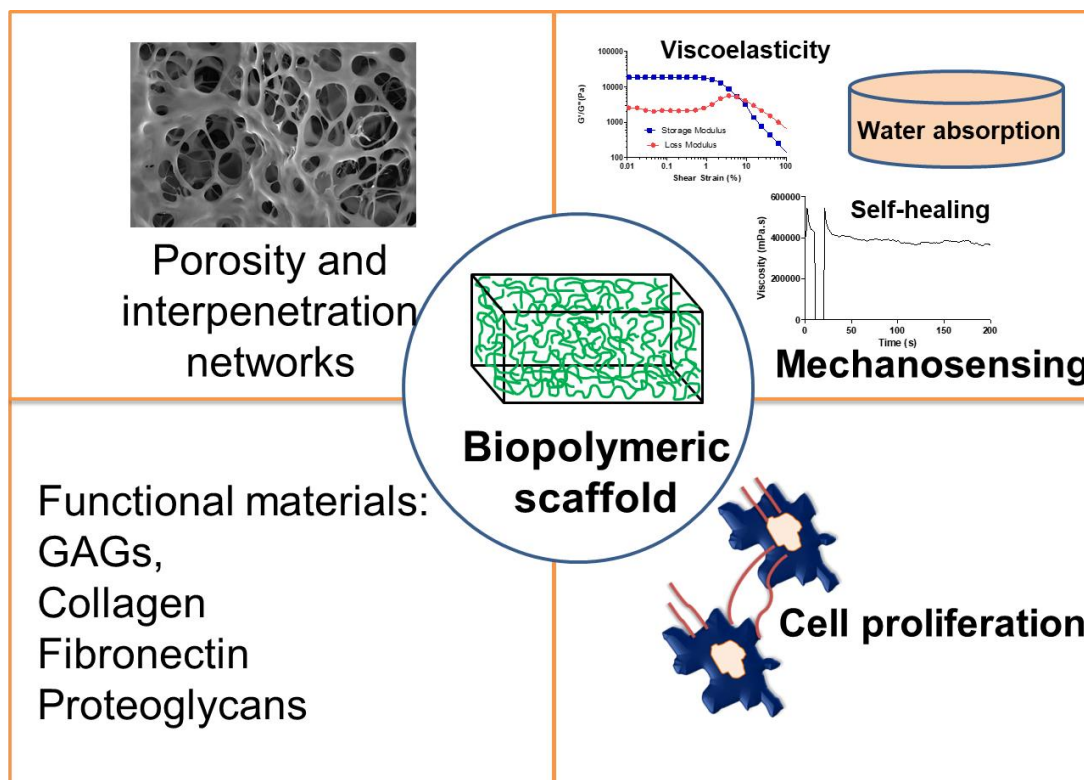
Fig.1.2 Properties of biopolymeric scaffold for the fabrication of ECM mimetic dressing

Hydrogel dressing can be used in all types of wounds. As they form an ECM-like 3D structure that helps in skin regeneration, they have a high potential as wound dressing. These hydrogels act as a carrier for encapsulating cells and growth factors and are also explored in drug delivery [93]. Various existing polymeric hydrogel-based dressings are listed in **Table 1.2**.

Table 1.2 Polymeric hydrogel-based dressings for wound management.

Polymer-based scaffold	Method	*In vivo* model	Outcomes	Ref
Chitosan-alginate loaded with hesperidin	Chemical cross-linking	Rodent	Hemocompatible ↑ Antibacterial↑ Wound contraction ↑	[94]
Chitosan-alginate loaded with silver nanoparticles	In-situ chemical reduction	Rodent	Antibacterial ↑ Cytocompatible	[95]
Chitosan/PVA/dextran hydrogel	Glutaraldehyde cross-linking	Rodent	Antibacterial ↑ Cytocompatible Cell proliferation ↑	[96]
Quaternized chitosan (QCS), methacrylate anhydride-modified collagen (CMA), and oxidized dextran (ODex)	Chemical reduction	Rodent	Angiogenesis ↑ Collagen deposition ↓ Wound closure ↑ Re-epithelialization ↑ Anti-inflammatory↑	[97]

poly(N-isopropylacrylamide$_{166}$-co-n-butyl acrylate$_9$)-poly(ethylene glycol)-poly(N-isopropylacrylamide$_{166}$-co-n-butyl acrylate$_9$) copolymer (P(NIPAM$_{166}$-co-nBA$_9$)-PEG-P(NIPAM$_{166}$-co-nBA$_9$), denoted as PEP) – Silver nanoparticles	Chemical cross-linking	Rodent	Hair follicle growth ↑ Wound closure ↑ Inflammation ↓ Cellular and vascular infiltration ↓ Regeneration ability↑ Antibacterial↑	[98]
poly(ethylene glycol-b-[DL-lactic acid-co-glycolic acid]-b-ethylene glycol) (PEG-PLGA-PEG)	In-situ chemical crosslinking	Rodent	Wound closure ↑ Inflammation ↓	[99]
Gelatin-bFGF hydrogel	Photo-crosslinking	Rodent	Angiogenesis ↑ Wound contraction ↑ Granulation tissue formation ↑	[100]
Polyethylene glycol-thioketal hydrogel loaded with epidermal growth factor	Bi-orthogonal click chemistry	Rodent	Wound closure ↑ Skin appendage formation ↑ ROS ↓ Antioxidant ↑	[101]
Seicin based hydrogel	Photo-crosslinking	Rodent	Granulation tissue formation ↑ Angiogenesis ↑ Collagen maturation ↑	[102]
Nanocellulose based hydrogel	Chemical modification	Human burns	Epithelialization ↑ Hair follicles ↑ Skin appendage formation ↑	[103]
Arginine-modified chitosan hydrogel	Radical polymerization	Rodent	Re-epithelialization ↑ Cell adhesion ↑ Inflammation ↓	[104]
Zinc-sodium alginate hydrogel	Chemical modification	Infected diabetic skin model (Rodent)	Inflammation ↓ Wound contraction ↑ Re-epithelialization ↑ Antibacterial ↑	[105]
Carboxymethyl cellulose-oxidized sodium alginate-based hydrogel	UV-Crosslinking	-	Double network porous hydrogel, hemostatic. Wound contraction ↑ Collagen expression↑	[106]

Catechol functionalized chitosan/oyster peptide microspheres	Wound contraction ↑ [107]
	Cell proliferation ↑

The hydrogel-based dressings are mainly fabricated by chemical reactions forming a covalent bond. The covalent cross-linking increases the stability of the polymeric scaffold by increasing its elasticity [108, 109]. However, the covalent cross-linking lead to the addition of various chemical cross-linkers like glutaraldehyde which are toxic and hence limits its use. Another limitation of using covalently cross-linked hydrogel is reduced thixotropic properties, which reduces their self-healing if the porous scaffold structure is broken during application [110].

On the other hand, physical cross-linking possesses a self-healing property, which can regain its shape even after deformation. Looking at these aspects, research has emphasized the development of self-healing scaffolds prepared using physical interactions. Scaffolds prepared using physical interaction have the added advantage of *in-situ* formation at the wound site. However, a review of the current literature revealed that no in-situ forming polymeric scaffold has been available for clinical use till now. Understanding the importance and benefit of the *in-situ* forming scaffold, few researchers have previously tried to develop such a product; however, all of them have used chemical methods for making a covalently cross-linked matrix. For example, Li *et al*. have reported an in-situ hydrogel composed of chemically cross-linked chitosan and alginate dialdehyde [111]. Xu *et al*. used a similar chitosan and alginate dialdehyde method to develop a similar scaffold for corneal wound healing [112]. Hartwell *et al*. have prepared such a scaffold by chemical cross-linking of polyvinyl alcohol-collagen-glycosaminoglycan [113]. Smeds and Grinstaff have developed a photo cross-linkable methacrylate-modified alginate and hyaluronan [114]. Balakrishnan *et al*. have reported an in-situ scaffold prepared by reacting alginate dialdehyde with gelatin in the presence of borax [115]. Kundu *et al*. have reported a physically entrapped silk sericin protein in a polyacrylamide scaffold as an in situ forming hydrogel [116]. However, no report was found for using electrostatic interaction to develop a cross-linked scaffold at the wound site. Electrostatic interactions have important advantages over chemical cross-linking. It does not need any catalyst or produce any byproducts in the process. The reaction kinetics is rapid, almost instantly it can produce a complex. Also, this type of interaction is very specific; only the charged counterparts interact, keeping the rest of the material undisturbed. Because of such

advantages, different types of such scaffolds have been prepared for various purposes ranging from drug delivery to tissue engineering and regeneration [117-131].

1.6 Hypothesis

A unique way of developing an *in-situ* scaffold is by cross-linking a polymer at the wound site. The problem with the normal cross-linking process is that it depends on chemical cross-linkers, which are toxic for use in an open wound. An ingenious way of making an *in-situ* cross-linked polymer is by using the poly-electrolyte complexation (PEC) strategy. In this approach, two oppositely charged poly-electrolyte polymers interact through the electrostatic bond formation to form a scaffold almost instantaneously. The exclusion of chemical cross-linkers makes the process simple, straightforward, and free of other chemicals. We propose making a bioactive, *in-situ* forming highly porous polymeric scaffold using the PEC strategy, which can have significant advantages over the currently used pre-formed scaffolds. We evaluated different polymer combinations for developing an ECM-mimetic scaffold in a preliminary screening. Among all the combinations tested, cationic polysaccharide chitosan (CH) and anionic glycosaminoglycan chondroitin sulfate (CS) exhibited the best physicochemical characteristics, like swelling and porosity. Based on that, CH and CS were selected to make a PEC-based wound healing scaffold. We hypothesized that as this *in-situ* forming scaffold would be directly applied at the wound site and would come in contact with the wound bed cells, it should stimulate the proliferation and function of the dermal and epidermal cells for improved wound healing.

1.7 Advantage of using chitosan and chondroitin sulfate

The natural polymers, chitosan and chondroitin sulfate, proposed to be used in this scaffold are reported to have significant wound healing efficacy. Paul *et al*. reviewed the role of chitosan and its derivatives in various biological activities. The author demonstrated the non-toxic, biocompatible, biodegradable, and low immunogenic properties of chitosan and its analogs [132]. Ahmad *et al*. synthesized and characterized a chitosan-based hydrogel membrane using a free radical solution polymerization technique for topical application against bacterial skin infections. They used mupirocin as a model antibiotic to check the controlled release of the drug through the prepared polymeric membrane [133]. Patreula *et al*. discussed the different

formulations of chitosan, like sponges, films, and polymeric scaffolds, used to manage wound healing effectively [134]. Wei *et al*. studied the cellular and molecular mechanisms underlying silver nanoparticle/chitosan/poly(vinyl alcohol) nanofiber-mediated wound healing. The authors confirmed the involvement of the TGF-β signaling pathway in the enhanced cell proliferation and increased cell migration when treated with the silver nanoparticles loaded chitosan PVA nanofibers [135].

The role of glycosaminoglycans in wound care is well documented [136]. Amongst the glycosaminoglycans (GAG), chondroitin sulfate has significant wound-healing efficacy [137]). The sulfated GAG is a part of proteoglycan, having significant advantages of being biodegradable, biocompatible, readily available, and highly versatile. Also, chondroitin sulfate-based materials promote wound healing and stimulate skin defect regeneration [138]. Olczyk *et al*. mentioned the role of the extracellular matrix in cutaneous wound healing. The author mentioned that chondroitin sulfate induces FGF-2 and henceforth helps cell proliferation and cell-cell adhesion [139]. Zou *et al*. investigated the role of chondroitin sulfate in palatal wound healing. The results depicted an increase in cell adhesion and growth in a dose-dependent manner and showed beneficial effects in palatal wound healing [140]. Dawlee *et al*. fabricated chondroitin sulfate/gelatin matrices, using gelatin as a crosslinker to prepare chondroitin sulfate matrices. The study concluded that the fabricated hydrogel matrix was biocompatible and beneficial in the early stage of wound healing and tissue repair [141].

Formulation of these polymers individually has its demerits as poor mechanical strength [142]. Few studies reported on using chitosan-based polyelectrolyte complexes for managing chronic wounds [128]. Pires *et al*. evaluated the effect of poly(dimethylsiloxane) on the mechanical properties of chitosan-alginate (CA) polyelectrolyte complexes (PECs) loaded with thymol and beta-carotene with potential application as wound dressing biomaterials [143]. You *et al*. fabricated silver nanoparticle-loaded collagen/chitosan scaffolds, which enhanced fibroblast migration and increased myofibroblast differentiation, showing faster wound repair [144]. Nian *et al*. investigated the characteristics and drug release properties of silver sulfadiazine incorporated into membranes of chitosan and alginate prepared via a casting/solvent evaporation technique. The membrane showed a controlled drug release with optimum porosity and water uptake capacity [145]. Also, Abdel *et al*. fabricated a chitosan–hyaluronic acid

composite sponge scaffold loaded with andrographolide lipid nanoparticles for enhanced wound healing. The research group prepared lipid nanocarriers of andrographolide loaded in a composite chitosan/hyaluronic acid scaffold, which enhanced wound healing with no scar and improved tissue quality [146]. Sarkar *et al*. developed chitosan/collagen electrospun nano/microfibrous mimicking the structural and functional attributes of native extracellular matrix for applicability in skin tissue engineering [147].

As discussed above, both chitosan and chondroitin sulfate have been extensively explored for wound healing applications. However, when used alone, they have low mechanical strength. Hence poly-electrolyte complexation strategy has been proposed, which leads to the formation of a porous scaffold with adequate mechanical strength by combining both the polycation (chitosan) and polyanion (chondroitin sulfate). Rodrigues *et al*. formulated chitosan/chondroitin sulfate membranes produced by poly-electrolyte complexation for cartilage engineering. The membranes sustain the adhesion of chondrocyte cells, inducing their rearrangement in cellular aggregates typical of chondrogenesis and the expression of cartilage markers [148]. However, this reported strategy did not focus on spontaneous (*in-situ*) scaffold formation, as well as the role of this scaffold on skin tissue repair and scaffold is yet to be explored.

Almost all currently available scaffolds are prefabricated by design [149-151]. Pre-formed scaffolds have several logistic issues associated with their use, including complicated fabrication, handling, packaging, etc. Furthermore, the most critical limitation of a pre-formed scaffold is its inability to interact with the basal skin cells of the denuded wound bed. Prefabricated scaffolds do not penetrate the uneven wound bed due to their stiffness, making their interaction with the basal skin cells to a minimum [152]. To overcome the limitation, *in-situ*-forming wound dressings can be developed. *In-situ* hydrogel-based dressings form the scaffold at the target site directly and come in direct contact with the surrounding cells providing a microenvironment for cell adhesion and growth.

References

1.   Yao, Z., J. Niu, and B. Cheng, *Prevalence of Chronic Skin Wounds and Their Risk Factors in an Inpatient Hospital Setting in Northern China.* 2020. **33**(9): p. 1-10.
2.   Shukla, V.K., M.A. Ansari, and S.K. Gupta, *Wound healing research: a perspective from India.* Int J Low Extrem Wounds, 2005. **4**(1): p. 7-8.
3.   Gupta, N., et al., *An Indian community-based epidemiological study of wounds.* J Wound Care, 2004. **13**(8): p. 323-5.
4.   Leveriza-Oh, M. and T.J. Phillips, *Chapter 8 - Dressings and Postoperative Care*, in *Surgery of the Skin*, J.K. Robinson, et al., Editors. 2005, Mosby: Edinburgh. p. 117-135.
5.   Fonder, M.A., et al., *Treating the chronic wound: A practical approach to the care of nonhealing wounds and wound care dressings.* Journal of the American Academy of Dermatology, 2008. **58**(2): p. 185-206.
6.   Sen, C.K., *Human Wound and Its Burden: Updated 2020 Compendium of Estimates.* Adv Wound Care (New Rochelle), 2021. **10**(5): p. 281-292.
7.   Gupta, S., et al., *Chronic wounds: Magnitude, socio-economic burden and consequences.* 2021. **4**: p. 8-14.
8.   Dickinson, L.E. and S. Gerecht, *Engineered Biopolymeric Scaffolds for Chronic Wound Healing.* 2016. **7**.
9.   Shi, C., et al., *Selection of Appropriate Wound Dressing for Various Wounds.* 2020. **8**.
10.   Okur, M.E., et al., *Recent trends on wound management: New therapeutic choices based on polymeric carriers.* Asian Journal of Pharmaceutical Sciences, 2020. **15**(6): p. 661-684.
11.   Potekaev, N.N., et al., *The Role of Extracellular Matrix in Skin Wound Healing.* J Clin Med, 2021. **10**(24).
12.   Eisinger, F., J. Patzelt, and H.F. Langer, *The Platelet Response to Tissue Injury.* Front Med (Lausanne), 2018. **5**: p. 317.
13.   Eisinger, F., J. Patzelt, and H.F. Langer, *The Platelet Response to Tissue Injury.* Frontiers in Medicine, 2018. **5**.
14.   Opneja, A., S. Kapoor, and E.X. Stavrou, *Contribution of platelets, the coagulation and fibrinolytic systems to cutaneous wound healing.* Thromb Res, 2019. **179**: p. 56-63.
15.   Sorg, H., et al., *Panta Rhei: Neovascularization, Angiogenesis and Nutritive Perfusion in Wound Healing.* Eur Surg Res, 2018. **59**(3-4): p. 232-241.
16.   Etulain, J., *Platelets in wound healing and regenerative medicine.* Platelets, 2018. **29**(6): p. 556-568.
17.   Saghazadeh, S., et al., *Drug delivery systems and materials for wound healing applications.* Adv Drug Deliv Rev, 2018. **127**: p. 138-166.
18.   Ebaid, H., *Neutrophil depletion in the early inflammatory phase delayed cutaneous wound healing in older rats: improvements due to the use of un-denatured camel whey protein.* Diagn Pathol, 2014. **9**: p. 46.
19.   Wilgus, T.A., S. Roy, and J.C. McDaniel, *Neutrophils and Wound Repair: Positive Actions and Negative Reactions.* Adv Wound Care (New Rochelle), 2013. **2**(7): p. 379-388.
20.   Kim, S.Y. and M.G. Nair, *Macrophages in wound healing: activation and plasticity.* Immunol Cell Biol, 2019. **97**(3): p. 258-267.
21.   Wynn, T.A. and K.M. Vannella, *Macrophages in Tissue Repair, Regeneration, and Fibrosis.* Immunity, 2016. **44**(3): p. 450-462.
22.   Mescher, A.L., *Macrophages and fibroblasts during inflammation and tissue repair in models of organ regeneration.* Regeneration (Oxf), 2017. **4**(2): p. 39-53.

23. Bainbridge, P., *Wound healing and the role of fibroblasts.* J Wound Care, 2013. **22**(8): p. 407-8, 410-12.

24. Xue, M. and C.J. Jackson, *Extracellular Matrix Reorganization During Wound Healing and Its Impact on Abnormal Scarring.* Adv Wound Care (New Rochelle), 2015. **4**(3): p. 119-136.

25. Volk, S.W., et al., *Diminished type III collagen promotes myofibroblast differentiation and increases scar deposition in cutaneous wound healing.* Cells Tissues Organs, 2011. **194**(1): p. 25-37.

26. Lovvorn, H.N., 3rd, et al., *Relative distribution and crosslinking of collagen distinguish fetal from adult sheep wound repair.* J Pediatr Surg, 1999. **34**(1): p. 218-23.

27. Hallock, G.G., et al., *Analysis of collagen content in the fetal wound.* Ann Plast Surg, 1988. **21**(4): p. 310-5.

28. Wojtowicz, A.M., et al., *The importance of both fibroblasts and keratinocytes in a bilayered living cellular construct used in wound healing.* Wound Repair Regen, 2014. **22**(2): p. 246-55.

29. Pastar, I., et al., *Epithelialization in Wound Healing: A Comprehensive Review.* Adv Wound Care (New Rochelle), 2014. **3**(7): p. 445-464.

30. Michopoulou, A. and P. Rousselle, *How do epidermal matrix metalloproteinases support re-epithelialization during skin healing?* Eur J Dermatol, 2015. **25 Suppl 1**: p. 33-42.

31. Han, G. and R. Ceilley, *Chronic Wound Healing: A Review of Current Management and Treatments.* Adv Ther, 2017. **34**(3): p. 599-610.

32. Das, S. and A.B. Baker, *Biomaterials and Nanotherapeutics for Enhancing Skin Wound Healing.* 2016. **4**.

33. Saghazadeh, S., et al., *Drug delivery systems and materials for wound healing applications.* Advanced Drug Delivery Reviews, 2018. **127**: p. 138-166.

34. Zhao, R., et al., *Inflammation in Chronic Wounds.* Int J Mol Sci, 2016. **17**(12).

35. Kim, H.S., et al., *Advanced drug delivery systems and artificial skin grafts for skin wound healing.* Advanced Drug Delivery Reviews, 2019. **146**: p. 209-239.

36. McCarty, S.M. and S.L. Percival, *Proteases and Delayed Wound Healing.* Adv Wound Care (New Rochelle), 2013. **2**(8): p. 438-447.

37. Liu, Y.-F., et al., *Therapeutic strategies for chronic wound infection.* Chinese Journal of Traumatology, 2022. **25**(1): p. 11-16.

38. Yue, B., *Biology of the extracellular matrix: an overview.* J Glaucoma, 2014. **23**(8 Suppl 1): p. S20-3.

39. Berghoff, S.A., et al., *Dietary cholesterol promotes repair of demyelinated lesions in the adult brain.* Nature Communications, 2017. **8**(1): p. 14241.

40. Tracy, L.E., R.A. Minasian, and E.J. Caterson, *Extracellular Matrix and Dermal Fibroblast Function in the Healing Wound.* Adv Wound Care (New Rochelle), 2016. **5**(3): p. 119-136.

41. Aziz, J., et al., *Molecular Mechanisms of Stress-Responsive Changes in Collagen and Elastin Networks in Skin.* Skin Pharmacology and Physiology, 2016. **29**(4): p. 190-203.

42. Sidgwick, G.P. and A. Bayat, *Extracellular matrix molecules implicated in hypertrophic and keloid scarring.* J Eur Acad Dermatol Venereol, 2012. **26**(2): p. 141-52.

43. Xiao, Y., S. Ahadian, and M. Radisic, *Biochemical and Biophysical Cues in Matrix Design for Chronic and Diabetic Wound Treatment.* Tissue Eng Part B Rev, 2017. **23**(1): p. 9-26.

44. Rosińczuk, J., et al., *Mechanoregulation of Wound Healing and Skin Homeostasis.* Biomed Res Int, 2016. **2016**: p. 3943481.

45. Kuehlmann, B., C.A. Bonham, and I. Zucal, *Mechanotransduction in Wound Healing and Fibrosis.* 2020. **9**(5).

46. Eckes, B., R. Nischt, and T. Krieg, *Cell-matrix interactions in dermal repair and scarring.* Fibrogenesis & Tissue Repair, 2010. **3**(1): p. 4.
47. Walma, D.A.C. and K.M. Yamada, *The extracellular matrix in development.* Development, 2020. **147**(10).
48. Comelles, J., et al., *Soft topographical patterns trigger a stiffness-dependent cellular response to contact guidance.* 2022: p. 2022.01.25.477731.
49. Kaiser, J.-P., A. Reinmann, and A. Bruinink, *The effect of topographic characteristics on cell migration velocity.* Biomaterials, 2006. **27**(30): p. 5230-5241.
50. Holle, A.W., et al., *Cell–Extracellular Matrix Mechanobiology: Forceful Tools and Emerging Needs for Basic and Translational Research.* Nano Letters, 2018. **18**(1): p. 1-8.
51. Wei, Q., et al., *Soft Hydrogels for Balancing Cell Proliferation and Differentiation.* ACS Biomaterials Science & Engineering, 2020. **6**(8): p. 4687-4701.
52. Rosińczuk, J., et al., *Mechanoregulation of Wound Healing and Skin Homeostasis.* BioMed Research International, 2016. **2016**: p. 3943481.
53. Dutta, B., R. Goswami, and S.O. Rahaman, *TRPV4 Plays a Role in Matrix Stiffness-Induced Macrophage Polarization.* Frontiers in Immunology, 2020. **11**.
54. Chen, M., et al., *Substrate stiffness modulates bone marrow-derived macrophage polarization through NF-κB signaling pathway.* Bioactive Materials, 2020. **5**(4): p. 880-890.
55. Spiller, S., et al., *Improvement of wound healing by the development of ECM-inspired biomaterial coatings and controlled protein release.* Biological Chemistry, 2021. **402**(11): p. 1271-1288.
56. Negut, I., G. Dorcioman, and V. Grumezescu, *Scaffolds for Wound Healing Applications.* Polymers, 2020. **12**(9): p. 2010.
57. Baker, B.M., et al., *Cell-mediated fibre recruitment drives extracellular matrix mechanosensing in engineered fibrillar microenvironments.* Nat Mater, 2015. **14**(12): p. 1262-8.
58. Wang, Y., et al., *Substrate stiffness regulates the proliferation, migration, and differentiation of epidermal cells.* Burns, 2012. **38**(3): p. 414-420.
59. Hosseini, M.S. and A.A. Katbab, *Effects of surface viscoelasticity on cellular responses of endothelial cells.* Rep Biochem Mol Biol, 2014. **3**(1): p. 20-8.
60. Rasoulianboroujeni, M., et al., *Dual Porosity Protein-based Scaffolds with Enhanced Cell Infiltration and Proliferation.* Scientific Reports, 2018. **8**(1): p. 14889.
61. Underwood, R.A., et al., *Quantifying the effect of pore size and surface treatment on epidermal incorporation into percutaneously implanted sphere-templated porous biomaterials in mice.* J Biomed Mater Res A, 2011. **98**(4): p. 499-508.
62. Woeller, C.F., et al., *Evaluating a Variable Porosity Wound Dressing With Anti-Scar Properties in a Porcine Model of Wound Healing.* Eplasty, 2018. **18**: p. e20.
63. Shi, C., et al., *Selection of Appropriate Wound Dressing for Various Wounds.* Frontiers in Bioengineering and Biotechnology, 2020. **8**.
64. Dhivya, S., V.V. Padma, and E. Santhini, *Wound dressings - a review.* Biomedicine (Taipei), 2015. **5**(4): p. 22.
65. Fan, F., S. Saha, and D. Hanjaya-Putra, *Biomimetic Hydrogels to Promote Wound Healing.* Front Bioeng Biotechnol, 2021. **9**: p. 718377.
66. Pan, Z., H. Ye, and D. Wu, *Recent advances on polymeric hydrogels as wound dressings.* APL Bioeng, 2021. **5**(1): p. 011504.
67. Kalva, S.N., et al., *Active agents loaded extracellular matrix mimetic electrospun membranes for wound healing applications.* Journal of Drug Delivery Science and Technology, 2021. **63**: p. 102500.

68.   Da, L.C., et al., *Membranous Extracellular Matrix-Based Scaffolds for Skin Wound Healing.* Pharmaceutics, 2021. **13**(11).

69.   Morissette Martin, P., et al., *Decellularized Adipose Tissue Scaffolds for Soft Tissue Regeneration and Adipose-Derived Stem/Stromal Cell Delivery.* Methods Mol Biol, 2018. **1773**: p. 53-71.

70.   Cottler, P.S., et al., *Immunomodulation of Acellular Dermal Matrix Through Interleukin 4 Enhances Vascular Infiltration.* Ann Plast Surg, 2022. **88**(5 Suppl 5): p. S466-s472.

71.   Hanson, S., R.N. D'Souza, and P. Hematti, *Biomaterial-mesenchymal stem cell constructs for immunomodulation in composite tissue engineering.* Tissue Eng Part A, 2014. **20**(15-16): p. 2162-8.

72.   Solarte David, V.A., et al., *Decellularized Tissues for Wound Healing: Towards Closing the Gap Between Scaffold Design and Effective Extracellular Matrix Remodeling.* Frontiers in Bioengineering and Biotechnology, 2022. **10**.

73.   Dziki, J.L., et al., *Solubilized extracellular matrix bioscaffolds derived from diverse source tissues differentially influence macrophage phenotype.* J Biomed Mater Res A, 2017. **105**(1): p. 138-147.

74.   Ramirez-Acuña, J.M., et al., *Diabetic Foot Ulcers: Current Advances in Antimicrobial Therapies and Emerging Treatments.* 2019. **8**(4).

75.   Zhao, Y., J. Fan, and S. Bai, *Biocompatibility of injectable hydrogel from decellularized human adipose tissue in vitro and in vivo.* J Biomed Mater Res B Appl Biomater, 2019. **107**(5): p. 1684-1694.

76.   Alizadeh, M., et al., *Evaluation of vacuum washing in the removal of SDS from decellularized bovine pericardium: method and device description.* Heliyon, 2019. **5**(8): p. e02253.

77.   Lin, W., et al., *A barrier against reactive oxygen species: chitosan/acellular dermal matrix scaffold enhances stem cell retention and improves cutaneous wound healing.* Stem Cell Res Ther, 2020. **11**(1): p. 383.

78.   Bankoti, K., et al., *Carbon nanodot decorated acellular dermal matrix hydrogel augments chronic wound closure.* J Mater Chem B, 2020. **8**(40): p. 9277-9294.

79.   Hsieh, C.M., et al., *A Novel Composite Hydrogel Composed of Formic Acid-Decellularized Pepsin-Soluble Extracellular Matrix Hydrogel and Sacchachitin Hydrogel as Wound Dressing to Synergistically Accelerate Diabetic Wound Healing.* Pharmaceutics, 2020. **12**(6).

80.   Wang, Y., et al., *Biogenetic Acellular Dermal Matrix Maintaining Rich Interconnected Microchannels for Accelerated Tissue Amendment.* ACS Appl Mater Interfaces, 2021. **13**(14): p. 16048-16061.

81.   Wang, L., et al., *Preparation and Characterization of Antibacterial Porcine Acellular Dermal Matrices with High Performance.* ACS Omega, 2020. **5**(32): p. 20238-20249.

82.   Paramasivam, T., et al., *Effect of PDGF-B Gene-Activated Acellular Matrix and Mesenchymal Stem Cell Transplantation on Full Thickness Skin Burn Wound in Rat Model.* Tissue Eng Regen Med, 2021. **18**(2): p. 235-251.

83.   Wang, C., et al., *Sulfated glycosaminoglycans in decellularized placenta matrix as critical regulators for cutaneous wound healing.* Acta Biomater, 2021. **122**: p. 199-210.

84.   Milan, P.B., et al., *Decellularized human amniotic membrane: From animal models to clinical trials.* Methods, 2020. **171**: p. 11-19.

85.   Ramakrishnan, R., et al., *Human-Derived Scaffold Components and Stem Cells Creating Immunocompatible Dermal Tissue Ensuing Regulated Nonfibrotic Cellular Phenotypes.* ACS Biomater Sci Eng, 2020. **6**(5): p. 2740-2756.

86.   Hashemi, S.S., et al., *The role of labeled cell therapy with and without scaffold in early excision burn wounds in a rat animal model.* Iran J Basic Med Sci, 2020. **23**(5): p. 673-679.

87.   Wang, B., W. Li, and J. Harrison, *An Evaluation of Wound Healing Efficacy of a Film Dressing Made from Polymer-integrated Amnion Membrane.* Organogenesis, 2020. **16**(4): p. 126-136.

88.   Ramasamy, P., et al., *Bio-Fabrication of Human Amniotic Membrane Zinc Oxide Nanoparticles and the Wet/Dry HAM Dressing Membrane for Wound Healing.* Front Bioeng Biotechnol, 2021. **9**: p. 695710.

89.   Yang, Y., et al., *A Sponge-Like Double-Layer Wound Dressing with Chitosan and Decellularized Bovine Amniotic Membrane for Promoting Diabetic Wound Healing.* Polymers (Basel), 2020. **12**(3).

90.   Echeverria Molina, M.I., K.G. Malollari, and K. Komvopoulos, *Design Challenges in Polymeric Scaffolds for Tissue Engineering.* Frontiers in Bioengineering and Biotechnology, 2021. **9**.

91.   Mogoşanu, G.D. and A.M. Grumezescu, *Natural and synthetic polymers for wounds and burns dressing.* International Journal of Pharmaceutics, 2014. **463**(2): p. 127-136.

92.   Maaz Arif, M., et al., *Polymer-based biomaterials for chronic wound management: Promises and challenges.* International Journal of Pharmaceutics, 2021. **598**: p. 120270.

93.   Lei, Z., et al., *Bone marrow-derived mesenchymal stem cells laden novel thermo-sensitive hydrogel for the management of severe skin wound healing.* Materials Science and Engineering: C, 2018. **90**: p. 159-167.

94.   Bagher, Z., et al., *Wound healing with alginate/chitosan hydrogel containing hesperidin in rat model.* Journal of Drug Delivery Science and Technology, 2020. **55**: p. 101379.

95.   Chalitangkoon, J., M. Wongkittisin, and P. Monvisade, *Silver loaded hydroxyethylacryl chitosan/sodium alginate hydrogel films for controlled drug release wound dressings.* International Journal of Biological Macromolecules, 2020. **159**: p. 194-203.

96.   Lin, S.-P., et al., *Evaluation of PVA/dextran/chitosan hydrogel for wound dressing.* Cellular Polymers, 2019. **38**(1-2): p. 15-30.

97.   Zhao, F., et al., *A chitosan-based multifunctional hydrogel containing in situ rapidly bioreduced silver nanoparticles for accelerating infected wound healing.* Journal of Materials Chemistry B, 2022. **10**(13): p. 2135-2147.

98.   Yan, X., et al., *Thermoresponsive in Situ Forming Hydrogel with Sol–Gel Irreversibility for Effective Methicillin-Resistant Staphylococcus aureus Infected Wound Healing.* ACS Nano, 2019. **13**(9): p. 10074-10084.

99.   Xu, W.-K., et al., *Accelerated Cutaneous Wound Healing Using an Injectable Teicoplanin-loaded PLGA-PEG-PLGA Thermogel Dressing.* Chinese Journal of Polymer Science, 2019. **37**(6): p. 548-559.

100.   Kushibiki, T., et al., *Photocrosslinked gelatin hydrogel improves wound healing and skin flap survival by the sustained release of basic fibroblast growth factor.* Scientific Reports, 2021. **11**(1): p. 23094.

101.   An, Z., et al., *Injectable thioketal-containing hydrogel dressing accelerates skin wound healing with the incorporation of reactive oxygen species scavenging and growth factor release.* Biomaterials Science, 2022. **10**(1): p. 100-113.

102.   Qi, C., et al., *Sericin hydrogels promote skin wound healing with effective regeneration of hair follicles and sebaceous glands after complete loss of epidermis and dermis.* Biomaterials Science, 2018. **6**(11): p. 2859-2870.

103.   Resch, A., C. Staud, and C. Radtke, *Nanocellulose-based wound dressing for conservative wound management in children with second-degree burns.* Int Wound J, 2021. **18**(4): p. 478-486.

104.   Zhao, N. and W. Yuan, *Highly adhesive and dual-crosslinking hydrogel via one-pot self-initiated polymerization for efficient antibacterial, antifouling and full-thickness wound healing.* Composites Part B: Engineering, 2022. **230**: p. 109525.

105.   Yao, S., et al., *Injectable Dual-Dynamic-Bond Cross-Linked Hydrogel for Highly Efficient Infected Diabetic Wound Healing.* Adv Healthc Mater, 2022: p. e2200516.

106.   He, Y., et al., *A double-network polysaccharide-based composite hydrogel for skin wound healing.* Carbohydrate Polymers, 2021. **261**: p. 117870.

107.   Zhang, D., et al., *Catechol functionalized chitosan/active peptide microsphere hydrogel for skin wound healing.* International Journal of Biological Macromolecules, 2021. **173**: p. 591-606.

108.   Han, B., et al., *Non-additive impacts of covalent cross-linking on the viscoelastic nanomechanics of ionic polyelectrolyte complexes.* RSC Advances, 2017. **7**(84): p. 53334-53345.

109.   Drozdov, A.D. and J. deClaville Christiansen, *Tuning the viscoelastic response of hydrogel scaffolds with covalent and dynamic bonds.* Journal of the Mechanical Behavior of Biomedical Materials, 2022. **130**: p. 105179.

110.   Fan, L., et al., *Advances in Synthesis and Applications of Self-Healing Hydrogels.* 2020. **8**.

111.   Li, X., et al., *In situ injectable nano-composite hydrogel composed of curcumin, N,O-carboxymethyl chitosan and oxidized alginate for wound healing application.* Int J Pharm, 2012. **437**(1-2): p. 110-9.

112.   Xu, W., et al., *An in situ hydrogel based on carboxymethyl chitosan and sodium alginate dialdehyde for corneal wound healing after alkali burn.* J Biomed Mater Res A, 2019. **107**(4): p. 742-754.

113.   Hartwell, R., et al., *An in-situ forming skin substitute improves healing outcome in a hypertrophic scar model.* Tissue Eng Part A, 2015. **21**(5-6): p. 1085-94.

114.   Smeds, K.A., et al., *Photocrosslinkable polysaccharides for in situ hydrogel formation.* J Biomed Mater Res, 2001. **54**(1): p. 115-21.

115.   Balakrishnan, B., et al., *Evaluation of an in situ forming hydrogel wound dressing based on oxidized alginate and gelatin.* Biomaterials, 2005. **26**(32): p. 6335-42.

116.   Kundu, B. and S.C. Kundu, *Silk sericin/polyacrylamide in situ forming hydrogels for dermal reconstruction.* Biomaterials, 2012. **33**(30): p. 7456-67.

117.   Alinejad, Y., et al., *An injectable chitosan/chondroitin sulfate hydrogel with tunable mechanical properties for cell therapy/tissue engineering.* Int J Biol Macromol, 2018. **113**: p. 132-141.

118.   Tan, C., M.J. Selig, and A. Abbaspourrad, *Anthocyanin stabilization by chitosan-chondroitin sulfate polyelectrolyte complexation integrating catechin co-pigmentation.* Carbohydr Polym, 2018. **181**: p. 124-131.

119.   Fan, M., et al., *Covalent and injectable chitosan-chondroitin sulfate hydrogels embedded with chitosan microspheres for drug delivery and tissue engineering.* Mater Sci Eng C Mater Biol Appl, 2017. **71**: p. 67-74.

120.   Jardim, K.V., et al., *Physico-chemical characterization and cytotoxicity evaluation of curcumin loaded in chitosan/chondroitin sulfate nanoparticles.* Mater Sci Eng C Mater Biol Appl, 2015. **56**: p. 294-304.

121.   Venkatesan, J., et al., *Chitosan-amylopectin/hydroxyapatite and chitosan-chondroitin sulphate/hydroxyapatite composite scaffolds for bone tissue engineering.* Int J Biol Macromol, 2012. **51**(5): p. 1033-42.

122.   Park, Y.J., et al., *Controlled release of platelet-derived growth factor-BB from chondroitin sulfate-chitosan sponge for guided bone regeneration.* J Control Release, 2000. **67**(2-3): p. 385-94.

123.   Concha, M., et al., *Aerogels made of chitosan and chondroitin sulfate at high degree of neutralization: Biological properties toward wound healing.* J Biomed Mater Res B Appl Biomater, 2018. **106**(6): p. 2464-2471.

124.   Umerska, A., O.I. Corrigan, and L. Tajber, *Design of chondroitin sulfate-based polyelectrolyte nanoplexes: Formation of nanocarriers with chitosan and a case study of salmon calcitonin.* Carbohydr Polym, 2017. **156**: p. 276-284.

125.   Yeh, M.K., et al., *Novel protein-loaded chondroitin sulfate-chitosan nanoparticles: preparation and characterization.* Acta Biomater, 2011. **7**(10): p. 3804-12.

126.   Huang, L., et al., *Preparation of chitosan/chondroitin sulfate complex microcapsules and application in controlled release of 5-fluorouracil.* Carbohydrate Polymers, 2010. **80**(1): p. 168-173.

127.   Sui, W., et al., *Preparation and properties of chitosan chondroitin sulfate complex microcapsules.* Colloids Surf B Biointerfaces, 2008. **65**(1): p. 69-73.

128.   Vasile, C., et al., *Chitosan/hyaluronic acid polyelectrolyte complex hydrogels in the management of burn wounds.* Rev Med Chir Soc Med Nat Iasi, 2013. **117**(2): p. 565-71.

129.   Kim, H.J., et al., *Polyelectroylte complex composed of chitosan and sodium alginate for wound dressing application.* J Biomater Sci Polym Ed, 1999. **10**(5): p. 543-56.

130.   Hong, H.J., et al., *Accelerated wound healing by smad3 antisense oligonucleotides-impregnated chitosan/alginate polyelectrolyte complex.* Biomaterials, 2008. **29**(36): p. 4831-7.

131.   Puppi, D., et al., *Microstructured chitosan/poly(γ-glutamic acid) polyelectrolyte complex hydrogels by computer-aided wet-spinning for biomedical three-dimensional scaffolds.* Journal of Bioactive and Compatible Polymers, 2016. **31**(5): p. 531-549.

132.   Paul, P., B. Kolesinska, and W. Sujka, *Chitosan and its derivatives - biomaterials with diverse biological activity for manifold applications.* Mini Rev Med Chem, 2019.

133.   Ahmad, S., et al., *Preparation and Evaluation of Skin Wound Healing Chitosan-Based Hydrogel Membranes.* AAPS PharmSciTech, 2018. **19**(7): p. 3199-3209.

134.   Patrulea, V., et al., *Chitosan as a starting material for wound healing applications.* Eur J Pharm Biopharm, 2015. **97**(Pt B): p. 417-26.

135.   Zi-Wei, L., et al., *The Cellular and Molecular Mechanisms Underlying Silver Nanoparticle/Chitosan Oligosaccharide/Poly(vinyl alcohol) Nanofiber-Mediated Wound Healing.* J Biomed Nanotechnol, 2017. **13**(1): p. 17-34.

136.   Ghatak, S., et al., *Roles of Proteoglycans and Glycosaminoglycans in Wound Healing and Fibrosis.* Int J Cell Biol, 2015. **2015**: p. 834893.

137.   Im, A.R., et al., *Wound healing and antibacterial activities of chondroitin sulfate- and acharan sulfate-reduced silver nanoparticles.* Nanotechnology, 2013. **24**(39): p. 395102.

138.   Sapru, S., et al., *Nonmulberry silk protein sericin blend hydrogels for skin tissue regeneration - in vitro and in vivo.* Int J Biol Macromol, 2019. **137**: p. 545-553.

139.   Olczyk, P., L. Mencner, and K. Komosinska-Vassev, *The role of the extracellular matrix components in cutaneous wound healing.* Biomed Res Int, 2014. **2014**: p. 747584.

140.   Zou, X.H., et al., *Chondroitin sulfate in palatal wound healing.* J Dent Res, 2004. **83**(11): p. 880-5.

141.   Dawlee, S., et al., *Oxidized chondroitin sulfate-cross-linked gelatin matrixes: a new class of hydrogels.* Biomacromolecules, 2005. **6**(4): p. 2040-8.

142.   Han, F., et al., *Preparation, characteristics and assessment of a novel gelatin-chitosan sponge scaffold as skin tissue engineering material.* Int J Pharm, 2014. **476**(1-2): p. 124-33.

143. Pires, A.L.R., et al., *Towards wound dressings with improved properties: Effects of poly(dimethylsiloxane) on chitosan-alginate films loaded with thymol and beta-carotene.* Mater Sci Eng C Mater Biol Appl, 2018. **93**: p. 595-605.

144. You, C., et al., *Silver nanoparticle loaded collagen/chitosan scaffolds promote wound healing via regulating fibroblast migration and macrophage activation.* Sci Rep, 2017. **7**(1): p. 10489.

145. Meng, X., et al., *Chitosan and alginate polyelectrolyte complex membranes and their properties for wound dressing application.* J Mater Sci Mater Med, 2010. **21**(5): p. 1751-9.

146. Sanad, R.A. and H.M. Abdel-Bar, *Chitosan-hyaluronic acid composite sponge scaffold enriched with Andrographolide-loaded lipid nanoparticles for enhanced wound healing.* Carbohydr Polym, 2017. **173**: p. 441-450.

147. Sarkar, S.D., et al., *Chitosan-collagen scaffolds with nano/microfibrous architecture for skin tissue engineering.* J Biomed Mater Res A, 2013. **101**(12): p. 3482-92.

148. Rodrigues, M.N., et al., *Chitosan/Chondroitin Sulfate Membranes Produced by Polyelectrolyte Complexation for Cartilage Engineering.* Biomacromolecules, 2016. **17**(6): p. 2178-88.

149. Qin, X., et al., *An Extracellular Matrix-Mimicking Hydrogel for Full Thickness Wound Healing in Diabetic Mice.* Macromol Biosci, 2018. **18**(7): p. e1800047.

150. Rahmani Del Bakhshayesh, A., et al., *Recent advances on biomedical applications of scaffolds in wound healing and dermal tissue engineering.* Artif Cells Nanomed Biotechnol, 2018. **46**(4): p. 691-705.

151. Zhu, C., et al., *Novel enzymatic crosslinked hydrogels that mimic extracellular matrix for skin wound healing.* Journal of Materials Science, 2018. **53**(8): p. 5909-5928.

152. Daristotle, J.L., et al., *Sprayable and biodegradable, intrinsically adhesive wound dressing with antimicrobial properties.* Bioeng Transl Med, 2020. **5**(1): p. e10149.

Chapter 2

**Rationale, gaps in existing research
and objectives of the study**

2.1 Rationale

Skin regeneration is a complex process that requires a coordinated integration of multiple components at the wound site. Among different components, the extracellular matrix (ECM) plays one of the most important roles in wound healing: it provides structural support and an attachment site for cell surface receptors and regulates cell migration, proliferation, and angiogenesis. ECM helps different cells, including fibroblasts, keratinocytes, endothelial, and smooth muscle cells, to migrate through the wound bed and proliferate to re-epithelialize the denuded surface. However, the ECM structure gets completely damaged in severe and chronic wounds, resulting in impaired wound healing. The lost ECM leads to an inadequate nutrient supply making the wound bed hypoxic and maintaining a hyper-inflammatory condition, leading to the development of chronic wounds. De-cellularized matrices are being used as a treatment regimen; however, their tendency to get a bacterial infection, high cost, and difficult fabrication limit their use.

Developing a polymer-based ECM-mimetic wound dressing would be highly useful for this purpose. Externally applied polymeric scaffolds act to substitute the damaged tissue matrix to improve the wound healing process. The main structural feature of any scaffold is a porous, mesh-like structure supported by a polymeric backbone. However, all of these polymeric scaffolds are pre-fabricated, limiting the scaffold's penetration to the deep wound crevices, providing limited mechanical support for the cell growth, partial cell-matrix contact, and thereby delayed cell growth and re-epithelialization.

This brings on to the demand for developing *in-situ* porous scaffolds with good mechanical strength. An ideal *in-situ* forming scaffold should provide cell-substrate contact and allow the dressing to enter the deep crevices of the wound. They should have a favorable viscoelastic property, mimicking the stiffness and elasticity of the skin ECM, supporting the cells to proliferate, and helping overall wound healing. Furthermore, they should have a sufficient antibacterial activity to prevent opportunistic infection. Another critical criterion is the modulation of inflammation at the wound site, as wound inflammation is one of the major causes of a chronic wound.

Physical crosslinking of the polymers directly at the wound site *in-situ* will overcome the limitations of traditional in-situ scaffolds. Traditional *in-situ* scaffolds demand the use of chemical

crosslinkers, which are toxic for use in an open wound. The polyelectrolyte complexation strategy is a unique, ingenious strategy to develop an *in-situ* crosslinked scaffold directly at the wound site. In this strategy, two oppositely charged polyions instantly interact to form a scaffold. Development of the complex without any chemical crosslinkers makes the process simple and straightforward. This instantly formed PEC has multiple advantages over the existing pre-fabricated scaffolds in terms of ease of development, ease of handling, packaging and storing, ease of application, etc. Functionally, its direct contact with the wound bed cells can stimulate dermal cell growth and enhance cell adhesion and tissue repair by providing an ECM-mimetic matrix. Furthermore, as both CH and CS have multifaceted wound healing activity, including promoting tissue regeneration, intracellular signaling, cell proliferation, cell adhesion, antibacterial, and immunomodulatory property, CH-CS PEC could exhibit a multidimensional wound healing efficacy due to its unique material property of coming in direct contact with the wound bed cells.

2.2 Gaps in existing research

Different types of PECs have been designed using CH as the cationic counterpart with diverse types of polyanions [1, 2]. A few examples of CH-based PECs for wound healing application are also there. Vasile *et al*. prepared a CH and hyaluronic acid PEC for the treatment of burn wounds [3]. Kim *et al*. developed a CH and sodium alginate-based PEC for wound dressing [4]. Similar CH/alginate PEC has also been reported by Hong *et al*. [5]. Puppi *et al*. prepared Chitosan/ poly(γ-glutamic acid) polyelectrolyte complex-based 3D scaffold for tissue engineering [6].

The main disadvantage of most of these PECs is that as they are composed of two high molecular weight polymers (CH/hyaluronic acid; CH/sodium alginate; etc.), their spontaneous mixing is impossible. Hence, the wound healing scaffolds need to be pre-fabricated for the application. However, if a low molecular weight polyanion is used, spontaneous mixing can occur, forming a PEC *in-situ*. The major advantage of spontaneous PEC formation is size and shape modulation which can be done relatively easily with this method. Structurally, a wound healing scaffold can be of mainly two types, amorphous or semi-stiff sheets (crystalline or semi-crystalline) [7]. Amorphous scaffolds have very low mechanical strength and can be packaged into a tube for ease of handling. It can also conform to the irregular depths of a wound bed. However, the porosity of amorphous scaffolds is significantly low. Hence it cannot absorb a high amount of tissue exudates.

Also, due to the lower mechanical strength of amorphous scaffolds, they cannot act as a basement membrane to stimulate dermal tissue proliferation. Contrarily, semi-stiff sheets that have enough structural strength have good porosity and absorption capacity and can stimulate dermal tissue growth by acting as a membrane. However, handling these sheets is difficult as they come pre-fabricated and need special packaging and handling. They also cannot take up the shape of the wound due to their stiffness. It would be highly beneficial if we could develop a scaffold that has the property of both types, i.e., it should be amorphous in nature for ease of application, storage, and handling, yet, after application, will have sufficient mechanical strength to act as a scaffolding material to improve tissue repair and absorb wound exudates.

In the current study, we have selected chondroitin sulfate (CS) as a polyanion to be used with CH to make a PEC scaffold. CS is an unbranched oligosaccharide containing two alternating monosaccharides: D-glucuronic acid (GlcA) and N-acetyl-D-galactosamine (GalNAc). CS has a wide range of bioactivity, including promoting tissue regeneration, intracellular signaling, cell proliferation, and cell adhesion [8]. Due to the presence of glucuronic acid moiety, CS has an overall negative charge. Few researchers have previously prepared CH-CS PEC for diverse applications. For example, Huang *et al*. have reported CH-CS PEC microcapsules for controlled release of 5-fluorouracil [9]. They prepared the microcapsules by an emulsion-chemical crosslinking method. Sui *et al*. have also reported a similar microcapsule using the same emulsion-chemical crosslink method [10]. Yeh *et al*. have prepared protein-loaded CH-CS PEC nanoparticles by ionic crosslinking of CS solution with CH [11]. When they mixed dilute solutions of CH and CS, NP suspension was formed. Similarly, Umerska *et al*. prepared calcitonin-loaded CH-CS PEC nanoparticles by ionic crosslinking method [12]. Similar CH-CS PEC nanoparticles were prepared by Tan *et al*. [13] and Jardim *et al*. [14] as well, encapsulating anthocyanins and curcumin, respectively. Fan *et al*. have reported the preparation of a covalently linked CH-CS hydrogel using Schiff's base reaction between amino and aldehyde groups of polysaccharides for crosslinking [15]. Alinejad *et al*. prepared an injectable PEC hydrogel using CH solution mixed with the beta-glycerophosphate / sodium hydrogen carbonate and CS solution [16]. The solutions were mixed thoroughly using two syringes and a Luer Lock connector to make the hydrogel. Park *et al*. have prepared a porous CH-CS sponge by freeze-drying and crosslinking CH and CS with tripolyphosphate [17]. Recently, Concha *et al*. reported preparing an aerogel using CH and CS

[18]. To develop the aerogel, they first prepared a colloidal suspension of CH-CS PEC and freeze-dried it to get the aerogel. However, until now, no one has explored the spontaneous mixing of high molecular weight CH and low molecular weight CS for making an in-situ scaffold for wound healing.

We have discovered that using a high molecular weight poly-cationic polymer, CH, with a low molecular weight counter ion, CS, can lead to spontaneous mixing and *in-situ* crosslinking almost instantly after application without generating any other by-products. Our method for developing a crosslinked scaffold directly at the wound site is unique because we are using two such moieties that can mix spontaneously, leading to the formation of a complex on its own without any external assistance. Additionally, none of the previous wound healing scaffolds have been reported to act to support all the phases of wound healing. They either act as antibacterial or some have been reported to support skin cell growth. The development of easy-to-fabricate clinically viable wound dressing can act at multiple stages of wound healing in an unmet clinical need.

The physicochemical properties of polymeric dressings can alter cell fate and behavior [19]. However, the influence of the biophysical properties of a polymeric scaffold on the major cells involved in wound healing, viz., keratinocytes, fibroblasts, and macrophages, has remained largely unexplored. As an *in-situ* forming scaffold will come in direct contact with the wound bed cells, it can potentially influence their function. Previously, multiple studies have been done to analyze the effect of wound dressing on skin cells. However, none of the studies focused on all the major cells associated with wound healing, viz., keratinocytes, fibroblasts, as well as macrophages. As illustrated in **Chapter 1**, **Table 1.2**, various polymeric dressings are documented for the management of wounds. Mittal *et al*. engineered a dimethylamino ethyl acrylate and hyaluronic acid hybrid polymeric dressing engrafted with the herbal extract. The developed dressing exhibited fast wound closure and ECM deposition [20]. However, vascularization and macrophage modulation behavior was not explored. Another study by Thangavel *et al.* demonstrated high collagen synthesis and angiogenic potential in L-glutamic acid-loaded hydrogel-treated diabetic wounds [21]. However, macrophage-mediated immunomodulation was not in that study. Similarly, Liang *et al*. developed a hemostatic, antibacterial dual crosslinked adhesive hydrogel sealant. However, the study lacks the hydrogel's efficacy on cell proliferation and neo-

angiogenesis [22]. Polymeric dressings demonstrating effective hemostatic as well as potent antibacterial efficacy are very well documented [23-25]. However, these dressing lacks angiogenic properties. From the angiogenesis perspective, some polymeric hydrogels embed a pro-angiogenic agent for supporting vascularization [26, 27]. However, this makes the already complicated fabrication methodology more intricate. Similarly, there are anti-inflammatory dressings studied. Nazir *et al*. illustrated the wound-healing efficacy of *Dictyophora indusiata* extracts. The study reported anti-inflammatory and collagen deposition mechanisms. Nevertheless, these dressings lack the hemostatic and pro-angiogenic aspects of the dressing. Similar works are reported with the other polymeric dressing [28, 29]. Likewise, Zhu *et al.* described the anti-inflammatory and pro-angiogenic potential of multifunctional nanocomposite hydrogel [30]. The study focused on the sustained release of magnesium ions supporting vascularization. However, that study did not evaluate collagen synthesis, ECM deposition, and cell proliferation.

Hence, there is an unmet clinical need for the development of a wound dressing that can show multidimensional wound healing efficacy.

2.3 Objectives of the study

1. Designing and fabrication of an *in-situ* forming viscoelastic scaffold for dermal wound healing. Detailed physicochemical characterization of the scaffold.

2. Evaluation of cellular wound healing mechanism in terms of cell proliferation and expression of functional markers in skin fibroblasts and keratinocyte cells. Confirmation of the activity in the acute wound model.

3. *In-vitro* analysis of the antibacterial efficacy and mechanism of action of the scaffold. Evaluation of macrophage polarization and phagocytic activity in an *in-vitro* infection model. Evaluation of the *in-vivo* efficacy against an infected wound model.

4. Incorporation of a suitable drug for wound healing in the scaffold. Evaluation of its efficacy in a chronic wound model.

References

1. Luo, Y. and Q. Wang, *Recent development of chitosan-based polyelectrolyte complexes with natural polysaccharides for drug delivery.* Int J Biol Macromol, 2014. **64**: p. 353-67.

2. An, Z., et al., *Injectable thioketal-containing hydrogel dressing accelerates skin wound healing with the incorporation of reactive oxygen species scavenging and growth factor release.* Biomaterials Science, 2022. **10**(1): p. 100-113.

3. Vasile, C., et al., *Chitosan/hyaluronic acid polyelectrolyte complex hydrogels in the management of burn wounds.* Rev Med Chir Soc Med Nat Iasi, 2013. **117**(2): p. 565-71.

4. Kim, H.J., et al., *Polyelectroylte complex composed of chitosan and sodium alginate for wound dressing application.* J Biomater Sci Polym Ed, 1999. **10**(5): p. 543-56.

5. Hong, H.J., et al., *Accelerated wound healing by smad3 antisense oligonucleotides-impregnated chitosan/alginate polyelectrolyte complex.* Biomaterials, 2008. **29**(36): p. 4831-7.

6. Puppi, D., et al., *Microstructured chitosan/poly(γ-glutamic acid) polyelectrolyte complex hydrogels by computer-aided wet-spinning for biomedical three-dimensional scaffolds.* Journal of Bioactive and Compatible Polymers, 2016. **31**(5): p. 531-549.

7. Ahmed, E.M., *Hydrogel: Preparation, characterization, and applications: A review.* Journal of Advanced Research, 2015. **6**(2): p. 105-121.

8. Lamme, E.N., et al., *Extracellular matrix characterization during healing of full-thickness wounds treated with a collagen/elastin dermal substitute shows improved skin regeneration in pigs.* J Histochem Cytochem, 1996. **44**(11): p. 1311-22.

9. Huang, L., et al., *Preparation of chitosan/chondroitin sulfate complex microcapsules and application in controlled release of 5-fluorouracil.* Carbohydrate Polymers, 2010. **80**(1): p. 168-173.

10. Sui, W., et al., *Preparation and properties of chitosan chondroitin sulfate complex microcapsules.* Colloids Surf B Biointerfaces, 2008. **65**(1): p. 69-73.

11. Yeh, M.K., et al., *Novel protein-loaded chondroitin sulfate-chitosan nanoparticles: preparation and characterization.* Acta Biomater, 2011. **7**(10): p. 3804-12.

12. Umerska, A., O.I. Corrigan, and L. Tajber, *Design of chondroitin sulfate-based polyelectrolyte nanoplexes: Formation of nanocarriers with chitosan and a case study of salmon calcitonin.* Carbohydr Polym, 2017. **156**: p. 276-284.

13. Tan, C., M.J. Selig, and A. Abbaspourrad, *Anthocyanin stabilization by chitosan-chondroitin sulfate polyelectrolyte complexation integrating catechin co-pigmentation.* Carbohydr Polym, 2018. **181**: p. 124-131.

14. Jardim, K.V., et al., *Physico-chemical characterization and cytotoxicity evaluation of curcumin loaded in chitosan/chondroitin sulfate nanoparticles.* Mater Sci Eng C Mater Biol Appl, 2015. **56**: p. 294-304.

15. Fan, M., et al., *Covalent and injectable chitosan-chondroitin sulfate hydrogels embedded with chitosan microspheres for drug delivery and tissue engineering.* Mater Sci Eng C Mater Biol Appl, 2017. **71**: p. 67-74.

16. Alinejad, Y., et al., *An injectable chitosan/chondroitin sulfate hydrogel with tunable mechanical properties for cell therapy/tissue engineering.* Int J Biol Macromol, 2018. **113**: p. 132-141.

17. Park, Y.J., et al., *Controlled release of platelet-derived growth factor-BB from chondroitin sulfate-chitosan sponge for guided bone regeneration.* J Control Release, 2000. **67**(2-3): p. 385-94.

18. Concha, M., et al., *Aerogels made of chitosan and chondroitin sulfate at high degree of neutralization: Biological properties toward wound healing.* J Biomed Mater Res B Appl Biomater, 2018. **106**(6): p. 2464-2471.

19. Cao, H., et al., *Current hydrogel advances in physicochemical and biological response-driven biomedical application diversity.* Signal Transduction and Targeted Therapy, 2021. **6**(1): p. 426.

20. Mittal, A.K., et al., *Acceleration of Wound Healing in Diabetic Rats through Poly Dimethylaminoethyl Acrylate–Hyaluronic Acid Polymeric Hydrogel Impregnated with a Didymocarpus pedicellatus Plant Extract.* ACS Omega, 2020. **5**(38): p. 24239-24246.

21. Thangavel, P., et al., *Accelerated Healing of Diabetic Wounds Treated with L-Glutamic acid Loaded Hydrogels Through Enhanced Collagen Deposition and Angiogenesis: An In Vivo Study.* Scientific Reports, 2017. **7**(1): p. 10701.

22. Liang, Y., et al., *Dual-Dynamic-Bond Crosslinked Antibacterial Adhesive Hydrogel Sealants with On-Demand Removability for Post-Wound-Closure and Infected Wound Healing.* ACS Nano, 2021. **15**(4): p. 7078-7093.

23. Zhao, X., et al., *Antibacterial anti-oxidant electroactive injectable hydrogel as self-healing wound dressing with hemostasis and adhesiveness for cutaneous wound healing.* 2017. **122**: p. 34-47.

24. Marulasiddeshwara, R., et al., *Nonwoven fabric supported, chitosan membrane anchored with curcumin/TiO2 complex: Scaffolds for MRSA infected wound skin reconstruction.* 2020. **144**: p. 85-93.

25. Liu, M., et al., *Magnesium oxide-incorporated electrospun membranes inhibit bacterial infections and promote the healing process of infected wounds.* 2021. **9**(17): p. 3727-3744.

26. Yu, M., et al., *Liraglutide-loaded PLGA/gelatin electrospun nanofibrous mats promote angiogenesis to accelerate diabetic wound healing via the modulation of miR-29b-3p.* 2020. **8**(15): p. 4225-4238.

27. Chereddy, K.K., et al., *Combined effect of PLGA and curcumin on wound healing activity.* Journal of Controlled Release, 2013. **171**(2): p. 208-215.

28. Brandi, J., et al., *Exploring the wound healing, anti-inflammatory, anti-pathogenic and proteomic effects of lactic acid bacteria on keratinocytes.* Scientific Reports, 2020. **10**(1): p. 11572.

29. Lavelle, E., L. Moran, and M. Andersson. *The impact of chitosan acetylation pattern on inflammation and toxicity*. in *The 14th International Chitin and Chitosan Conference (14th ICCC)*. 2018.

30. Zhu, S., et al., *Engineered multifunctional nanocomposite hydrogel dressing to promote vascularization and anti-inflammation by sustained releasing of Mg2+ for diabetic wounds.* Composites Part B: Engineering, 2022. **231**: p. 109569.

Chapter 3

Designing and fabrication of an *in-situ* forming viscoelastic scaffold. Detailed physicochemical characterization

3.1 Background

Skin damage causes extracellular matrix damage, miscommunication between the surrounding cells, and an improper supply of nutrients and oxygen. Therefore there is a demand for developing wound dressings that can provide cell support and nutrients. With the increasing demand for biocompatible materials, extensive research has been done on advanced functional materials with tunable physicochemical properties [1]. Various natural polymers are used in this field because of their excellent biocompatibility and biodegradability. The common polymers used in skin regeneration include collagen, chitosan, alginate, and hyaluronic acid [2]. These polymers provide mechanical support to the cells surrounding the wound bed to proliferate and migrate at the wound site. Due to their poor mechanical properties, most of these polymers are either used in combination or by some chemical crosslinking [3, 4].

Polyelectrolyte complexation (PEC) is one approach for improving the polymeric scaffold's mechanical strength [5]. Generally, oppositely charged polyions (polycations or polyanions) undergo electrostatic interactions between them, resulting in the formation of PEC. In this strategy, an electrostatic bond is formed between the oppositely charged polymers forming a porous crosslinked scaffold. The PEC-based scaffolds are reported to have good water absorption capacity with a porous network supporting the cells to migrate and proliferate at the wound site. Various PEC-based dressings are evaluated [6, 7]. However, all of these dressings are prefabricated by design [8-11]. The limitations of prefabricated scaffolds have already been discussed in the previous chapter.

In the current study, we have used different poly-cations and poly-anions to develop an ideal wound dressing *in-situ,* providing a moist environment and support to the cells for overall tissue development. The major advantage of spontaneous PEC formation is its modulation to different size and shape to penetrate the wound's deep crevices, creating cell-substrate contact. This chapter focuses on the selection of polymers for the development of PEC-based wound dressing *in-situ*. Further, it discusses the solid-state characterization to confirm the PEC formation, followed by its physicochemical and rheological evaluation and hematological estimation.

3.2 Materials and methods

Sodium alginate and hyaluronic acid were procured from Tokyo chemical industry Co. Ltd. High molecular weight CH (MW≈700 kDa, DD: min 90%), medium molecular weight CH (MW≈310 kDa, DD: min 90%) and low molecular weight CH (MW≈190 kDa, DD: min 90%) was purchased from Sisco Research Laboratories (SRL) Pvt. Ltd. (Maharashtra, India). Chondroitin 6-sulfate (PubChem CID: 24766) monosodium salt, MW 475.39 Da was procured from Tokyo Chemical Industry Co. Ltd. and Bovine serum albumin were procured from S.D. fine chemicals Ltd. (Maharashtra, India). DSC aluminum pans were procured from Toshwin Pharma Ltd. All other chemical reagents used were of A.R. grade.

3.2.1 Screening of polymers

The aim of the current study was the development of a polymeric scaffold using polyelectrolyte complexation technology. The polyelectrolyte complex is formed by electrostatic interaction between the oppositely charged polymers. In the current study, we chose gelatin and chitosan as the cationic polymers and chondroitin sulfate, sodium alginate, and hyaluronic acid as the anionic polymers. The polymers were chosen on the basis of the wound healing efficacy as reported in the literature [12-16]. Water absorption capacity is one of the important parameters required for effective wound healing. We have used a combination of CH & CS, gelatin (G)-Chondroitin sulfate and chitosan- hyaluronic acid (HA) in 1:1 v/v ratio for the preliminary screening. The final polymer selection for the formulation of polyelectrolyte complex was evaluated on the basis of their water absorption capacity and their mechanical strength in the aqueous media.

3.2.2 Preparation of polyelectrolyte complex

All the polymeric solutions were prepared separately by dissolving the weighed amount in MQ water. CH was solubilized in 1%v/v of glacial acetic acid. CH solution was then dialyzed using a 10 kDa cut-off membrane against MQ water to remove the acetic acid. Dialysis was stopped when the pH of the CH solution became more than or equal to 6. PEC was prepared by mixing the polymers of the mentioned combination ion 1:1 v/v ratio. Briefly, a highly viscous CH solution was poured on the mold initially. On top of that, an equal quantity of CS solution was added drop-wise. After a few seconds, an opaque crosslinked scaffold was observed, confirming the development of a polyelectrolyte complex by forming an ionic bond between the oppositely charged polyions. For the physicochemical evaluation of the prepared CH-CS PEC scaffold, the prepared PEC was lyophilized for 24 h to make it dry. After selecting the polymers, the formulation was optimized by exploring the Quality-By-Design approach using 3^3 Box Behnken Design (BBD). The experimental design matrix was prepared and run in Stat-Ease Design-Expert version 8.0.0.7 software.

3.2.3 Characterization of CH-CS PEC complex

1. Fourier Transform Infrared Spectroscopy

FTIR spectroscopy was performed to confirm the formation of CH-CS PEC scaffold. Fourier transform infrared spectroscopy was done using IR Prestige FTIR instrument (Shimadzu). CH-CS PEC was dried by lyophilization and the dry powder used for FTIR analysis. The samples were prepared using KBr pressed pellet method in 1:100 ratio of the sample and KBr. The sample was analyzed in between 400- 4000 cm^{-1}. FTIR spectroscopy of CH, CS, and the CH-CS PEC was done separately.

2. Differential Scanning Calorimetry

Differential scanning calorimetric (DSC) measurements were performed in a DSC-60 plus thermal analyzer (Shimadzu). The DSC curves were executed under a dynamic nitrogen atmosphere (40 mLmin^{-1}) using sample mass as 2–5 mg and heating rates 10°Cmin^{-1}. Accurately weighed samples

were placed into a covered aluminum sample holder. Empty aluminum sample holder was kept as a reference and the run was performed by heating the samples from 25°C up to 480°C.

3. Solid-state CP MAS 13C NMR spectroscopy

High-resolution, solid-state 13C NMR experiments were conducted at room temperature using a JEOL ECZR series 600MHz NMR spectrometer. The 13C CP MAS spectra were measured with a 20μs 90° pulse, a 5 s pulse delay time with 1102 scans. A MAS rate of 20.0 kHz was used to eliminate resonance broadening due to the anisotropy of chemical shift tensors.

4. Thermogravimetric analysis (TGA)

TGA was performed using a TGA-50 (Shimadzu) instrument. The mass of each sample was 3–5 mg. The carrier gas was nitrogen at a flow rate of 50 ml/min. The samples were heated from 30 to 500 °C.

5. X-ray diffraction studies

The X-ray diffraction patterns were collected using a Desktop X-ray diffractometer, Miniplex-II (Rigaku) at 40 kV and 40 mA, in theta-theta configuration, secondary monochromator with Cu-Kα radiation, and a PIXcel solid-state detector at room temperature.

6. Swelling Studies

The swelling index was calculated by the method reported by Im *et al*. [17]. Briefly, the pre-weighed CH-CS PEC scaffold was immersed in PBS (pH 7.4). The weight of the prepared PEC was calculated at different time points till 5 h. swelling ratio was calculated by:

Swelling ratio$= ((W_w - W_i)/W_i) \times 100$

Where W_i was the initial weight of the sample and W_w was the wet weight of the samples at the respective time interval.

7. Porosity Studies

The porosity studies were performed by alcohol displacement method. Pre-weighed CH-CS PEC scaffold was dipped in a graduated cylinder containing ethanol and soaked for 24 h. The final

weight of the wet sample was noted as W_f % porosity was determined using formula reported by Im *et al.* [17].

Porosity%$= ((W_f – W_i / \rho_{ethanol})/V) \times 100$

W_f and W_i indicates the weight of samples before and after immersion in alcohol, respectively. V is the volume of alcohol used in the study ρ ethanol is the density of ethanol. The porosity was further confirmed by microscopic observation of the pores using scanning electron microscopy.

8. Scanning Electron Microscopy and EDS

The surface morphology of the CH-CS PEC was studied using the scanning electron microscopy. SEM images of the CH-CS PEC scaffold was taken at high vacuum mode in Apreo-S FEI instrument at 20 µm scale for observing the morphology of the CH-CS PEC. The images of scaffold prepared with the different molecular weight of CH and scaffold prepared with CH alone were also captured for comparison purpose. Further surface characterization was performed using Elemental dispersive spectroscopy (EDS).

9. X-ray Photoelectron spectroscopy

The surface-bound elemental analysis was performed using Shimadzu Kratos Supra Spectrophotometer (Shimadzu Analytical Corp. Tokyo) with a monochromatic Aluminum Kα source at a power of 15 Kv with 10 mA. The study was performed in the fixed analyzer transmission mode where the pressure was between 10^{-9} and 10^{-8} mbar. The study was performed to confirm the elements present on the polymeric surface. To obtain more detailed information about chemical structure, oxidation states etc., and high-resolution spectra were recorded from individual peaks at either 20 or 40 eV serial energy (yielding a typical peak width for polymers of 0.8–1.0 eV). Survey spectra were acquired at a pass energy of 160 eV. All elements present were identified from survey spectra database. The atomic concentrations of the detected elements were calculated using integral peak intensities and the sensitivity factors supplied by the manufacturer. Binding energies were referenced to the C 1s, O 1s, peak at 285 eV for aliphatic hydrocarbon [18].

10 Rheological characterization

Rheological measurements were performed on Anton Paar (MCR 92) rotational rheometer, using a plane plate (PP25), 25 mm in diameter. The samples were loaded on the disc, putting a gap of 1 mm between the disc and PP25. Oscillatory amplitude and frequency sweep tests were performed to study the viscoelastic nature of the scaffold. The amplitude sweep test was performed at a constant frequency of 100 rads/s to find the scaffold's linear viscoelastic region (LVER). After confirming the LVER region, the frequency sweep test was performed within the LVER limit. The viscoelastic behavior was analyzed in terms of storage modulus (G') and loss modulus (G"). Further, the thixotropic analysis of the scaffold was performed by evaluating the recovery rate at different strains. Change in viscosity was evaluated at initial strain of 0.25% for 10s, 1000% strain for 10s, and then 0.25% strain for a further 200s. Also, a macroscopic evaluation of the self-healing property of CH-CS PEC was performed. The CH-CS PEC was prepared as two separate disc-shaped scaffolds, amongst which one was stained with Rhodamine B. Both the discs were kept in surface contact for 3 min; after that, their physical integrity was evaluated and photographed.

3.2.4 Blood-cell interaction study of CH-CS PEC

1. *In-vitro* hemolysis test

In-vitro hemolysis was studied to check the hemocompatibility of the prepared CH-CS PEC. The hemolysis ratio of CH-CS PEC scaffold was tested with different concentrations of CH-CS PEC (2 mg/ml to 0.008 mg/ml). The samples were pre-weighed in the required quantity and were UV sterilized for 30 min. The samples were crushed in a mortar and pestle, and the required concentrations were prepared by suspending the sample in PBS. The blood was withdrawn from the Wister rat via the retro-orbital route. To prevent it from clotting, it was mixed with the required amount of 0.1 M EDTA (20 µl/ml blood). The blood sample was then centrifuged at 7500 rpm twice for 7 min to isolate RBCs. The supernatant was removed, and the RBC pellet was washed with PBS (pH 7.4). Finally, the RBCs were suspended in 1 ml PBS (pH 7.4). From the suspension of RBC 100 µl of the sample was added to different concentrations of CH-CS PEC. The blood sample mixed with distilled water was taken as a negative control. The samples were incubated for 1h with gentle shaking. The samples were then again centrifuged at 3500 rpm for 1 min to

remove intact RBCs. The supernatant was isolated and analyzed using UV spectrophotometer at 408 nm. The percentage hemolysis was calculated using the formula:

$$\% \text{ Hemolysis} = \left(\frac{Ds - Dn}{Dp - Dn}\right) \times 100$$

Where Ds, Dn, and Dp are the absorbance of the sample, normal saline mixed with samples, and distilled water mixed with samples, respectively.

2. Whole blood clotting study and cell adhesion test

The whole blood clotting study was performed to check the hemostatic potential of the CH-CS PEC scaffold. The smaller the blood clotting index is, the stronger the hemostatic potential of the material. The blood was collected via a retro-orbital route from the Wister rat. The study was performed by putting 0.2 mL of citrated whole blood onto the pre-weighed scaffold. On top of the treated scaffold, 20 µL of 0.2 M $CaCl_2$ solution was added to initiate coagulation. After 10 min, red blood cells (RBCs) that were not trapped in the clot were hemolyzed with 20 mL of deionized water, and the absorbance of the resulting hemoglobin solution was measured at 408nm. A blood sample without CH-CS PEC was taken as blank. The study on blood clotting mainly evaluates the hemostatic potential of the wound dressing to induce thrombosis in blood by a performance evaluation parameter called blood-clotting index (BCI). The blood cells trapped in the CH-CS PEC were fixed by treating the treated sample with 4% glutaraldehyde solution for 15 min. The sample was then dried, and its morphology was studied using scanning electron microscopy (Apreo-S FEI) to check the amount of the RBCs adhered on the surface of CH-CS PEC. The blood clotting index was calculated using the formula:

BCI = As/Ab × 100

Where A_s is the Abs of the sample and A_b is the Abs of the blank [19].

3. Protein adsorption study

The adsorption of bovine serum albumin (BSA) was done via the batch contact method [20]. An increase in the adsorption of bovine serum albumin implies better thrombotic properties. The samples were first soaked in 20 mL of 0.2 wt. % BSA solution in PBS (pH=7.4) and then shaken

for 1h to prevent the solution-air interface formation. The supernatants were analyzed to determine the residual BSA in solution using a UV spectrophotometer at 280 nm. The amount of protein adsorbed on the CH-CS PEC was calculated using the formula:

Adsorbed BSA (mg/g) = $((C_o - C_a)/w) \times V)$

Where C_0 and C_a are the BSA concentrations (mg/mL) before and after adsorption, respectively, W is the weight of the swollen CH-CS PEC (g), and V is the volume of the BSA solution (mL).

3.2.5 Statistical analysis

All data are expressed as mean ± SEM. Statistical analysis was conducted with the two-tailed unpaired t-test for two-group comparison or one-way ANOVA, followed by the Tukey multiple comparison tests by using GraphPad Prism (for three or more groups). A difference with $p < 0.05$ was considered to be statistically significant.

3.3 Results and Discussion

3.3.1 Screening of polymers for the polyelectrolyte complex formation

In the current study, we wanted to develop a simple and scalable technique free from all the chemical crosslinkers. We herein used the poly-cations CH and Gelatin (G), and the polyanions, namely CS, Alginic acid (AA), and HA. The use of these polymers in wound healing is already known. We used this poly-cation−poly-anion combination to develop spontaneous polyelectrolyte complex formation at the wound site. The formation of PEC was observed in the CH-CS, CH-HA, G-CS and G-AA polymer combination in 1:1 ratio from different combinations of cationic and anionic polymers. These PEC were further lyophilized and screened based on their water absorption capacity and strength in aqueous media. The CH-CS PEC and CH-HA PEC showed the best water absorption capacity compared to other polyelectrolyte complexes **(Table 3.1)**. Hence, for further studies, we fixed CH-CS PEC for further design and optimization.

Table 3.1 Swelling index (%) of polyelectrolyte complex of different drug combinations

Polyelectrolyte complex	Swelling (%)
G-CS	516 ±116
G-AA	654.9±43.21
CH+HA	634±13.56
CH+CS	857±12.04

The CH-CS PEC showed a spontaneous formation of PEC due to the ease of penetration of low molecular weight CS into the high molecular weight CH. Hence, for further studies, we used CH-CS PEC for further design optimization and other studies.

3.3.2 Design and fabrication of CH-CS PEC

CH is a linear polysaccharide composed of randomly distributed β-(1→4)-linked D-glucosamine. Due to the presence of the free −NH$_2$ group in the glucosamine unit, CH can readily get protonated in the acidic medium and carry a positive charge. Conversely, CS is an oligosaccharide composed of a chain of alternating sugars, sulfated N-Acetylgalactosamine, and glucuronic acid. CS carries a negative charge due to the presence of sulfate group and glucuronic acid moiety.
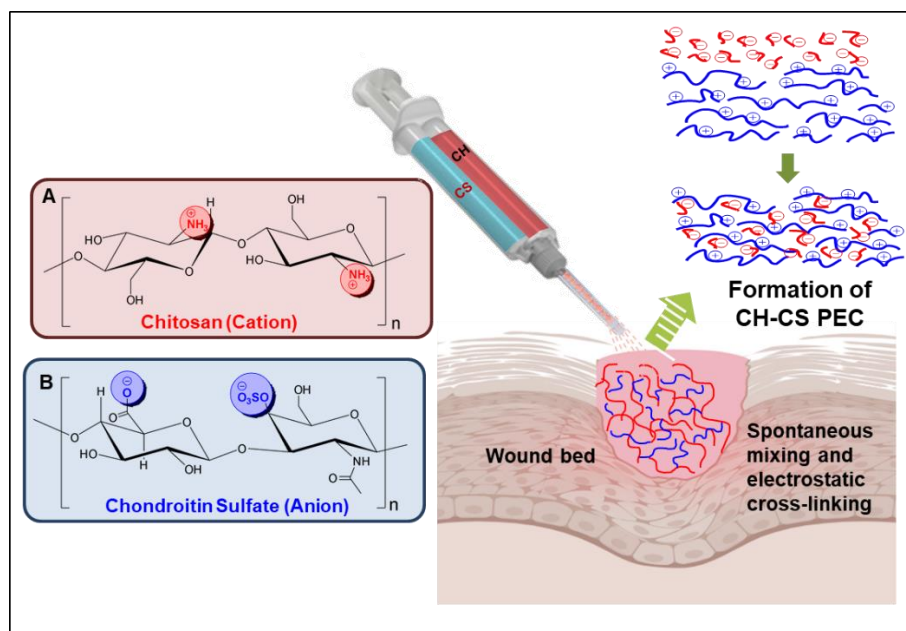
Fig. 3.1 Schematic representation of CH-CS PEC formation.

As CH and CS carry opposite charges, these two polysaccharides can spontaneously interact to form a polyelectrolyte complex (PEC) **(Fig. 3.1)**. The advantages of PEC include quick and spontaneous formation, stability, etc. [21]. Along with these, CH and CS have the added advantage of spontaneous mixing. We have used a disaccharide form of CS (6 sulfate, monosodium salt) in this study with a molecular weight of 475 Da. As CH has a significantly higher molecular weight than CS, CH solution is highly viscous, whereas CS solution of the same concentration has a very low viscosity. Due to this, CS solution can easily percolate into the viscous CH solution, making crosslinks on the way, forming the PEC and leading to instant scaffold formation, while with other PEC formations, the polymer solutions need to be mechanically mixed. When poured into a Petri dish, CH solution formed a thick and viscous layer. We added CS solution on top of it, which easily penetrated the CH solution, rapidly forming the CH-CS-PEC as a solid scaffold. This spontaneous formation is highly beneficial over prefabricated scaffolds used for wound healing, as size and shape modulation can be done relatively easily with this method.

1. Optimization of the CH-CS-PEC design based on swelling and porosity analysis

After confirming that CH and CS can spontaneously interact to produce a PEC, we wanted to determine the best ratio of CH and CS to produce the most useful scaffold for wound healing. The Box Behnken design was chosen to find out the best ratio of CH and CS to optimize CH-CS-PEC. Based on our preliminary experiment and understanding, three independent variables were chosen for optimization, the concentration of CH and CS, and the MW of CH. Three different concentrations of CH and CS (2, 5, and 8 mg/mL) and three different MW of CH (low, medium and high) were selected, as depicted in **Table 3.2**. The experiments were run as per the design matrix obtained by the software. The critical quality attributes (CQA) were selected as the concentration of CH (X_1), the concentration of CS (X_2), and the molecular weight of CH (X_3). The quality target product profile (QTPP) was chosen as per the formulation requirement of the ideal wound dressing, namely % swelling and % porosity of the prepared CH-CAS PEC scaffold. **Table 3.2** shows the design matrix obtained by using BBD design. Based on this design matrix, PEC was prepared and tested for their efficacy. We have chosen swelling and porosity as the quality target product profile (QTPP) as these two properties are essential requirements of a wound dressing material. Higher swelling and porosity properties define that the dressing will absorb wound

exudates, promoting wound healing. The swelling and porosity of different batches of PEC are depicted in **Table 3.3**, **Fig. 3.2A,** and **3.2B**. Among the three variables, MW of CH was found to have the most significant impact on the QTPP of the CH-CS-PEC, and high MW showed enhanced swelling and porosity compared to the low and medium MW CH (**Fig 3.2A**, **3.2B**; **Table 3.3**). This may be due to the longer chain length of the high MW CH, which increases the entanglement of the polymer, increasing porosity. The effect of MW of polymer on the porosity of PEC has been studied before, and a similar phenomenon has been observed [22]. Other variables, namely the concentration of CH and CS, were found to have a moderate effect on the QTPP, and higher concentrations of both CH and CS generally increased the QTPP slightly. We also found that more than 5 weight % of high MW CH was very difficult to dissolve

Table 3.2 Experimental Design, Factors, and Responses

Independent Variables	Levels		
	-1	**0**	**+1**
X_1 = **Concentration of CH (%)**	2	5	8
X_2 = **Concentration of CS (%)**	2	5	8
X_3 = **mol. wt of CH (KDa)**	low	Medium	High
Dependent variables			
Y1= Swelling study			
Y2= Porosity			

Table 3.3 Composition of design matrix and Quality target product profile of CH-CS PEC

Batches	Factor			Responses	
	Concentration of CH (X_1)	Concentration of CS (X_2)	MW of CH (X_3)	Swelling (%)	Porosity (%)
1	5	8	High	928.98	104.2
2	8	5	High	**Batch didn't form**	
3	2	5	High	879.49	81.49
4	5	2	High	865.12	108.65
5	5	5	Medium	345.05	56.79
6	8	2	Medium	385.23	65.06
7	8	8	Medium	232.23	70.18
8	2	2	Medium	247.63	76.77
9	2	8	Medium	278.00	20.76
10	5	2	Low	219.06	22.45
11	5	8	Low	234.67	28.84
12	8	5	Low	235.71	20.42
13	2	5	Low	167.76	18.09

2. Influence of independent variables on the swelling property of CH-CS-PEC

Next, we analyzed the effect of the independent variables on the swelling property and porosity of the CH-CS-PEC. As a higher swelling property was found with high MW CH (X_3), it was kept constant. The 3-D contour plot (**Fig. 3.2C**) describes the effect of changes in concentrations of both the polymers on % swelling. It extrapolated that as the concentration of CH and CS increased, the % swelling of the polyelectrolyte complex was also increased. The quadratic model was considered to be the best-fit model for the swelling property of the polyelectrolyte complex with a p-value of 0.0369. The model followed the polynomial equation $Y=+155.67X_1-69.12X_2+586.09X_3-17.55X_1^2+8.59X_2^2+133.27X_3^2-2.72X_1X_2-78.82X_1X_3+6.104X_2X_3$. The equation determines that the variables concentration of CH (X_1) and MW of CH (X_3) significantly impact the swelling property of CH-CS PEC.
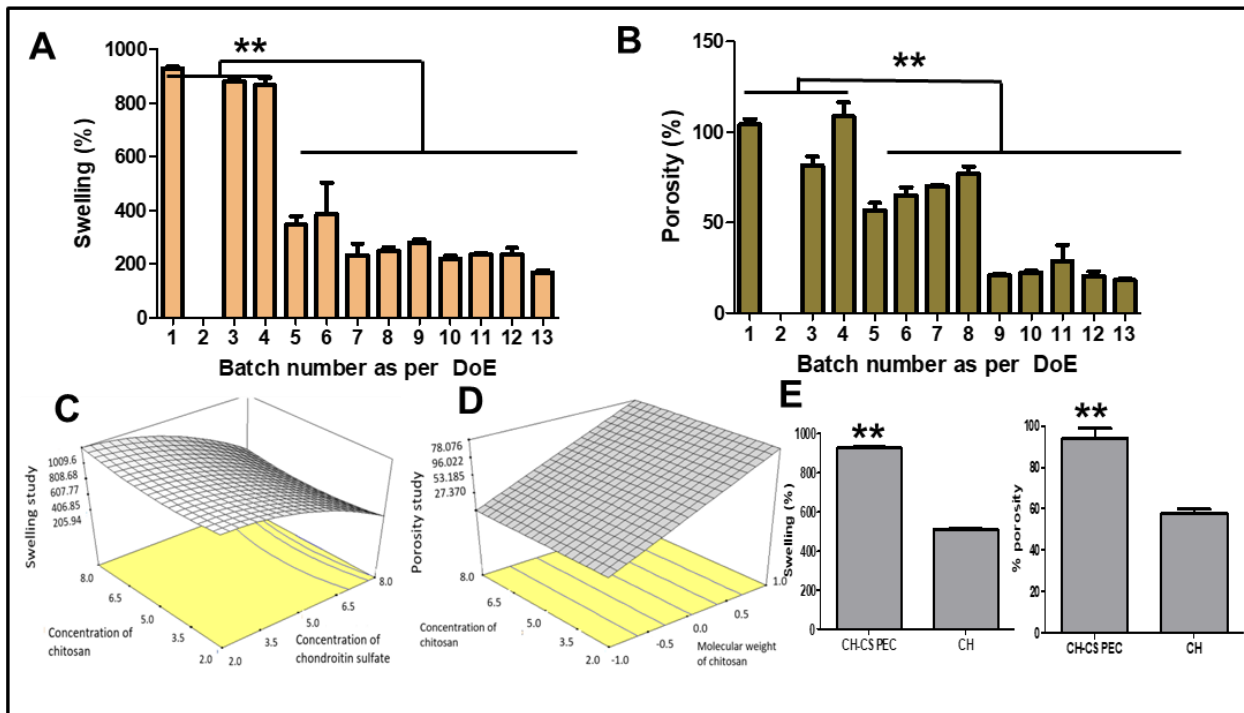
Fig. 3.2 Optimization of the CH-CS-PEC design based on swelling and porosity analysis. A. % Swelling and B. % Porosity of different batches. C. 3-D contour plot of concentrations of both the polymers vs. % swelling. D. 3-D contour plot of concentration of CH and molecular weight of CH vs. % porosity. E. Comparison between CH scaffold and the optimized CH-CS PEC in terms of swelling and porosity.

Fig 3.2D depicts the 3D contour plot of the effect of independent variables on the % porosity of CH-CS PEC. It was found that there was no significant impact of the change in CS concentration on the CH-CS PEC's porosity, and henceforth was kept constant. The other two factors i.e., the concentration of CH and molecular weight of CH, showed a significant impact on the % porosity of the CH-CS PEC. The best model fit for % porosity was a linear model. The contour plot described the positive impact of MW of CH on the porosity property of the PEC. The graph determined an increase in porosity with an increase in CH's concentration and molecular weight. The polynomial equation defining the model is $y = +53.12 - 5.12X_1 - 5.29X_2 + 52.25X_3$. The p-value for the model was 0.0136, and the lack of fit value was 7.86.

3. Validation of the Design Analysis approach

To validate the use of the Design Analysis approach for determining the best composition, some combinations of checkpoint were generated by the software predicting the range of independent and dependent variables. Three batches were selected randomly amongst the combinations and

evaluated for the dependent variables. The performed dependent variables should match the predicted solutions obtained by the software. The % prediction error should be less than 5 % for the design to be validated. As depicted in **Table 3.4**, the predicted error was found to be less than 5% in all the tested samples, validating the design analysis.

Table 3.4 Evaluation of the checkpoint batches and model validation

Batch Id	Independent variables			Predicted responses		Observed responses		% Predicted error	
	X_1	X_2	X_3	Y1	Y2	Y_1	Y_2	Y_1	Y_2
CH-1	5.4	4.2	high	927.84	94.84	912.54 ±23.58	91.63 ±3.45	0.31	4.31
CH-2	5.13	3.48	high	876.42	87.68	875.04 ±13.04	85.86 ±3.72	0.18	2.67
CH-3	5.47	5.77	high	930.1	92.76	914.41 ±15.47	95.97 ±1.89	2.14	2.46

Based on the observed effect of the influence of MW of CH, and concentration of both CH and CS on the properties of the CH-CS-PEC, we have selected high MW CH and 5 weight% concentration for both CH and CS for our further study. For the physicochemical evaluation of the prepared CH-CS PEC scaffold, the prepared PEC was lyophilized for 24 h to make it dry and dried PEC was used for analysis.

4. Morphology of the CH-CS PEC

The morphology of the lyophilized PEC samples was studied using scanning electron microscopy (**Fig. 3.3A-D**). The images of the CH (high molecular weight, 5 weight% concentration, (**Fig. 3.3A**) scaffold and CH-CS PEC made up with 5 weight% concentration of low molecular weight (**Fig. 3.3B**), medium molecular weight (**Fig. 3.3C**) and high molecular weight CH (**Fig. 3.3D**) along with 5 weight % of CS was taken to check the crosslinked structure and pore size of the formed PEC. The images were taken at 20 µm scale at high vacuum mode in an Apreo-S FEI instrument. The images showed a change in the pore size of the scaffold with a different molecular weight of CH. The scaffold prepared with only CH was brittle, and the morphology showed microscopically uneven structures (**Fig. 3.3A**). In the CH-CS PEC, the structure was found to be much less brittle physically and more uniform in the microscopic analysis. However, with low

molecular weight CH, the pores were less definite (**Fig. 3.3B**) compared to the PEC prepared with higher molecular weight CH (**Fig. 3.3C-D**). As indicated in the %swelling and %porosity studies, the pore size increased proportionately based on the molecular weight of CH, and high molecular weight CH exhibited the best porosity, which is also corroborated by the SEM analysis (**Fig. 3.3D**).
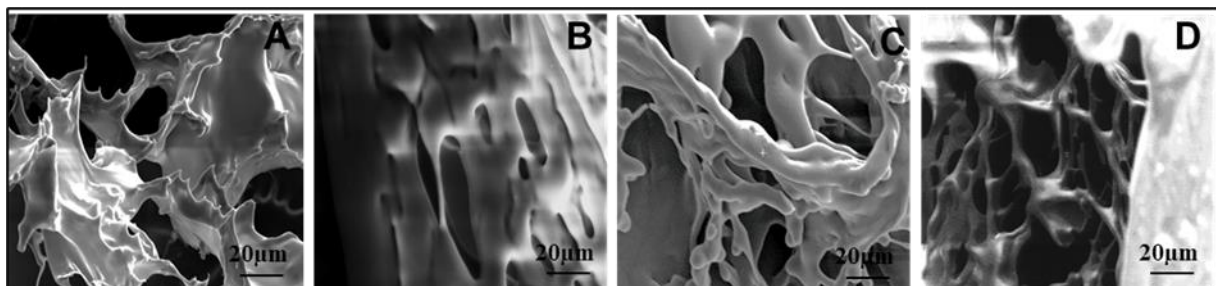
Fig. 3.3 SEM analysis of CH scaffold (A), and CH-CS PEC prepared with LMW CH (B), MMW CH (C), and HMW CH (D).

5. Comparison of the swelling index and porosity of the CH-CS PEC scaffold with CH scaffold

A formulation chosen for wound dressing should provide adequate porosity for the gaseous exchange and to maintain a moist environment. CH is a natural polymer that undergoes formation of hydrogel at acidic pH. Due to the gelling properties of CH, the polymer provides a suitable moist and porous environment for the healing of wounds. To determine the difference between the CH-CS PEC and CH scaffold, the swelling and porosity of the optimized CH-CS PEC were compared with that of the scaffold prepared with only CH (**Fig. 3.2E**). The prepared CH-CS PEC showed better swelling and porosity properties as compared with that of the scaffold prepared with the same concentration of CH alone. **Fig. 3.2E** showed the % porosity and swelling of CH scaffold and CH-CS PEC. Only CH scaffold exhibited a swelling of ~510% and porosity of ~58%, whereas CH-CS PEC exhibited a swelling of ~925% and porosity of ~95%. The reduction in the swelling ability of the CH gel could be because of its structure and lack of void volume. The cross-linking of CS with CH in the CH-CS PEC probably led to increased swelling and porosity of the CH-CS PEC than that of the scaffold prepared from the same concentration of CH alone. As described in **Fig. 3.4**, due to the absence of crosslinking, CH scaffolds exhibited a low void volume, whereas CH-CS scaffold maintained a large void volume, exhibiting significantly increased porosity and swelling.
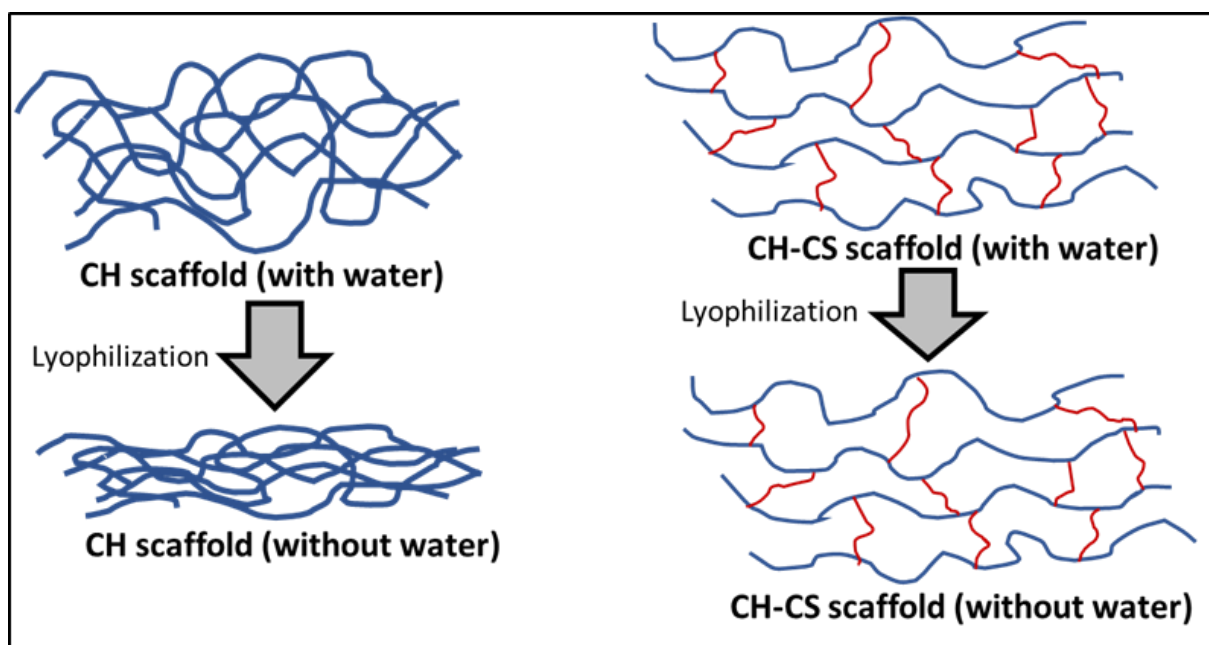
Fig. 3.4. Graphical representation of the swelling and porosity property of CH-CS PEC and CH scaffold

3.3.3 Physicochemical characterization of the CH-CS-PEC

1. FT-IR spectroscopic analysis

After fabricating the scaffold, we wanted to verify whether a PEC is forming between CH and CS or it's only a physical mixture. FTIR studies were conducted with the powder prepared from dried (lyophilized) CH-CS PEC. **Fig. 3.5A** describes the FTIR spectra of CH, CS, and the CH-CS-PEC prepared with high molecular weight chitosan and chondroitin sulfate. The peak for $-NH_2$ group bending and stretching appeared around 1642 cm^{-1} and 3486 cm^{-1}, respectively, present in the FT-IR spectra of the CH. However, it disappeared in the CH-CS-PEC, indicating modification in the $-NH_2$ group. The intensity of the peak assigned to the negatively charged $-OSO^{3-}$ group in the CS, which was coming at 1,217 cm^{-1}, was reduced in the CH-CS-PEC. The carbonyl carbon (C=O) peak of CS at 1650 cm^{-1} also shifted and reduced in intensity in the CH-CS-PEC. These data confirm the ionic bond formation between the positively charged amino group of CH and the negatively charged sulfate and the carbonyl group of CS.

2. DSC analysis

Next, we confirmed the formation of the CH-CS-PEC with DSC thermogram analysis. This study was performed with the powder prepared from dried (lyophilized) CH-CS PEC. As depicted in **Fig. 3.5B**, native CH exhibited an endothermic peak at ~70 °C and an exothermic peak at ~300 °C. CS exhibited an endothermic peak at ~93 °C and a sharp exothermic peak at ~240 °C. Compared to that, with the CH-CS-PEC, a completely new endothermic peak was detected at ~62 °C and two exothermic peaks at ~308 °C and ~460 °C (**Fig. 3.5B**). This data indicates that the complex formation was successful.

3. Thermogravimetric analysis (TGA)

TGA was performed to study the change in CH-CS PEC's thermal stability compared to CH and CS. As depicted in **Fig. 3.6B**, both CH and CS showed rapid weight loss, between 270°C to 330°C for CH and 240°C to 270°C for CS, with more than 33% and 25% weight loss, respectively. However, CH-CS PEC did not show such rapid weight loss; instead, a slow weight loss was observed from 220°C to 500°C. As both CH and CS are highly polar due to $-NH_2$ and $-COOH$ groups, they can bind with a high amount of water molecules. The release of this water might be responsible for the rapid weight loss observed with them. In the CH-CS PEC, those $-NH_2$ and $-COOH$ groups were no longer accessible, leading to no rapid weight loss, rather slow thermal degradation of the PEC. A similar observation in the TGA pattern has been made with the chitosan and sodium alginate polyelectrolyte complex [23].
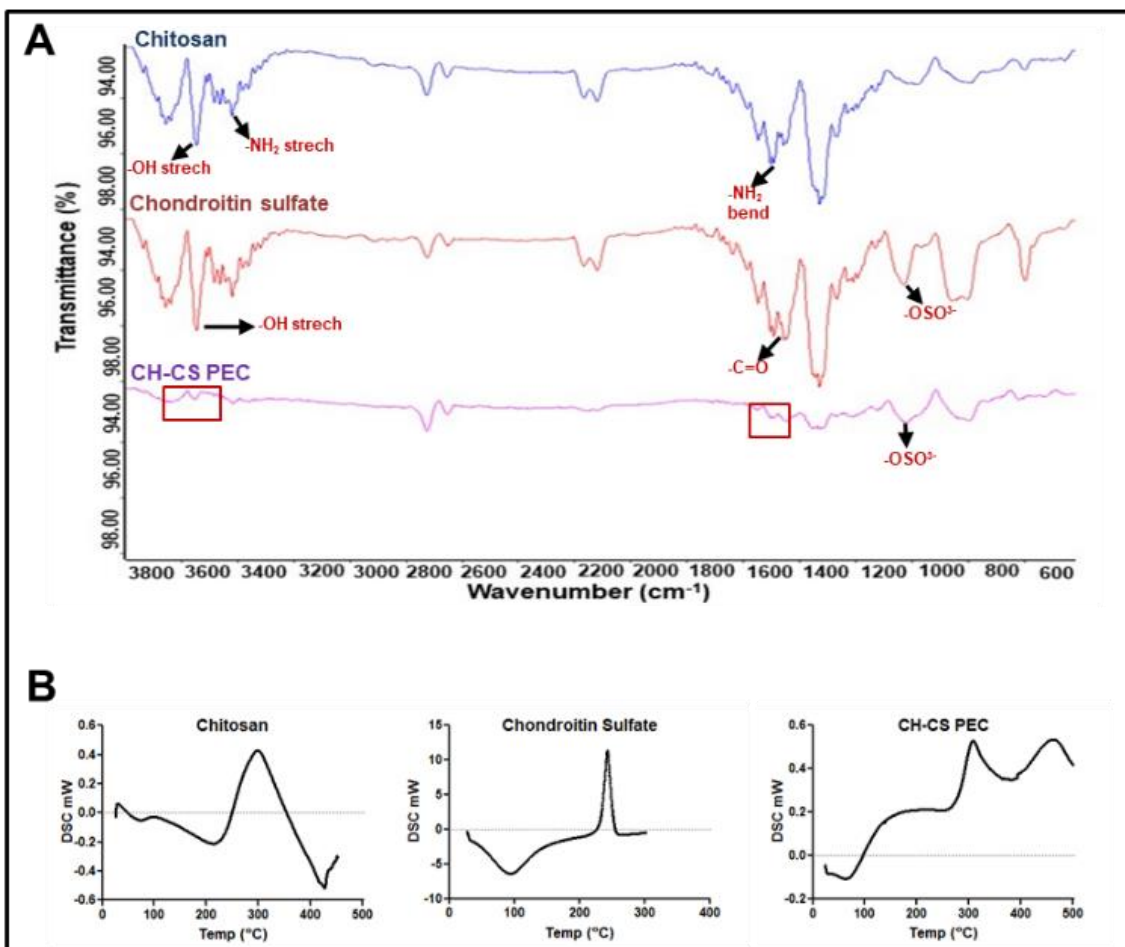
Fig. 3.5 Physicochemical characterization of the CH-CS-PEC. A. FT-IR spectroscopic analysis of CH, CS and CH-CS PEC; B. DSC analysis of CH,CS and CH-CS PEC.

4. X-ray diffraction (XRD) analysis

The X-ray diffraction pattern of CH, CS, and CH-CS PEC was performed to evaluate the change in crystallinity after complexation (**Fig. 3.6A**). The CH showed a characteristic sharp peak at 19.99° [24], indicating the crystallinity of CH, while CS showed a broad peak at 20.19° [25]. All these peaks disappeared in the CH-CS PEC, indicating an amorphous, crosslinked structure formation. CH and CS made a complex with each other during the PEC formation through electrostatic interaction, leading to a loss of the ordered, crystalline structure in the crosslinked scaffold. Similar observations have been made with other PECs as well [26].
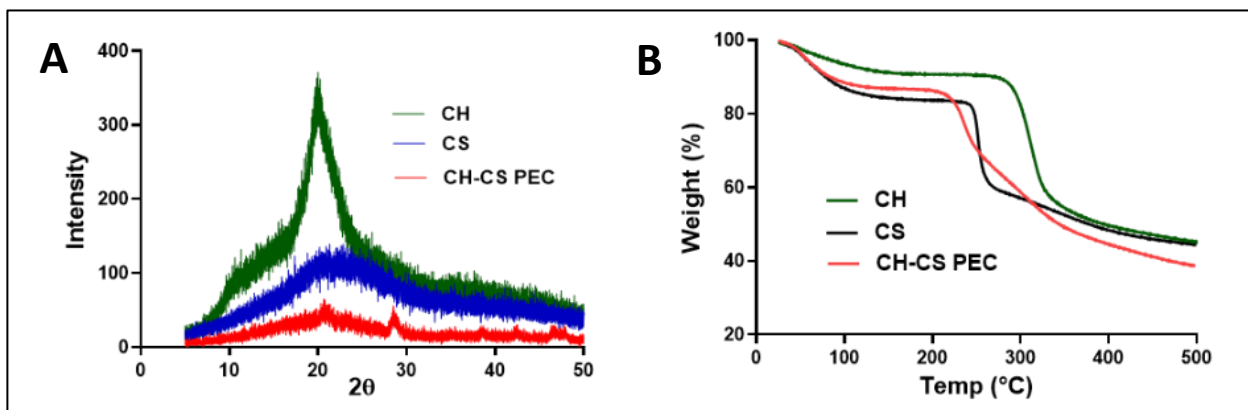
Fig. 3.6 Physicochemical characterization of the CH-CS PEC. A. XRD analysis of CH, CS, and CH-CS PEC. B: TGA analysis of CH, CS, and CH-CS PEC

5. Solid-state CP MAS 13C NMR analysis

Another method for the complexation of PEC formation is by performing its NMR. As the PEC was insoluble in any solvent, solid-state 13C NMR was performed to confirm the CH-CS PEC formation. CH is composed of β-(1,4)-[2-amino-2-deoxy-β-D-glucan], whereas CS is an alternating copolymer of D-glucuronic acid and N-acetyl-D-galactosamine, joined through β-(1,3) linkages. As depicted in **Fig. 3.7,** the CP MAS 13C spectra of CH showed characteristics peaks at 105.899 ppm corresponding to the carbon atom at the C1 position, 85.494 ppm for the carbon atom at C4, 76.236 ppm for C5 and C3 carbon atoms, and at 61.678 and 58.024 ppm, two convoluted peaks are observed, which were attributed to carbon C6 and C2 [27]. Similarly, the CP MAS 13C spectra of CS exhibited peaks at 103.340 ppm corresponding to the C1 carbon atom, convoluted peaks between 77.169 ppm and 74.165 ppm corresponding to C3 and C4 carbon atoms, 69.170 ppm for the C5 carbon atom of the glucuronic acid moiety. The C2 carbon atom peaked at 53.055 ppm, and 24.463 ppm depicts the N-acetyl methyl group's peak. [28]. CH and CS were hypothesized to crosslink by electrostatic interactions between the –NH$_2$ group of CH and the –COOH group of CS to form the CH-CS PEC. The peak corresponding to the C2 carbon atom of CH at 58.024 ppm exhibited a shift in the CH-CS PEC to 57.476, which may be due to the interaction of the –NH$_2$ group attached to the C2 carbon. Similarly, the peak assigned to the C5 carbon atom of the glucuronic acid moiety of CS at 69.170 ppm disappeared in the CH-CS PEC (**Fig. 3.7**). This data confirmed the interaction of the –COOH group of CS with the –NH$_2$ group of CH in the CH-CS PEC.
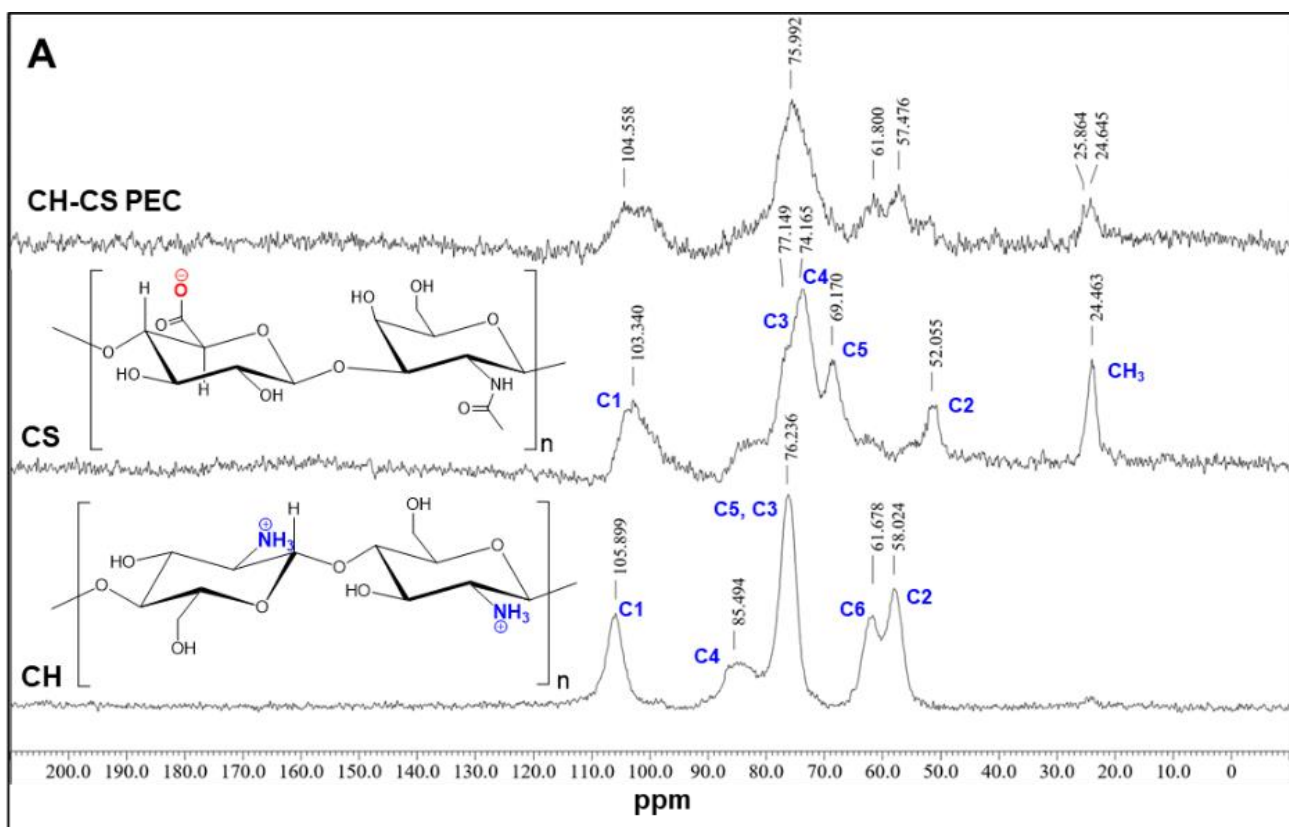
Fig. 3.7 Solid-state CP MAS 13C NMR of CH, CS, and CH-CS PEC.

6. Elemental analysis of CH-CS PEC

After establishing the electrostatic complex formation between CH and CS, we wanted to evaluate the surface properties of this scaffold. FESEM-EDS was performed to analyze the elements present on the surface and to evaluate the material's surface chemistry. As presented in **Fig. 3.8** and **Table 3.5**, the presence of nitrogen (5.55%) in the CH-CS PEC was lower than that of CH (8.91% nitrogen. The change in the elemental composition confirmed the interaction between the CH and CS and the formation of CH-CS PEC. The reduction in the nitrogen charge density of CH-CS PEC depicted the change in the surface chemistry due to the interaction of the poly-cation and poly-anion.

Table 3.5 Elemental analysis of CH and CH-CS PEC

Map Sum Spectrum	Wt% (CH-CS)	Wt% (CH)
C	23.97	40.19
N	5.55	8.91
O	55.45	49.60
Na	5.77	1.15
S	10.26	0.17
Total	100.00	100.00
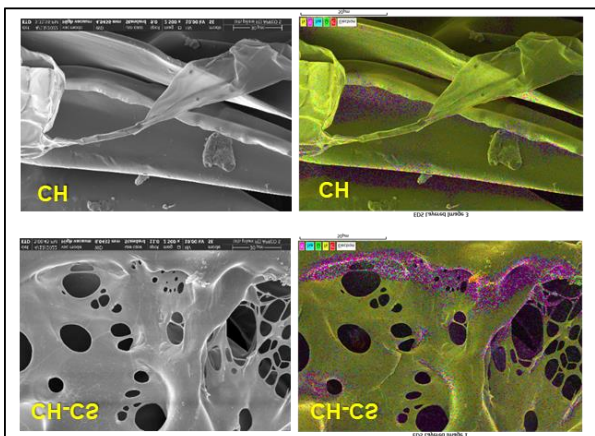
Fig. 3.8 FESEM-EDS scanning of CH and CH-CS PEC for elemental analysis.

7. X-ray Photon electron microscopy

X-ray photon spectroscopy (XPS) was performed to evaluate the surface material chemistry, which was done to analyze the elements present on the surface and to evaluate the material surface chemistry. As presented in **Fig. 3.9**, the presence of nitrogen 1s (5.4 %) and sulfur 2p (1.4 %) in the CH-CS PEC was lower than that of CH (7.0% nitrogen and no sulfur) and CS (6.5% nitrogen 1s and 1.8% sulfur, 2p) alone. The FWHM (*ev*) values for C 1s (3.63), N1s (2.55) O 1s (2.67 for CH and s 2p (2.74), C 1s (3.91) N 1s (2.59) O 1s (3.03) and Na 1s (2.75) for CS. These binding energy significantly changes with CH-CS-PEC compost indicating the surface elemental energy shift and binding phenomenon. The change in the elemental composition confirmed the interaction between the CH and CS and the formation of CH-CS PEC. The reduction in the nitrogen charge density of CH-CS PEC depicted the change in the surface chemistry due to the interaction of the poly-cation and poly-anion and the shift in the binding energy.

Elemental composition of CH, CS and CH-CS PEC

Elements	BE [eV]	Atomic conc. [%]		
		CH-CS PEC	CH	CS
Si 2p	101.2	0.75	0	0
S 2p	168.2	1.48	0	1.86
C 1s	285.2	54.92	63.93	53.56
N 1s	398.2	5.65	7.05	6.51
O 1s	531.2	35.51	29.02	33.85
Na 1s	1070.2	1.68	0	4.22
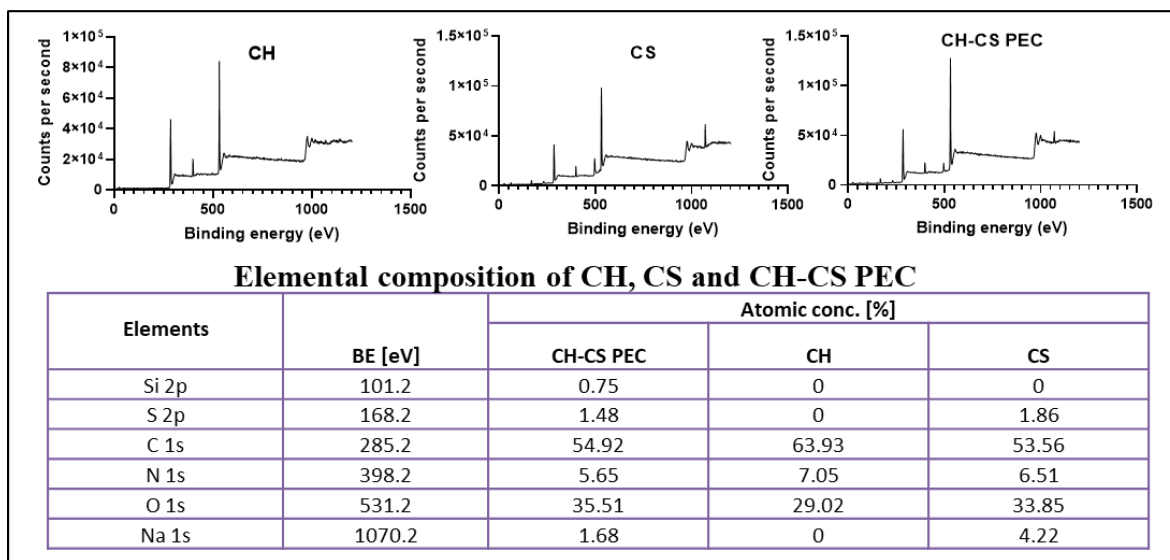
Fig. 3.9 XPS data of CH, CS, and CH-CS PEC. The evaluation of the elemental composition of CH, CS, and CH-CS PEC by XPS spectra

8. Evaluation of the viscoelastic properties of the CH-CS PEC

The electrostatically crosslinked CH-CS PEC should have sufficient viscoelastic properties to be useful as a wound dressing material. The matrix's viscoelasticity determines the primary cellular responses like cell adhesion, cell spreading, and cell proliferation [29]. The viscoelasticity of the CH-CS PEC scaffold was evaluated with respect to the storage modulus (G`) and loss modulus (G``). The storage modulus (G`) describes the elastic response of the solid material and depicts the degree of crosslinking in the scaffold, while the loss modulus (G``) determines the viscous, irreversible response resulting in the deformation [30]. Oscillatory tests, namely amplitude and frequency sweep tests, were performed to analyze CH-CS PEC's viscoelastic behavior. The initial step in studying viscoelasticity is determining the linear viscoelastic region (LVER). LVER is the amplitude below which the scaffold will undergo linear strain with no deformation, which is determined by the amplitude sweep test. An amplitude sweep test was done at an angular frequency of 100 rad/s, with 0.01 to 100 % shear strain. CH exhibited a significantly lower value of G' (~60 Pa, **Fig. 3.10A**), than that of G`` (~90 Pa), indicating the fluidic nature of CH. Low G` of CH has been reported earlier as well [31]. On the other hand, CH-CS PEC exhibited a significantly higher G` (~17000 Pa) compared to G`` (~7800 Pa), which indicated better crosslinking and mechanical strength (**Fig. 3.10B**). The LVER for CH-CS PEC was at 3.5% shear strain. We have also studied the changes in viscoelasticity of CH-CS PEC with a frequency sweep test. As CH exhibited lower

G` than G`` in the amplitude sweep test, indicative of no crosslinking, it was excluded from the frequency sweep test. The study was performed below the LVER region, at a constant shear strain of 1%, with a change in frequency from 0.1-100 rad/s. Here also, a significantly higher G` value was detected compared to the G`` with the CH-CS PEC, indicating considerable structural rigidity of the scaffold (**Fig. 3.10C**). The G` value gradually increased from ~9800 Pa to ~21600 Pa with the increase in angular frequency. The increase in the G` indicated that the electrostatic crosslinking within the polymer matrix acted like fixed network junctions, increasing the ability of the crosslinked scaffold to store the applied energy, leading to elastic-like characteristics. The high elasticity of a matrix has been reported to support cell proliferation and migration [32]. A significant increase in the G` with the CH-CS PEC compared to CH alone implied that a strong ionic crosslinked scaffold was formed with good stability and viscoelasticity when CH was mixed with CS.

Next, we studied the CH-CS PEC's self-healing property by performing the thixotropic study at different levels of strains. The study was conducted at 0.25% strain for 10s and 1000% strain for 10s, and then the recovery was observed at 0.25% strain for 200s by measuring the change in viscosity. The results depicted low initial viscosity with CH (1643 mPa.s at 0s at 0.25% strain) compared to CH-CS PEC (404000 mPa.s at 0s at 0.25% strain) (**Fig. 3.10DandE**). Higher viscosity with the CH-CS PEC indicated a crosslinked structure. While applying 1000% strain for 10s, a highly significant decrease in the viscosity was observed with both CH and CH-CS PEC. In the recovery stage at 0.25% strain, CH exhibited a moderate increase in viscosity (40% of the initial). However, a rapid and significant increase in the viscosity was observed with the CH-CS PEC, with more than 90% recovery to the earlier level. Rapid recovery in the viscosity indicated quick restoration of the crosslinked structure in the CH-CS PEC. The self-healing ability was further confirmed by macroscopic evaluation. In this study, the CH-CS PEC was prepared in two discs. One of the discs was stained with Rhodamine B dye, and the other was kept colorless. Then both the CH-CS PEC disc was kept in close contact. After 3 min, both the disks formed deep interconnection within themselves, depicting the CH-CS PEC's efficient self-healing and adhesive potential (**Fig. 3.10F**). As the scaffold was formed due to ionic interactions, if disrupted, it can quickly regenerate due to rapid ionic bond formation, unlike covalent bonds. This self-healing property has also been observed with other polyelectrolyte complexes [26]. Disruption of the

scaffold structure's integrity due to body movements can reduce the efficacy of the scaffold. Developing a self-healing scaffold that can automatically repair the damage without external intervention can be highly beneficial [33, 34].
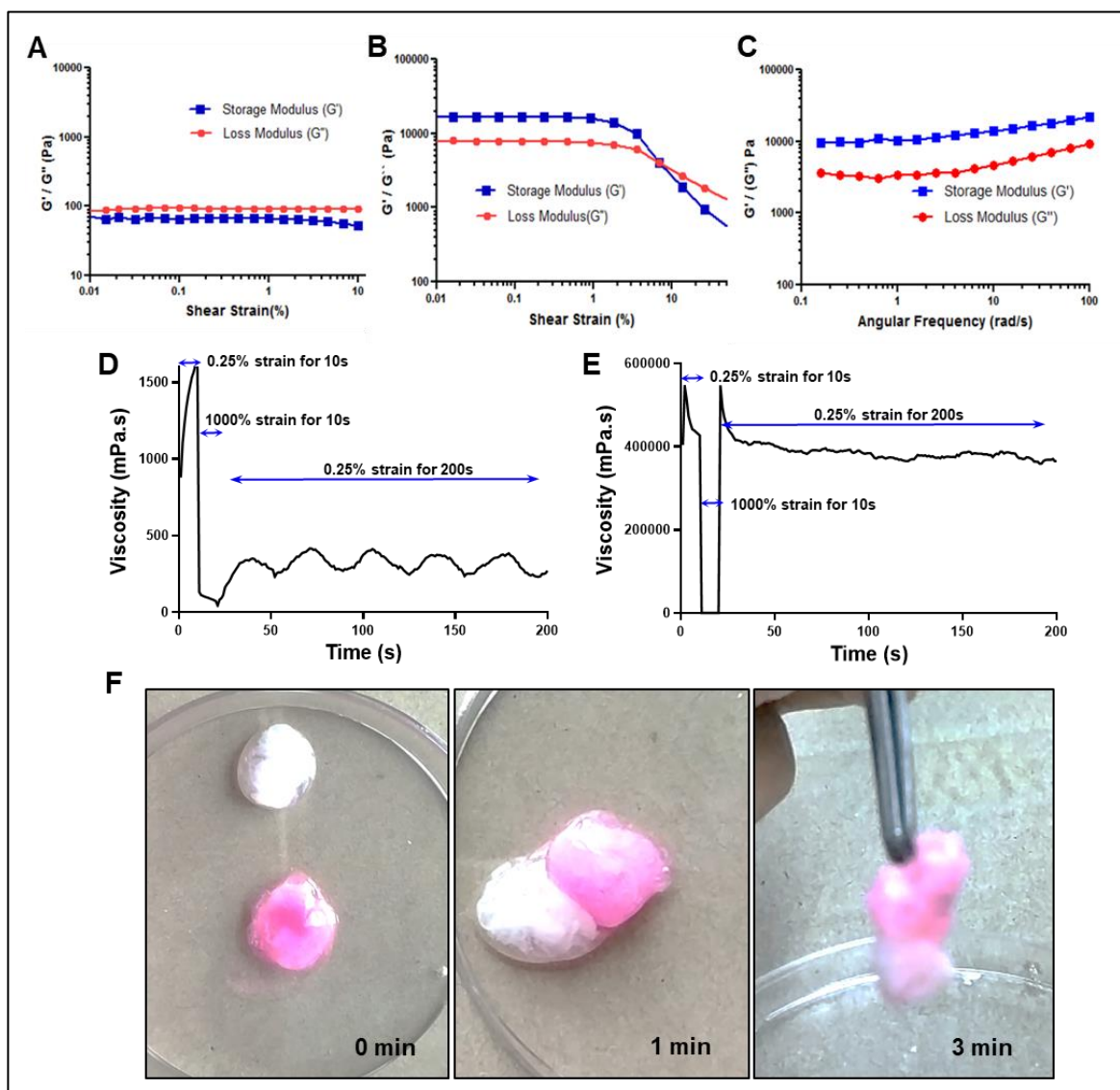
Fig. 3.10 Rheological characterization of the CH gel and CH-CS PEC. A: Amplitude sweep test for CH and B: CH-CS PEC. The graph depicts the change in storage modulus (G') and loss modulus (G") with a change in the shear strain at an angular frequency of 100rad/s. C: Frequency sweep test for CH-CS PEC depicting the change in G' and G" with a change in angular frequency from 0.1- 100 rad/s within the LVER region. D: Thixotropic analysis of CH and E: CH-CS PEC. The graph depicts the change in the viscosity at different % strain. F: Macroscopic evaluation of the self-healing property of CH-CS PEC.

3.3.4 Blood-cell interaction study of CH-CS PEC

1. *In vitro* hemolysis study

Biocompatibility is one of the most important properties of a wound-healing scaffold. As they directly come in contact with the blood, hematological stability indicates their biocompatibility. It is regarded that lower hemolysis is an indicator of better blood compatibility [35]. According to the American Society for Testing and Materials (ASTM), any material would be called non-hemolytic if it causes below 2% hemolysis [36]. We tested different concentrations of prepared CH-CS-PEC ranging from 2mg/mL to 0.008mg/mL. Maximum hemolysis was observed with 2mg/mL CH-CS-PEC at 1.26±0.45% (**Fig. 3.11A-B**). So the prepared CH-CS-PEC scaffold was considered a non-hemolytic material.

2. Whole blood clotting and cell adhesion

Another essential criterion for a good wound dressing material is its hemostatic ability. It is particularly important for the treatment of open wounds which are bleeding. Induction of thrombosis can arrest the bleeding and stop blood loss. We evaluated the hemostatic potential of the CH-CS-PEC and compared it with CH scaffold based on its blood clotting index (BCI). A smaller value of BCI indicates a stronger hemostatic potential of the material. CH-CS-PEC demonstrated significantly higher hemostatic ability (**35.46% BCI**) compared to CH scaffold (**83.64% BCI**) (**Fig. 3.11C**). The higher hemostatic ability of the CH-CS-PEC compared to CH scaffold may be due to the higher porosity and swelling of the CH-CS-PEC compared to CH. A blood cell adhesion study was performed using scanning electron microscopy. The samples were treated the same way as those treated for the blood clotting studies. Both CH-CS PEC and CH scaffold treated with blood were fixed with 4% formaldehyde solution for 15 minutes and dried at 37°C. The SEM images of the CH and CH-CS PEC blood pretreated scaffold showed that CH-CS PEC showed better blood cell adhesion (**Fig. 3.10E**) compared to the scaffold prepared with CH alone (**Fig. 3.11F**).
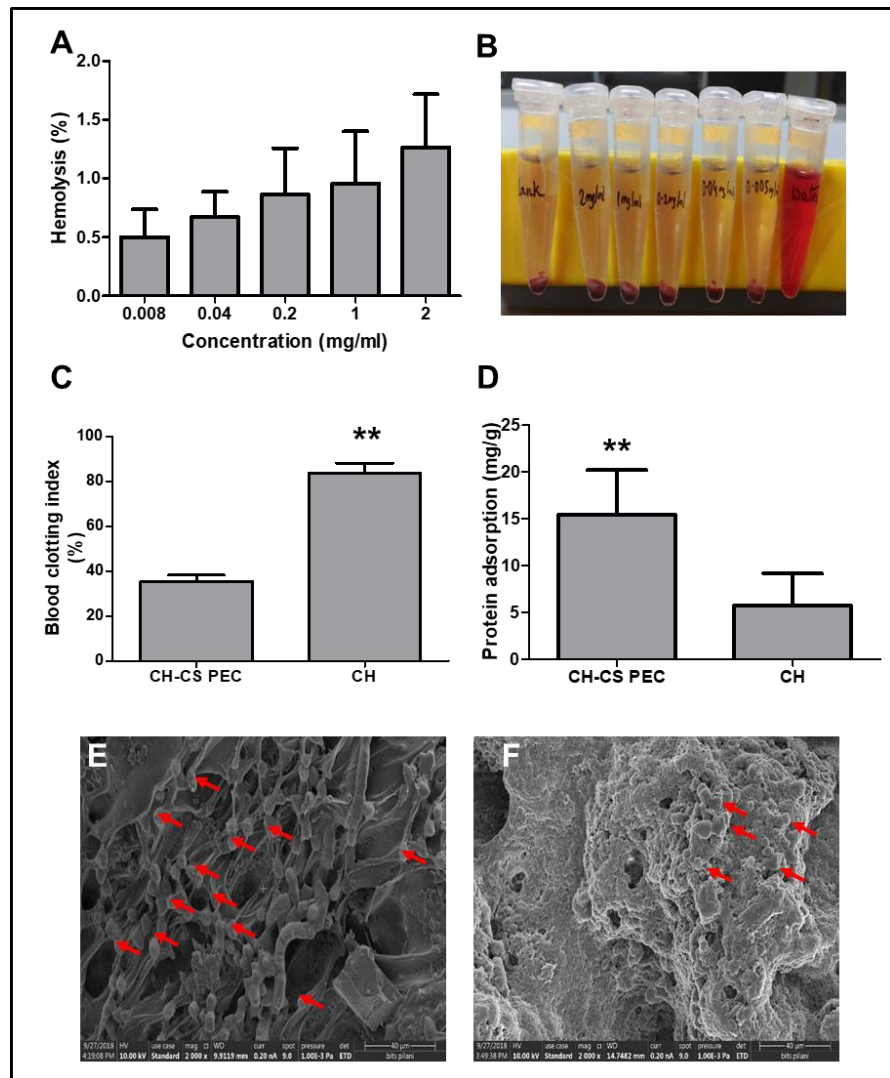
Fig.3.11 Determination of hemocompatibility and hemostatic ability of CH-CS PEC. A. Hemolysis study. B. Pictorial representation of the hemolysis. C. Comparison of blood clotting index and D. protein adsorption on CH-CS PEC with that of CH scaffold. E. SEM image of blood cell adhesion on CH-CS PEC and F. that on the CH scaffold. Cells were indicated with arrow. ** represents a significant difference ($p < 0.05$) as compared to other groups.

3. Protein adsorption studies

After demonstrating high hemostatic activity with the CH-CS-PEC, we wanted to find the underlying cause for this. It is generally accepted that the first step of thrombosis formation is the protein adsorption on the surface of the scaffold. Better hydration and increased water absorption improve the protein adsorption capacity of any scaffold. The aqueous layer is then replaced with

the adsorbing protein molecules, forming a new 3D interphase. In this way, as the water absorption capacity of the scaffold increases, protein adsorption improves [37]. In agreement with the % swelling data, a significantly higher amount of BSA was found to be adsorbed on the CH-CS PEC (15.4 mg/gm) than that of CH scaffold (5.7 mg/gm) (**Fig. 3.11D**), as the water uptake capacity of the CH-CS PEC is higher and may lead to better thrombogenic property. The protein adsorption studies showed that the CH-CS PEC exhibited an almost 3-fold increase in protein adsorption potential than that of the scaffold prepared with CH alone.

3.4 Conclusion

In the current chapter, we have demonstrated the screening of different polymers for the formation of PEC, which can form the scaffold *in-situ*. The selected polymers, high molecular weight CH and CS solution can spontaneously mix to form a PEC. This property can be highly beneficial for developing an *in-situ* scaffold for wound healing purposes. We have established that the physicochemical properties of the PEC are greatly influenced by the molecular weight of CH and moderately affected by the concentration of both CH and CS. Higher molecular weight CH has exhibited better porosity and swelling. The optimum concentration for both CH and CS was found to be 5% w/v in terms of porosity and swelling characteristics. The CH-CS PEC was found to be hemocompatible with less than 2% hemolysis at the highest concentration studied (2 mg/mL). It also exhibited significantly higher blood clotting ability and protein absorption capacity than CH scaffold. These data indicate that the CH-CS PEC has a high potential to be developed into an ideal wound dressing material. Overall, the CH-CS PEC's detailed characterization and biochemical estimation make it an ideal candidate for a wound dressing.

References

1. Sood, A., A. Gupta, and G. Agrawal, *Recent advances in polysaccharides based biomaterials for drug delivery and tissue engineering applications.* Carbohydrate Polymer Technologies and Applications, 2021. **2**: p. 100067.

2. Sahana, T.G. and P.D. Rekha, *Biopolymers: Applications in wound healing and skin tissue engineering.* Molecular Biology Reports, 2018. **45**(6): p. 2857-2867.

3. Tsao, C.T., et al., *Evaluation of chitosan/γ-poly(glutamic acid) polyelectrolyte complex for wound dressing materials.* Carbohydrate Polymers, 2011. **84**(2): p. 812-819.

4. Wang, J., et al., *Antimicrobial hydroxyapatite reinforced-polyelectrolyte complex nanofibers with long-term controlled release activity for potential wound dressing application.* Colloids and Surfaces A: Physicochemical and Engineering Aspects, 2021. **624**: p. 126722.

5. Meka, V.S., et al., *A comprehensive review on polyelectrolyte complexes.* Drug Discov Today, 2017. **22**(11): p. 1697-1706.

6. Vasile, C., et al., *Chitosan/hyaluronic acid polyelectrolyte complex hydrogels in the management of burn wounds.* Rev Med Chir Soc Med Nat Iasi, 2013. **117**(2): p. 565-71.

7. Puppi, D., et al., *Microstructured chitosan/poly(γ-glutamic acid) polyelectrolyte complex hydrogels by computer-aided wet-spinning for biomedical three-dimensional scaffolds.* Journal of Bioactive and Compatible Polymers, 2016. **31**(5): p. 531-549.

8. Qin, X., et al., *An Extracellular Matrix-Mimicking Hydrogel for Full Thickness Wound Healing in Diabetic Mice.* Macromol Biosci, 2018. **18**(7): p. e1800047.

9. Rahmani Del Bakhshayesh, A., et al., *Recent advances on biomedical applications of scaffolds in wound healing and dermal tissue engineering.* Artif Cells Nanomed Biotechnol, 2018. **46**(4): p. 691-705.

10. Zhu, C., et al., *Novel enzymatic crosslinked hydrogels that mimic extracellular matrix for skin wound healing.* Journal of Materials Science, 2018. **53**(8): p. 5909-5928.

11. Daristotle, J.L., et al., *Sprayable and biodegradable, intrinsically adhesive wound dressing with antimicrobial properties.* Bioeng Transl Med, 2020. **5**(1): p. e10149.

12. Singh, R., K. Shitiz, and A. Singh, *Chitin and chitosan: biopolymers for wound management.* Int Wound J, 2017. **14**(6): p. 1276-1289.

13. Prasathkumar, M. and S. Sadhasivam, *Chitosan/Hyaluronic acid/Alginate and an assorted polymers loaded with honey, plant, and marine compounds for progressive wound healing-Know-how.* Int J Biol Macromol, 2021. **186**: p. 656-685.

14. Hussain, Z., et al., *Recent Advances in Polymer-based Wound Dressings for the Treatment of Diabetic Foot Ulcer: An Overview of State-of-the-art.* Curr Drug Targets, 2018. **19**(5): p. 527-550.

15. Alven, S. and S. Peter, *Polymer-Based Wound Dressing Materials Loaded with Bioactive Agents: Potential Materials for the Treatment of Diabetic Wounds.* 2022. **14**(4).

16. Suarato, G., R. Bertorelli, and A. Athanassiou, *Borrowing From Nature: Biopolymers and Biocomposites as Smart Wound Care Materials.* Frontiers in Bioengineering and Biotechnology, 2018. **6**.

17. Im, A.R., et al., *Wound healing and antibacterial activities of chondroitin sulfate- and acharan sulfate-reduced silver nanoparticles.* Nanotechnology, 2013. **24**(39): p. 395102.

18. Fujimura, N., et al., *Evaluation of valence band top and electron affinity of SiO_2 and Si-based semiconductors using X-ray photoelectron spectroscopy.* Japanese Journal of Applied Physics, 2016. **55**(8S2): p. 08PC06.

19. Ong, S.Y., et al., *Development of a chitosan-based wound dressing with improved hemostatic and antimicrobial properties.* Biomaterials, 2008. **29**(32): p. 4323-32.

20. Golafshan, N., et al., *Nanohybrid hydrogels of laponite: PVA-Alginate as a potential wound healing material.* Carbohydr Polym, 2017. **176**: p. 392-401.

21. Lankalapalli, S. and V.R. Kolapalli, *Polyelectrolyte Complexes: A Review of their Applicability in Drug Delivery Technology.* Indian J Pharm Sci, 2009. **71**(5): p. 481-7.

22. Zhang, W., Q. Zhao, and J. Yuan, *Porous Polyelectrolytes: The Interplay of Charge and Pores for New Functionalities.* Angew Chem Int Ed Engl, 2018. **57**(23): p. 6754-6773.

23. Kulig, D., et al., *Study on Alginate(-)Chitosan Complex Formed with Different Polymers Ratio.* Polymers (Basel), 2016. **8**(5).

24. Eddya, M., B. Tbib, and K. El-Hami, *A comparison of chitosan properties after extraction from shrimp shells by diluted and concentrated acids.* Heliyon, 2020. **6**(2): p. e03486.

25. Ebube, N.K., W. Mark, and H. Hahm, *Preformulation studies and characterization of proposed chondroprotective agents: glucosamine HCl and chondroitin sulfate.* Pharm Dev Technol, 2002. **7**(4): p. 457-69.

26. Barroso, N., et al., *Self-healable hyaluronic acid/chitosan polyelectrolyte complex hydrogels and multilayers.* European Polymer Journal, 2019. **120**.

27. Heux, L., et al., *Solid state NMR for determination of degree of acetylation of chitin and chitosan.* Biomacromolecules, 2000. **1**(4): p. 746-751.

28. Winter, W.T., et al., *Solid-state 13C NMR and X-ray diffraction of dermatan sulfate.* Biochem Biophys Res Commun, 1986. **137**(1): p. 87-93.

29. Hosseini, M.S. and A.A. Katbab, *Effects of surface viscoelasticity on cellular responses of endothelial cells.* Rep Biochem Mol Biol, 2014. **3**(1): p. 20-8.

30. Guimarães, C.F., et al., *The stiffness of living tissues and its implications for tissue engineering.* Nature Reviews Materials, 2020. **5**(5): p. 351-370.

31. Heidenreich, A.C., et al., *Collagen and chitosan blends for 3D bioprinting: A rheological and printability approach.* Polymer Testing, 2020. **82**: p. 106297.

32. Chan, B.P. and K.W. Leong, *Scaffolding in tissue engineering: general approaches and tissue-specific considerations.* Eur Spine J, 2008. **17 Suppl 4**: p. 467-79.

33.   Zhang, A., et al., *Research status of self-healing hydrogel for wound management: A review.* Int J Biol Macromol, 2020. **164**: p. 2108-2123.

34.   Yang, B., et al., *Injectable Adhesive Self-Healing Multicross-Linked Double-Network Hydrogel Facilitates Full-Thickness Skin Wound Healing.* ACS Appl Mater Interfaces, 2020. **12**(52): p. 57782-57797.

35.   Panico, A., F. Paladini, and M. Pollini, *Development of regenerative and flexible fibroin-based wound dressings.* J Biomed Mater Res B Appl Biomater, 2018.

36.   Archana, D., et al., *Chitosan-PVP-nano silver oxide wound dressing: in vitro and in vivo evaluation.* Int J Biol Macromol, 2015. **73**: p. 49-57.

37.   Vogler, E.A., *Protein adsorption in three dimensions.* Biomaterials, 2012. **33**(5): p. 1201-37.

Chapter 4

In-vitro and *in-vivo* evaluation of cell proliferation
and cell function in skin fibroblasts and keratinocytes

4.1 Background

The previous chapter highlighted the physicochemical characteristics such as viscoelasticity, self-healing capability, and CH-CS PEC's porosity demonstrating the relatable biophysical properties compared to the normal skin's ECM. Further, the in-situ fabrication of the CH-CS PEC provides direct cell-substrate contact supporting cell adhesion and migration. Fibroblasts, keratinocytes, and macrophages are key players in the healing process. Fibroblasts and keratinocytes participate in the proliferation and re-epithelialization stage [1]. These cells respond to the inflammation signals followed by proliferation and tissue repair. Fibroblasts migrate and proliferate at the wound site, and they are responsible for synthesizing and remodeling the extra-cellular matrix proteins. [2]. These cell types communicate with the surrounding cells via paracrine signaling and activate keratinocytes which migrate to the wound bed for wound closure.

In the present study, we have evaluated the cell proliferation, migration, and bio-functions of keratinocyte and fibroblast cells seeded on this scaffold. Finally, the efficacy of this *in-situ* forming scaffold was studied in the *in-vivo* skin excision wound model in rats.

4.2 Materials and methods

High molecular weight chitosan (MW≈700kDa, DD: more than 90%) was purchased from Sisco Research Laboratories (SRL) Pvt. Ltd. (India). Chondroitin sulfate monosodium salt (MW 475.39 Da) was procured from Tokyo Chemical Industry Co. Ltd. HaCaT Cell line, and primary human dermal fibroblasts were obtained as a gift from IGIB, New Delhi. Dulbecco modified Eagle medium, 10% fetal bovine serum was obtained from HiMedia Laboratories Ltd., India. α-smooth muscle actin antibody, β1-integrin antibody, proliferating cell nuclear antigen (PCNA) antibody, β-actin antibody, and DAB substrate were procured from Cell Signaling Technology (USA). All the primers were procured from Imperial Life sciences, India. SYBR green qPCR kit and cDNA synthesis kit were procured from Bio-Rad. All other chemical reagents used were of A.R. grade.

4.2.1 Fabrication of CH-CS PEC

CH-CS PEC was fabricated using the process reported in our previous work [3]. Briefly, 5% w/v of CH solution was prepared in 1% v/v of glacial acetic acid and further dialyzed to remove the glacial acetic acid, until the pH of the solution became ~7.5% w/v chondroitin sulfate was prepared in Milli-Q water. CH solution was sterilized by autoclaving, and CS solution was

filtered through a 0.22 µm membrane. CH-CS PEC was prepared by mixing CH and CS solution in a 1:1 v/v ratio using a custom-made double-barreled syringe

4.2.2 Cell morphometric analysis

Cell morphology was observed by microscopic examination of keratinocyte (HaCaT) and fibroblast (HDF) cells. Briefly, cells (0.4×10^6 cells/6 well plate) were seeded on the CH scaffold and CH-CS PEC (**Fig. 4.1**). For CS treatment, the cells were seeded and directly treated with the CS solution. The cells were incubated for 48h and were observed under a phase-contrast microscope. Further, the cell morphology was confirmed by FESEM imaging.

Preformed scaffold(CH/CH-CS PEC)   Cells   Cells seeded on the scaffold
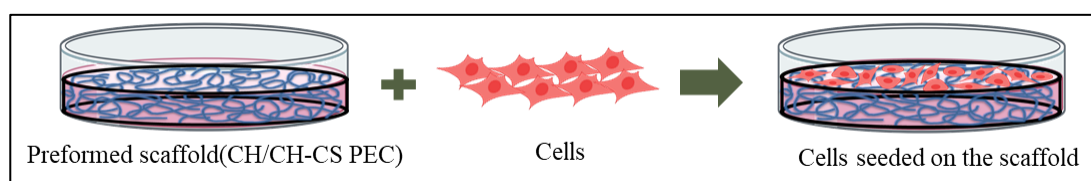
Fig.4.1 Schematic representation of the in-vitro experiment protocol

4.2.3. *In-vitro* cell proliferation and migration assay

In-vitro cell proliferation and migration studies were conducted with both HaCaT and HDFs cells. The cells (0.4×10^6 cells/6 well plate) were seeded on the scaffold-coated coverslips for the cell proliferation study. After incubation for a specific time, cells were fixed with 100% methanol, mounted with DAPI stain, and observed using a fluorescent microscope (Zeiss). All the samples were observed at $10\times$ magnification. For the cell migration assay, the cells were seeded on the scaffold coated (CH-CS PEC, CH, and CS) culture vessel supported with µ-dish culture insert (ibidi insert, Martinsried, Germany) (**Fig. 4.2**). Cells grown on plain culture vessels (TPP-Techno Plastic Products AG., Trasadingen, Switzerland) were used as control. When the cells became confluent, culture inserts were slowly removed without disturbing the edge to mimic the wound. Cells were photographed at various time-lapse periods (0, 8, 16, and 24 h). All the samples were observed at $20\times$ magnification. The rate of cell migration (mm) in various groups was calculated by using Image J software (NIH, Washington, --USA). Live cell migration was recorded by a time-lapse video device (Cyto smart-II, Lonza, Inc., Morristown, NJ, USA).
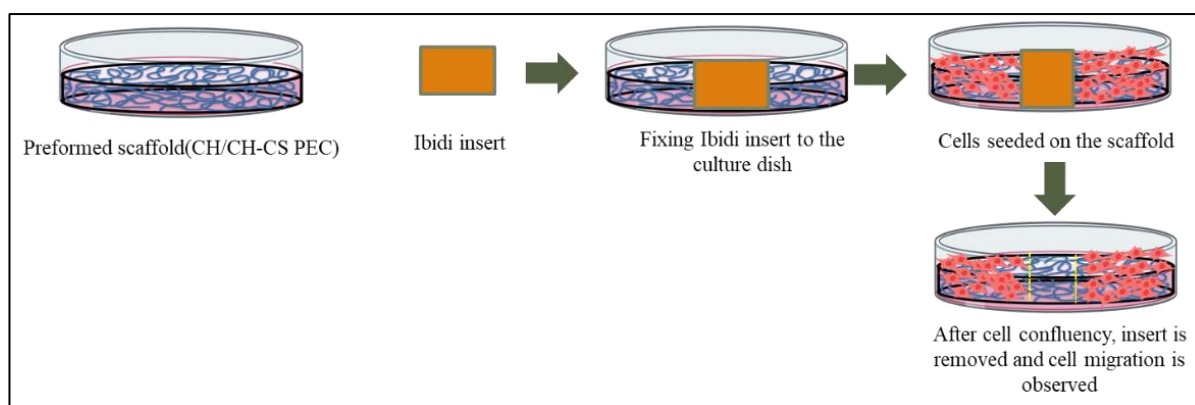
Fig. 4.2 Schematic representation for the cell migration study protocol

4.2.4 qPCR analysis

All the qPCR studies were performed on CFX Thermocycler (Bio-Rad). Cells (0.4×10^6 cells/6 well plate) were grown on different scaffolds, as described previously. Total RNA was isolated using TRI reagent and was used to synthesize cDNA using a cDNA synthesis kit (Bio-Rad). The transcript levels of the gene of interest were measured by quantitative PCR (qPCR). The qPCR reactions were performed using the SYBR Green chemistry. The data were normalized against GAPDH as a housekeeping gene. The primers used for qPCR are mentioned in **Table 4.1**.

Table 4.1 Primer sequence used in the study.

Gene	Forward (5'-3')	Reverse (5'-3')
GAPDH	ACCCAGAAGACTGTGGATGG	TCTAGACGGCAGGTCAGGTC
Col-I	TCTGCGACAACGGCAAGGTG	GACGCCGGTGGTTTCTTGGT
COL-III	TGAAAGGACACACAGAGGCTTCG	GCACCATTCTTACCAGGCTC
α-SMA	TGGCTATTCCTTCGTTACTACTGCT	CATCAGGCAACTCGTAACTCTTCTC
Involucrin	TCCTCCTCCAGTCAATACCC	GCTGATCCCTTTGTGTT
PCNA	TCACAGGGCAGTGTCTTCATT	GGGTGACTGTAGCTGGGAAT
β1-integrin	ACTCTCAGCACAGCATAAATAAAG	GGGAGAACCTTTCACCCCAT
HGF	GCTCGTGAGGATACTGAGAATC	CTGAGCTCGCCAGTGAAATG

4.2.5 Immunoblotting analysis

Both the HaCaT and HDF cells were grown on different scaffolds, as described previously. The cells were then lysed using RIPA buffer (Sigma- Aldrich), and total protein was measured. The protein was denatured in 5X loading buffer by heating (100° C for 10 min) and cooling on ice. Equal concentrations of the total protein were resolved using denaturing polyacrylamide

gels (5% stacking and 10% resolving). The resolved protein was then transferred to a PVDF membrane (Millipore). It was then blocked with a blocking buffer (Nacalai, Tesque, Tokyo, Japan). The blots were probed with antibodies against PCNA (Cell signaling Technologies, USA) and loading control beta-actin (Cell signaling Technologies, USA). The secondary antibodies used were horseradish peroxide-conjugated goat anti-rabbit IgG (Cell Signaling Technologies, USA). The protein intensity was detected using the LAS 4000 digital imaging system (Fujifilm, Tokyo, Japan). The band intensities were quantified using Image Quant TL software (GE Health care, Chicago, Illinois, USA).

4.2.6 *In-vivo* wound healing study

All animal experiments were conducted following the regulation of the Animal Ethics Committee, BITS-Pilani (Protocol number: IAEC/RES/25/3). The *in-vivo* wound healing study was performed in the Wistar rats with a full-thickness excisional wound of 2×2 cm^2 area. Four groups were included in the study: i) control (untreated), ii) lyophilized CH-CS PEC (as a preformed scaffold), iii) *in-situ* CH-CS PEC, and iv) a market-available CH-based preformed scaffold. *In-situ* CH-CS PEC treatment was given through a custom-made double-barreled syringe, with CH solution in one chamber and CS solution in the other chamber. For application, both the pistons of the double-barreled syringe were compressed simultaneously, leading to the ejection of both solutions at the same rate using a custom-made double-barreled syringe. The solutions were mixed in the wound bed itself, leading to the formation of the *in-situ* scaffold. The wound healing was analyzed by taking images of treated wounds every second day.

4.2.7 Histology and collagen staining

Representative animals from each group were sacrificed on day 7 and day 14. Their skin from the wound area was fixed, paraffin-embedded, sectioned, and stained with H&E dye. H&E staining was used to determine cellular and tissue morphology.

For collagen staining, the method described by Coelho et al. was used [4]. Briefly, skin sections were dewaxed and rehydrated. They were then incubated for 1h in 0.5% Direct red 80 (Sigma Aldrich) dye prepared in a saturated picric acid solution. After 1h, the sections were washed with acidified water (0.5% v/v of glacial acetic acid) to remove the excess stain. The samples were washed with Milli-Q water thrice and dehydrated. The stained sections were examined under brightfield microscopy. The images were taken at $4 \times$ and $20 \times$ magnification.

4.2.8 Immunohistochemistry

Immunohistochemical analysis of β1-integrin and α-SMA was performed in the skin sections. The sections were dewaxed and rehydrated. Antigen unmasking was performed by heating the sections in the citrate buffer (pH 6.0) in a water bath at 80°C for 15 min. Further, the samples were incubated with 3% hydrogen peroxide to quench endogenous peroxidase for 10 minutes. For IHC staining, the samples were washed and blocked with 5% w/v of bovine serum albumin in Tris Buffered Saline with Tween 20 for 2h. Further, the sections were incubated with anti-rat β1-integrin and anti-rat α-SMA antibody (1:500 dilutions, CST) at 4°C overnight. The sections were washed and incubated with HRP conjugated secondary antibody (1:1000 dilution, CST) for 2h at room temperature. The color was developed using the DAB substrate (CST). The image quantification was done using the method reported by Crowe et al., using the image J color deconvolution method [5]. The healthy skin's area fraction was considered the standard (100%) for the % estimation.

4.2.9 Statistical analysis

The data were analyzed using GraphPad Prism software version 8. Comparison among data sets was statistically determined using one-way or two-way ANOVA; post hoc Tukey's test was performed to compare each group's means with every other group. Data were represented as mean $\pm$ SD.

4.3 Results and discussion

4.3.1 Fabrication of the *in-situ* forming CH-CS PEC

In a previous study, we established that mixing CH and CS at a 1:1 v/v ratio would lead to a cross-linked scaffold formation due to electrostatic interaction between the positively charged CH and negatively charged CS [3]. We have used a high molecular weight CH (MW≈700kDa) and low molecular weight CS (disaccharide form; MW 475 Da). Due to low MW, the CS solution's viscosity is less, allowing it to spontaneously mix with the viscous CH solution, making electrostatic cross-links, and leading to instant scaffold formation. We have used a custom-made double-barreled syringe to prepare the scaffold. The in-situ CH-CS PEC further showed enhanced viscoelasticity and high porosity, making it suitable for fibroblasts and keratinocyte migration.

4.3.2 Cellular morphometric analysis

After establishing the CH-CS PEC's enhanced viscoelastic properties, we studied the ability of this scaffold to support cellular function in terms of morphology and adhesion. HaCaT and HDF cells seeded on the glass coverslips (control), CS, and CH-CS PEC were found to have normal morphology (**Fig. 4.3A** and **B**). In contrast, HaCaT and HDF cells seeded on the CH film were found to have lower cellular spreading, with many cells having abnormal spherical morphology (**Fig. 4.3 A** and **B**). A similar observation has also been reported with CH film [6]. The results were further confirmed by FESEM images. As the non-cytotoxic nature of CH film has been reported extensively [7-9], the morphological abnormality may be due to the low viscoelastic properties of the CH film, which can influence cell morphology [10, 11]. The SEM images of the fibroblasts grown on CH and CH-CS PEC supported the brightfield images (**Fig. 4.3C** and **D**).
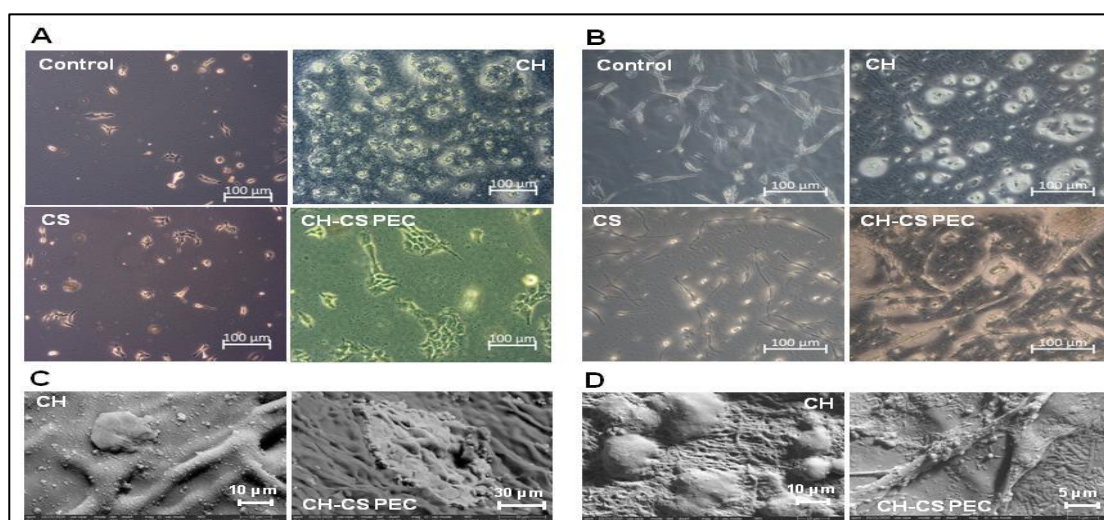
Fig. 4.3 Phase-contrast and FESEM microscopic evaluation of the A& C: HaCaT and B&D: HDF cells grown on different polymeric scaffolds for 48h

4.3.3 Cell proliferation and migration studies

Enhanced proliferation and migration of the dermal and epidermal cells is one of the primary criteria for successful wound healing. It has previously been demonstrated that viscoelastic scaffolds can provide mechanical support to the cells, augmenting their proliferation rate [11, 12]. Cell proliferation and wound healing assay were performed to evaluate the effect of the CH-CS PEC scaffold on the proliferation and migration of both HaCaT and HDF cells, and cell proliferation and wound healing assay were done. In both the cell types, significantly increased proliferation was observed with the CH-CS PEC than with the CH, CS, and control cells (**Fig. 4.5A** and **B**). In the wound healing assay, significantly improved migration was

observed in both HaCaT and HDF cells when grown on the CH-CS PEC, as depicted in **Fig. 4.4A** and **B.** Cells grown on CH and CS exhibited similar migration to control cells grown on a petri dish. The migration rate was found to be better in HDF than in the HaCaT cells.
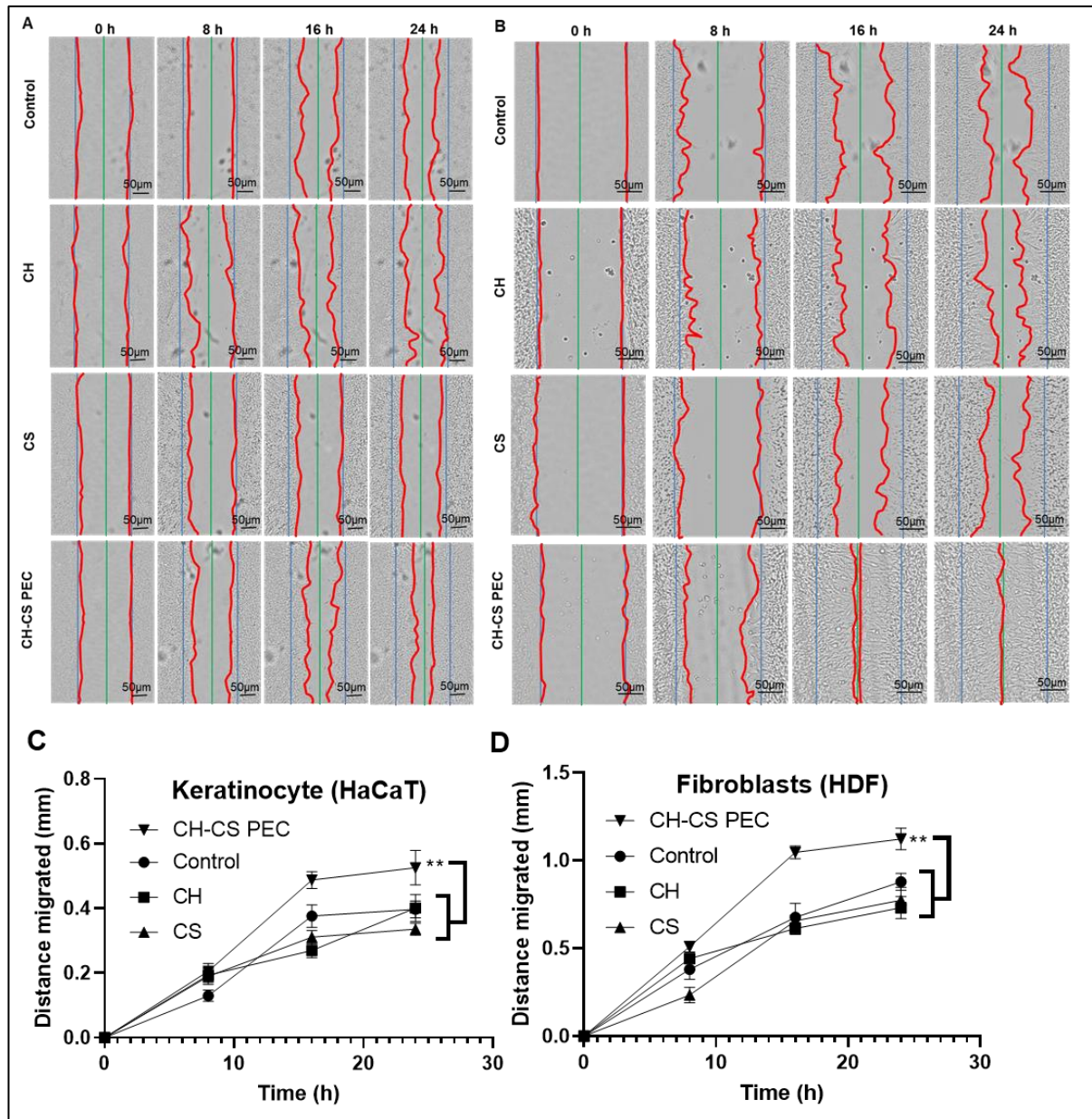
Fig. 4.4 *In-vitro* wound healing assay with HaCaT (A) and HDF (B) cells. Time-lapse microscopic images of the cells after incubating them for specific time points (0, 8, 16, and 24 h) with different polymeric scaffolds. Cells grown on the petri plate were used as the control. Blue line: starting point of cell migration. Green line: middle point of cell migration. Red line: migratory cell edge. Photographs were taken in bright field microscope with a magnification of 20×. C&D. Quantification of cell migration. A and B: Analysis of the distance migrated by both HaCaT and HDF cells grown on different polymeric scaffolds. Statistical analysis was done using 2-way ANOVA with Tukey multiple comparison test. ** denotes p-value < 0.05.
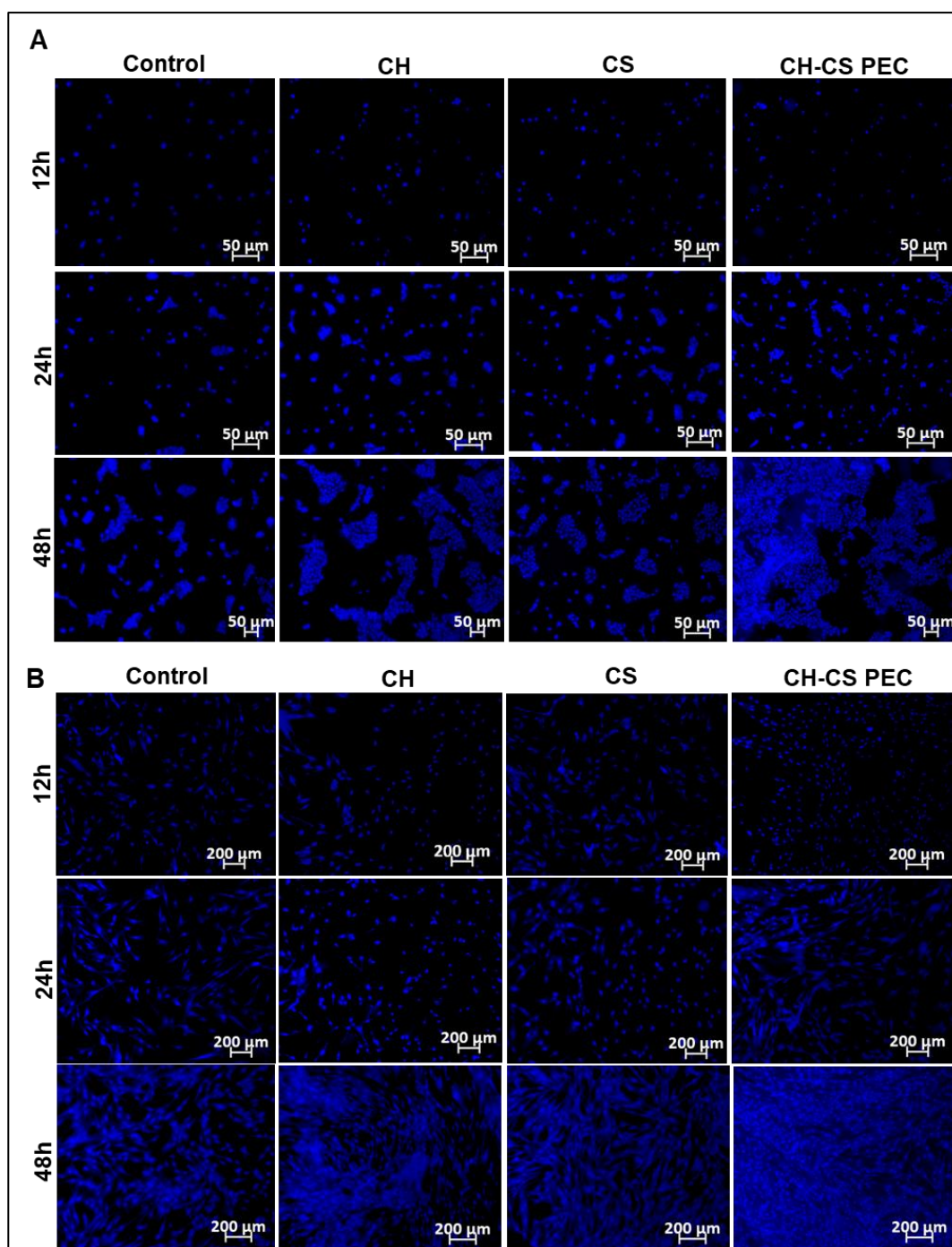
Fig.4.5 Cell proliferation study of keratinocytes and fibroblasts. A) Fluorescent microscopic image of the HaCaT cells after incubating them for specific time points with different polymeric scaffolds. Scale bar, 50μm. B) Fluorescent microscopic image of the HDF cells after specific time points. Scale bar, 200μm.

The quantitative analysis of the migratory potential of these cells is depicted in **Fig. 4.4C and D**. In both the cell types, a significant increase in migration was observed with the CH-CS PEC than other treatments. The average distance migrated by the HaCaT cells was found to be 0.53 ± 0.05 mm when grown on the CH-CS PEC, compared to 0.40 ± 0.04 mm with CH, 0.34 ± 0.02 mm with CS, and 0.40 ± 0.03 mm in the control cells after 24 h (**Fig. 4.4C**). Similarly, in

the case of HDF, after 24 h, the average migration was 1.12 ± 0.06 mm with the CH-CS PEC, compared to 0.73 ± 0.06 mm with CH, 0.77 ± 0.07 mm with CS, and 0.88 ± 0.05 mm in the control cells (**Fig.4.4D**). This data suggests that the CH-CS PEC can support and stimulate the growth of the dermal fibroblasts and epidermal keratinocytes.

4.3.4 Evaluation of the expression of proliferation markers by keratinocytes and fibroblasts

After observing enhanced cell migration with the CH-CS PEC, we evaluated the expression of proliferating cell nuclear antigen (PCNA) as a proliferation marker in both HaCaT and HDF cells by both real-time qPCRs as well as western blot analysis. The relative change in the mRNA expression was determined by the Livak-Schmittgen method [2(-Delta Delta C(T))] [13]. Fold-change in the expression was calculated by normalizing against untreated cells (cells grown on regular Petri plates) and using GAPDH as the housekeeping gene. In the HaCaT cells, the CH-CS PEC group showed a 5.6-fold increased expression of PCNA, compared to 2.5-fold in CH and 1.5-fold in CS (**Fig. 4.6A**). In the HDF cells, a 4.5-fold increase in PCNA expression was observed with the CH-CS PEC-grown cells, compared to both CH (0.8-fold) and CS (0.7-fold) (**Fig. 4.6B**).
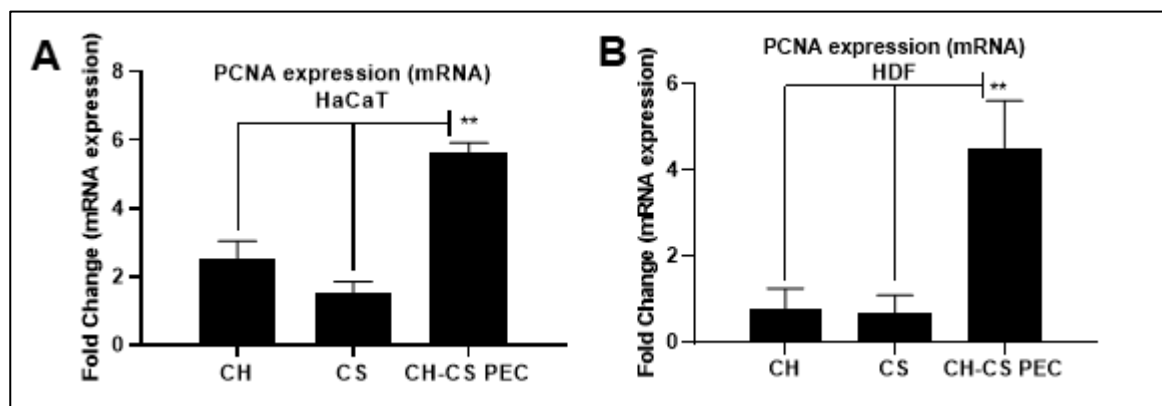
Fig. 4.6 Evaluation of the expression of PCNA as a cell proliferation marker in **A** and **B**: HaCaT and HDF cells by qRT-PCR. Statistical analysis was done using 2-way ANOVA with Tukey multiple comparison test. ** denotes p-value < 0.05.

The western blot of PCNA protein expression analysis also corroborates the qPCR data. A significantly increased PCNA expression was observed with both HaCaT and HDF cells grown on the CH-CS PEC compared to cells grown on a regular Petri plate, as well as with CH and CS treatment (**Fig. 4.7A-D**). PCNA expression increased 1.4 and 1.7-fold in the HaCaT and HDF cells, respectively, when grown on the CH-CS PEC compared to the control. The increased expression of PCNA in the cells grown on the CH-CS PEC substantiates the microscopic observation of higher proliferation in the similarly treated cells.
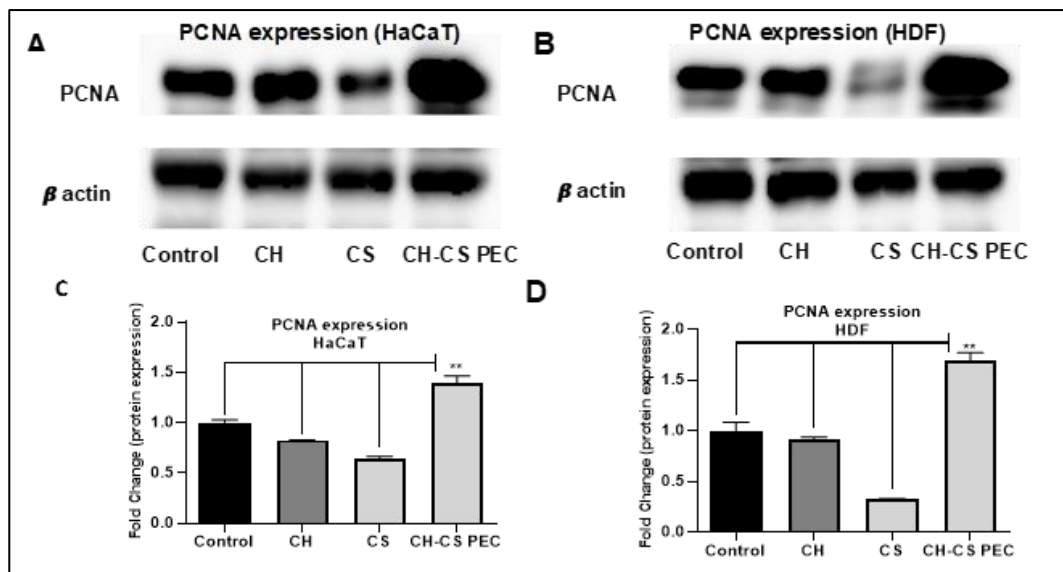
Fig. 4.7 A and B: Western blot analysis of PCNA expression in the HaCaT and HDF cells. C and D: Densitometric analysis of the PCNA western blot. Statistical analysis was done using 2-way ANOVA with Tukey multiple comparison test. ** denotes *p*-value < 0.05

4.3.5 Evaluation of the expression of functional markers by keratinocytes and fibroblasts

Next, we studied the functional efficacy of another vital skin cell, fibroblasts, by analyzing the expression of collagen-I, collagen-III, and α-SMA as functional markers. Fibroblasts are the principal skin cells that generate the dermal tissue's extra-cellular matrix (ECM). Collagen proteins, produced by fibroblasts, are the most crucial structural and functional component of the ECM, which is responsible for the skin's mechanical strength [14]. There are 28 types of collagen [15], which are divided into two groups, fibrillar collagens (type I, III, and V), and fibril-associated collagens (types XII, XIV, XVI, and VI). The fibrillar collagens have higher tensile strength [16]. Amongst the fibrillar collagens, type I (Col-I) and type III (Col-III) are the most predominant in the skin. Col-III helps in forming a provisional ECM structure at the early stage of wound healing [17]. Expression of Col-III also supports wound contraction [17]. Volk et al. have demonstrated increased scar tissue formation in Col-III deficient mice [18]. On the other hand, Col-I is mechanically stronger than Col-III and responsible for maintaining skin structure and tissue integrity [17]. Both collagens play a vital role in the wound-healing process. In our study, increased expression of both Col-I and Col-III was observed with the CH-CS PEC (Col-I: 3.8-fold, Col-III: 2.9-fold), compared to CH (Col-I: 0.4-fold, Col-III: 0.1-fold) and CS (Col-I: 1.8-fold, Col-III: 0.2-fold) (**Fig. 4.8A**). Interestingly, the Col-I to Col-III ratio was calculated to be 4:1 and 9:1 with CH and CS, respectively, while in the case of CH-CS PEC, it was 1.3:1. Though the mechanism is not clearly understood yet, the 1:1 ratio of Col-I to Col-III has been associated with scarless wound healing [17]. It has been shown that in the fetal skin, Col-I to Col-III ratio varies from 2.3:1 to 0.7:1, compared to 9:1 to 4:1 in the

adult [19, 20]. The higher amount of Col-III expression by the wounded fetal skin may influence scarless wound healing seen in the fetus [20]. In the adult skin, scar tissue was found to have a Col-I to III ratio of 6:1 to 17:1 [21]. As with the CH-CS PEC treatment, the Col-I/III ratio was found to be almost 1:1, similar to that of the fetal skin, scarless wound healing could be possible with the CH-CS PEC.
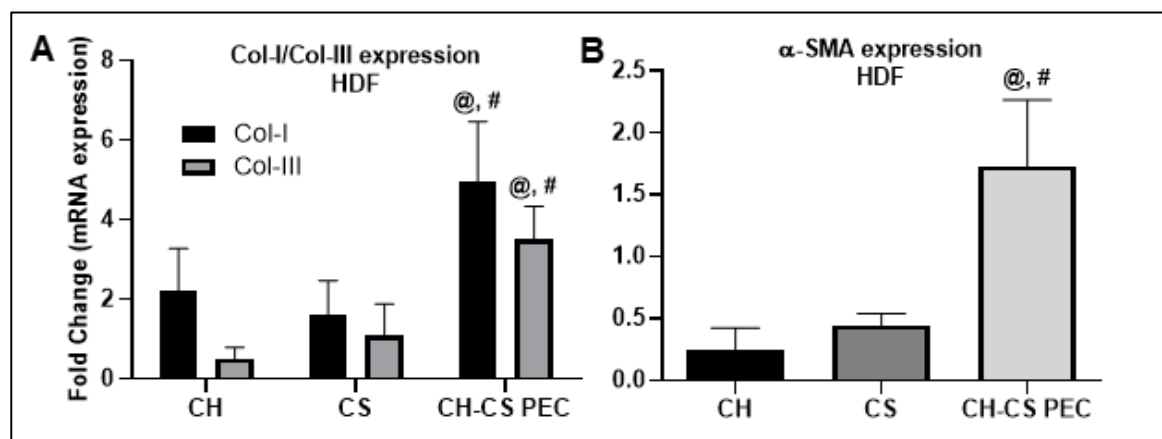
Fig. 4.8 The qRT-PCR analysis of the expression of functional markers in the HDF cells treated with different polymeric scaffolds for 48h. The following markers were analyzed in the HDF cells: A: Col-I and Col-III, and B: α-SMA. Statistical analysis was done using 1-way ANOVA with Tukey multiple comparison test. @ denotes p-value < 0.05 compared to CH, # denotes p-value < 0.05 compared to CS, $ denotes p-value < 0.05 compared to CH-CS PEC.

Apart from Col-I and III, we have also analyzed the expression of α-SMA in fibroblasts. α-SMA expression is associated with the structural and mechanical properties of the matrix [22, 23] and is responsible for generating contractile force in the skin [24]. α-SMA is a marker of myofibroblasts, which are differentiated fibroblasts with smooth muscle-like features and play a significant role in wound healing [25]. We found a 1.7-fold increase in α-SMA expression with the CH-CS PEC treatment, whereas, with CH and CS, it was 0.2 and 0.4-fold, respectively (**Fig. 4.8B**). These data suggest that the fibroblasts grown on the CH-CS PEC were functionally more active, which can benefit the wound healing process.
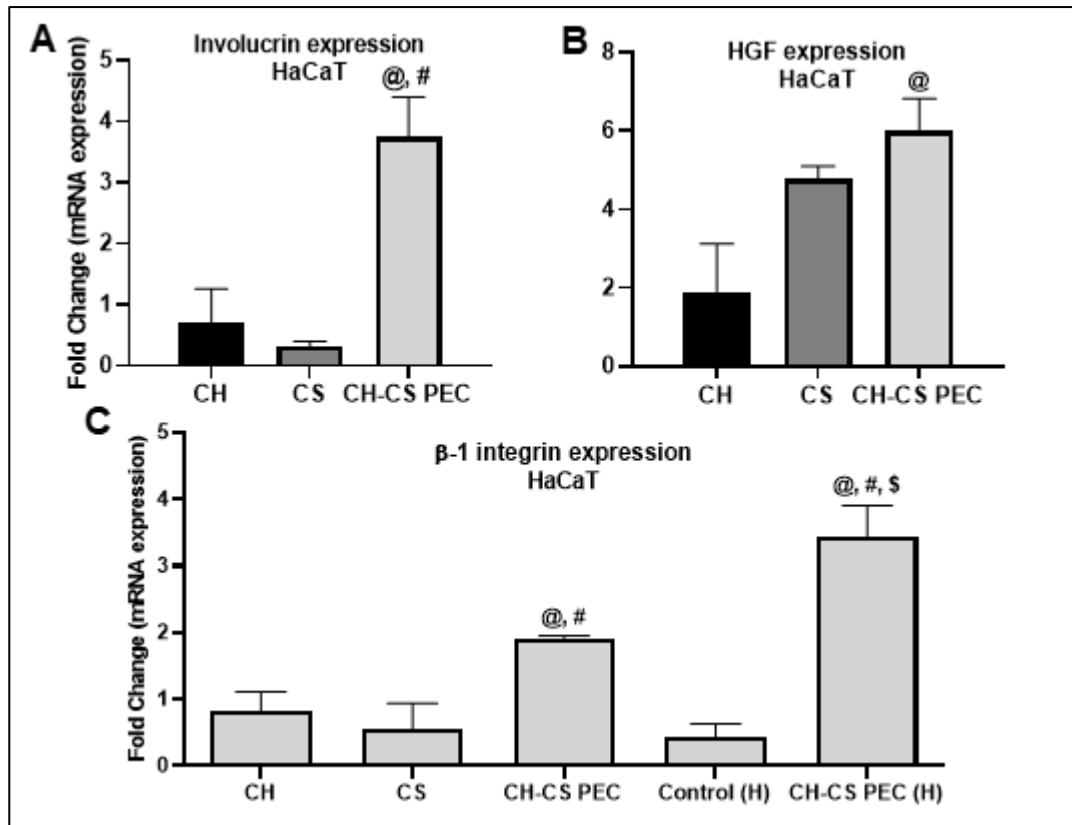
Fig. 4.9 The qRT-PCR analysis of the expression of functional markers in the HaCaT cells treated with different polymeric scaffolds for 48h. In the HaCaT cells, the following markers were analyzed: A: involucrin, B: HGF, and C: β1-integrin. β1-integrin expression was compared with the CH-CS PEC-grown cells treated with HDF-conditioned media [CH-CS PEC(H)]. Control(H) denotes HaCaT cells grown on a Petri plate treated with HDF-conditioned media. Statistical analysis was done using 1-way ANOVA with Tukey multiple comparison test. @ denotes p-value < 0.05 compared to CH, # denotes p-value < 0.05 compared to CS, \$ denotes p-value < 0.05 compared to CH-CS PEC.

Next, we studied the functional potential of these cells grown on the CH-CS PEC scaffold. Functionally active keratinocytes at the wound healing site get differentiated to express involucrin, a precursor of the epidermal cornified envelope [26]. This differentiation is crucial for making the external barrier. Previous studies have shown that growing keratinocytes on polymeric scaffolds can augment involucrin expression [27, 28], which is dependent on the structural and mechanical properties of the scaffold [6]. In the current study, we observed only a basal level of involucrin expression with CH and CS treatment (less than a 1-fold increase) at 48h.

On the contrary, with CH-CS PEC, a 3.7-fold increase in involucrin expression was observed (**Fig. 4.9A**). Similar observations with CH film have also been reported earlier [6]. Apart from involucrin, we have also analyzed the expression of HGF. HGF expression accelerates wound healing, reduces fibrosis [29], and promotes granulation tissue and angiogenesis [30]. With the CH-CS PEC treatment, a 6-fold increase in the expression of HGF was observed, compared to

a 1.9-fold and 4.7-fold increase with CH and CS, respectively (**Fig. 4.9B**). These data indicated that the keratinocyte cells were functionally more active when grown on the CH-CS PEC.

We have also analyzed the scaffold-seeded HaCaT cells' response treated with HDF-conditioned media to evaluate the cellular crosstalk between keratinocytes and fibroblasts [1, 31]. It has been demonstrated that the expression of β1-integrin by the keratinocytes is augmented by factors secreted by the fibroblasts [32]. Cells grown on CH or CS expressed very low levels of β1-integrin (0.8 and 0.6-fold, respectively). In contrast, a 1.9-fold increase in the β1-integrin expression was observed with HaCaT cells grown on CH-CS PEC without conditioned media treatment, indicating the interaction with the viscoelastic CH-CS PEC may enhance expression (**Fig. 4.9C**). Importantly, with HDF-conditioned media treatment, HaCaT cells grown on CH-CS PEC exhibited a 3.5-fold increase in the expression of β1-integrin (**Fig. 4.9C**). In contrast, HaCaT cells grown in standard culture plate treated with HDF conditioned media showed only a basal level of β1-integrin expression (0.4-fold), suggesting the role of the CH-CS PEC scaffold for its expression, consistent with previous reports that a matrix structure is important for the expression of integrins [33, 34].

4.3.9 *In-vivo* wound healing activity

After demonstrating enhanced cell proliferation and functional efficacy of both keratinocytes and fibroblasts treated with the CH-CS PEC, we evaluated the *in-vivo* wound healing activity of the *in-situ* forming scaffold and compared it with the lyophilized CH-CS PEC, as well as a market available chitosan-based scaffold. The study was performed in the Wistar rats with a full-thickness excisional wound of 2×2 cm^2 area. The animals were divided into four groups, untreated, lyophilized CH-CS PEC, *in-situ* CH-CS PEC, and a market-available CH-based preformed scaffold. *In-situ* CH-CS PEC treatment was given using a custom-made double-barreled syringe, with CH solution in one chamber and CS solution in the other. For application, both the pistons of the double-barreled syringe were compressed simultaneously, leading to the ejection of both solutions at the same rate. The solutions were mixed in the wound bed itself, leading to the formation of the *in-situ* scaffold. The wound healing was analyzed by taking images of treated wounds every second day.
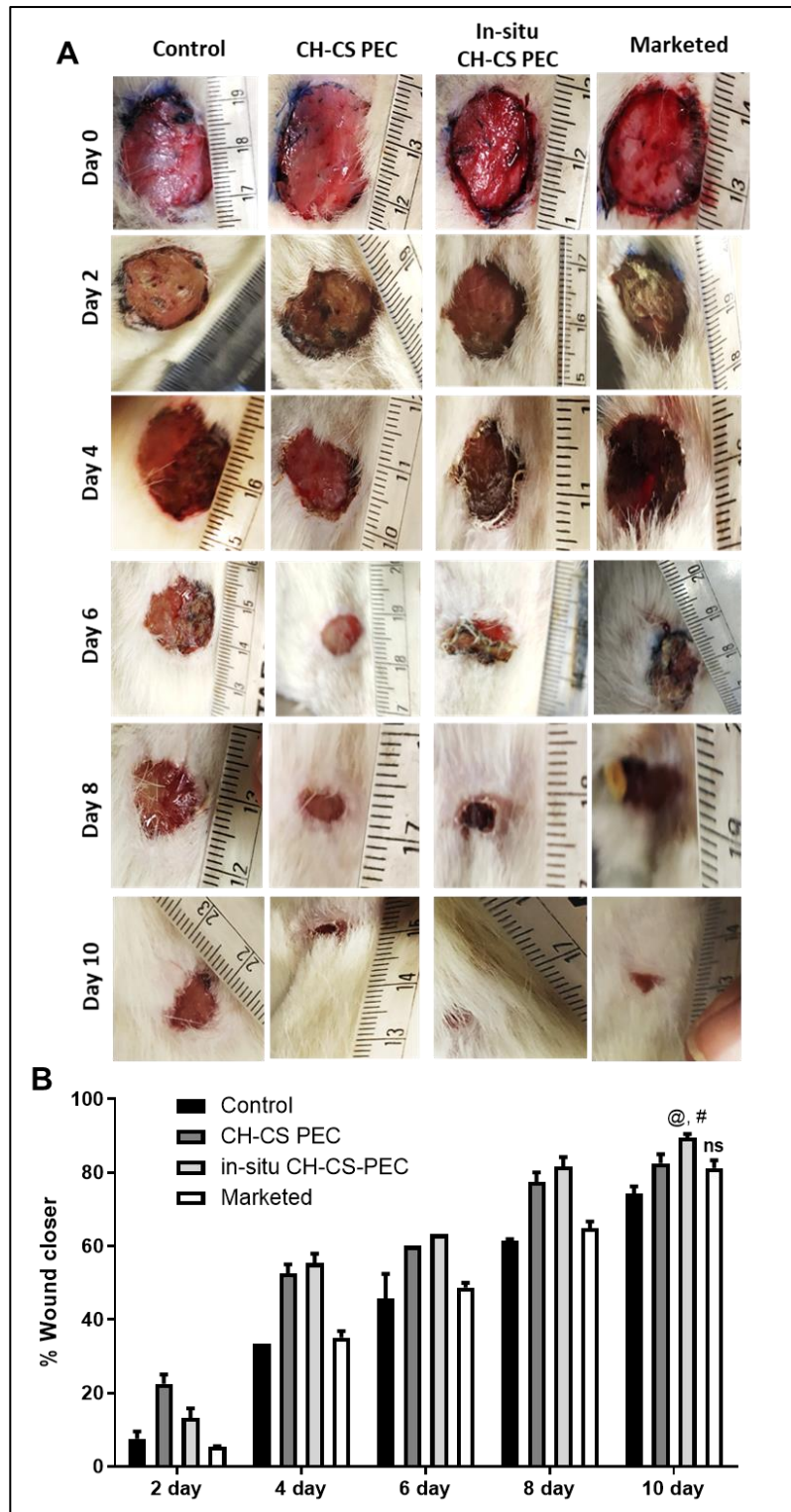
Fig. 4.10 A: *In-vivo* wound healing efficacy in rat excisional wound model. B: % Wound closer rate with different treatments. Statistical analysis was done using 2-way ANOVA with Tukey multiple comparison test. @ denotes *p* value < 0.05 compared to control, # denotes *p* value < 0.05 compared to marketed. ns: not significant compared to control.

Compared to all others, significantly faster wound closure was observed with the *in-situ* CH-CS PEC group (**Fig. 4.10A** and **B**). At day 10, the mean % wound closer was calculated to be

89.5±0.26% with the *in-situ* CH-CS PEC, compared to 82.5±2.5%, 81.1±2.19%, and 74.2±1.98% with the lyophilized CH-CS PEC, marketed, and untreated control, respectively (**Fig. 4.10B**). Compared between the *in-situ* CH-CS PEC and the market-available chitosan-based scaffold, the former exhibited significantly increased wound closure at the final time point, indicating that *in-situ* scaffold formation may improve wound healing activity. The market-available chitosan-based scaffold used in this study is prepared by the electrospinning technique. As there is no cross-linking, it has no significant mechanical properties (data not shown), probably due to which its wound healing activity was only marginally better than the untreated control. Moreover, CH-CS PEC had both CH and CS present in it. CH and CS have been reported to have significant wound-healing activity. CH helps in myofibroblast differentiation, enhances collagen synthesis, and increases fibroblast proliferation [35, 36], whereas CS can induce cell proliferation, improve cell adhesion, and stimulate cell migration [37, 38]. The enhanced wound closure rate of *in-situ* CH-CS PEC could be due to CH and CS properties and the physicochemical properties of the CH-CS PEC *in-situ*, including enhanced support to the basement cells in the wound bed.

4.3.10 Histology studies

After confirming efficient wound closure with the CH-CS PEC, histological evaluation of the wounds was performed 7-days and 14-days post-treatment in the four groups (**Fig. 4.11**). On the 7th-day post-treatment, a considerable amount of granulation tissue was observed in all the groups except the control, suggesting initiation of healing in the three groups. The control group exhibited the presence of granulation tissue as late as day 14, while the other three groups showed the presence of neo-epidermis formation and a healed dermal layer on the 14th day. Significantly improved re-epithelization was observed in the animals treated with the PEC scaffold and *in-situ* CH-CS PEC group compared to the market-available chitosan-based scaffold-treated group (broken epidermis marked with an arrow) (**Fig. 4.11**). Dermal appendages were observed in all three treated groups, with most appendages seen in the *in-situ* CH-CS PEC group (marked with a star) (**Fig. 4.11**).
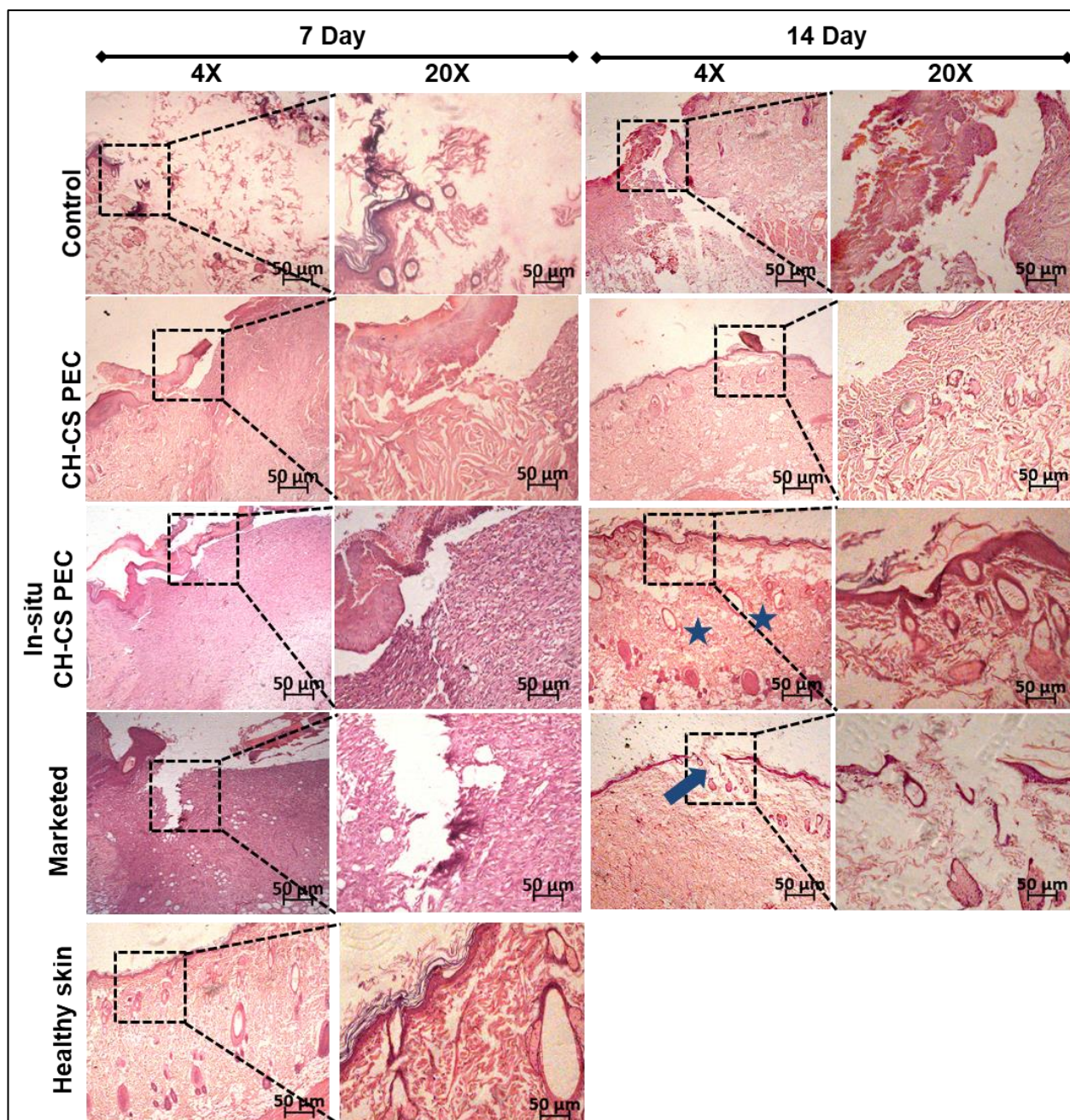
Fig. 4.11 Histopathological evaluation of the skin at 4X and 20X magnification, at 7th day and 14th day after the treatment. Scale bar 50 μm

4.3.10 Collagen staining

We examined the total collagen concentration by performing the picrosirius staining in the animal skin collected on day 14 post-treatment. The control (untreated) group detected a low amount of collagen, indicating reduced ECM formation (**Fig. 4.12**). A moderate increase in collagen content was found with the CH-CS PEC treatment, whereas patchy collagen staining was observed with the marketed CH scaffold (**Fig. 4.12**). In contrast, treatment with the *in-situ* CH-CS PEC showed a uniform distribution of collagen in both epidermal and dermal layers, signifying enhanced ECM formation (**Fig.4.12**). We have previously noted enhanced collagen

synthesis by the CH-CS PEC-seeded HDF cells (**Fig. 4.8A**). Detection of a high amount of collagen in the skin of the *in-situ* CH-CS PEC-treated animals corroborated that observation. Collagen is one of the most essential components of the extra-cellular matrix, which provides mechanical support to the tissue and aids cell adhesion and tissue repair [39]. The high total collagen content in the group treated with the *in-situ* CH-CS PEC suggested faster ECM remodeling, which could aid the faster re-epithelization and be the reason for faster wound closure observed with the *in-situ* CH-CS PEC.
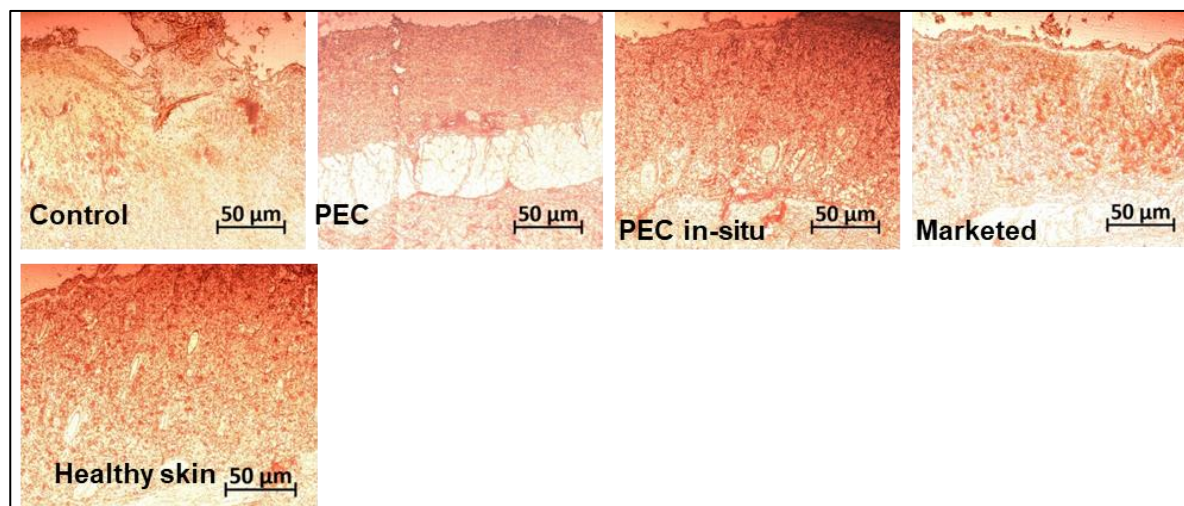
Fig. 4.12 Brightfield microscopic images of total collagen staining of the skin samples at 14th day post-treatment by picrosirius red staining. Scale bar 50 μm.

3.3.11 IHC analysis

After analyzing the efficient wound closure, and confirming the enhanced collagen content in the *in-situ* CH-CS PEC treated group, we wanted to analyze the molecular markers of wound healing in the treated animals. We evaluated the expression of α-smooth muscle actin (α-SMA) and β1-integrin in all the treated groups by immunohistochemical analysis. As depicted in **Fig. 4.13**, the expression of α-SMA was minimal in the control group (32±2% of the healthy skin). No significant difference was found in the α-SMA level in the lyophilized CH-CS PEC (47±2%) as well as marketed product (42±4%) treatment groups compared to the control (**Fig. 4.13**). The level of α-SMA in the *in-situ* CH-CS PEC group was 75±9% of the healthy skin, significantly higher than the control (**Fig. 4.13**). The *in-vitro* study also found enhanced expression of α-SMA by the CH-CS PEC-seeded HDF cells (**Fig. 4.8B**). Expression of α-SMA indicates wound contraction and faster granulation tissue formation, leading to faster cell proliferation and re-epithelialization [40].
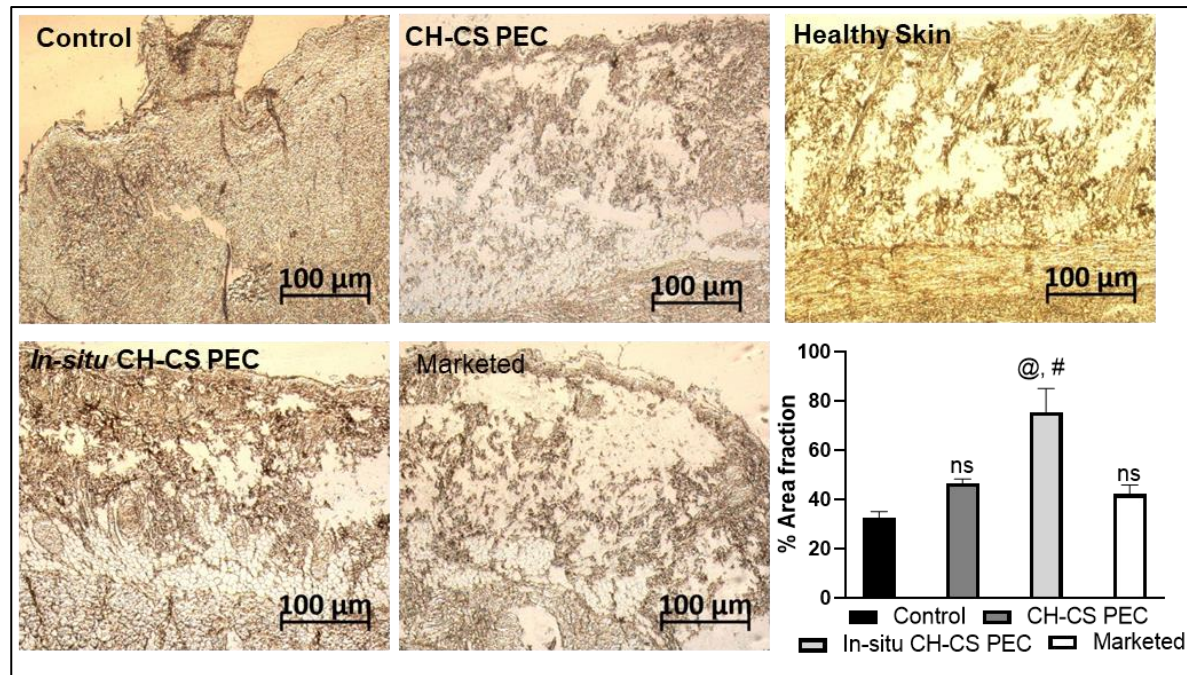
Fig. 4.13 Immunohistochemical staining of α-SMA in the skin tissue sections collected 14th-day post-treatment. The expression of the markers was compared with the skin section of the healthy skin. Scale bar 100 μm. Statistical analysis was done using 1-way ANOVA with Tukey multiple comparison test. @ denotes p-value < 0.05 compared to control, # denotes p-value < 0.05 compared to marketed. ns: not significant compared to control.

We have also analyzed the expression of β1-integrin. As depicted in **Fig. 4.14**, deficient expression was found in the control group (39±7% of the healthy skin). In the marketed CH scaffold-treated group, only a moderate increase (statistically insignificant) in the β1-integrin expression was observed (55±3%). A significant increase was detected with the lyophilized CH-CS PEC-treated group (67±7%) compared to the control; however, it was not significantly different from the marketed CH scaffold-treated group. With the *in-situ* CH-CS PEC treatment, a significantly higher amount of β1-integrin was detected (78±3%) than the control and the marketed product. As observed in the *in-vitro* study (**Chapter 3**), the presence of a viscoelastic matrix-like structure can significantly improve the mechano-sensing by the cells, which can modulate the expression of β1-integrin [41, 42]. *In-situ* application of the CH-CS PEC directly at the wound bed can provide a viscoelastic scaffold for functional maturation of the wound bed cells, stimulating the expression of markers like β1-integrin.
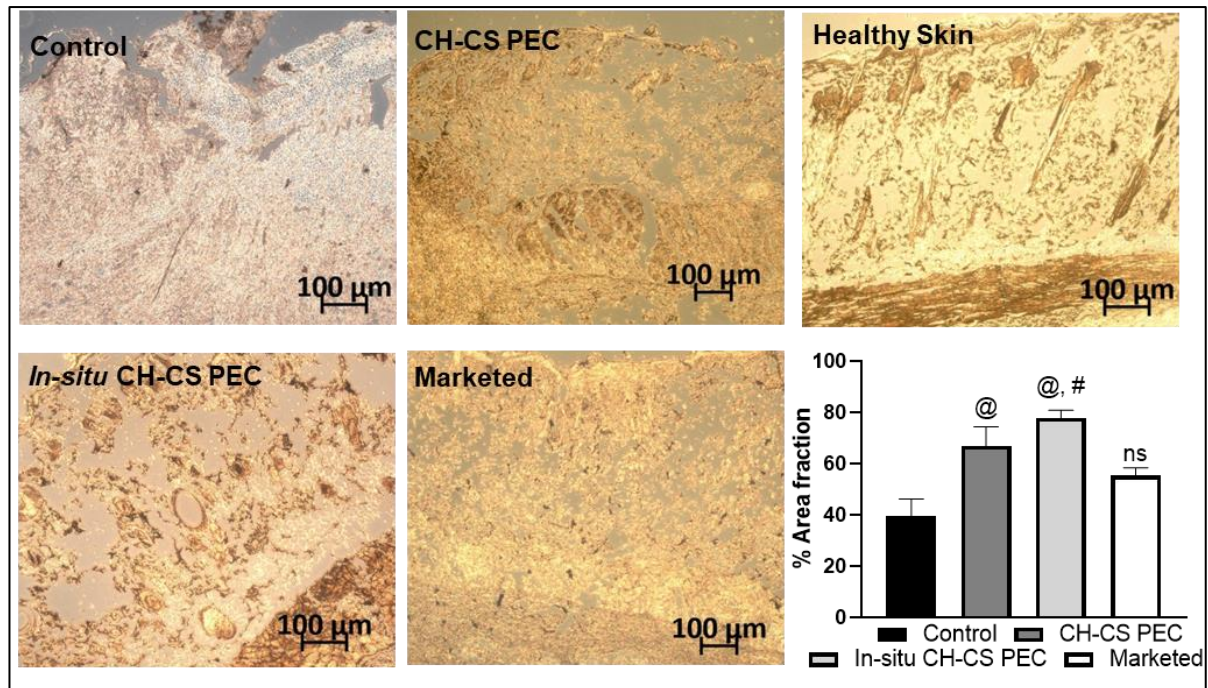
Fig. 4.14. Immunohistochemical staining of **β1 integrin** in the skin tissue sections collected 14th-day post-treatment. The expression of the markers was compared with the skin section of the healthy skin. Scale bar 100 μm. Statistical analysis was done using 1-way ANOVA with Tukey multiple comparison test. @ denotes p-value < 0.05 compared to control, # denotes p-value < 0.05 compared to marketed. ns: not significant compared to control.

4.4 Conclusion

In-situ forming scaffolds could exhibit enhanced wound healing properties due to direct contact with the wound bed cells. Previous attempts to make *in-situ* wound healing scaffolds involved chemical reactions, making them unsuitable for clinical application. Also, complicated design makes their large-scale production very challenging [43-46]. In the present study, we demonstrated the effect of viscoelastic in-situ formed CH-CS PEC on keratinocytes and fibroblasts. The data illustrated a significant increase in keratinocyte and fibroblast proliferation and function. In the rat skin-excisional wound model, treatment with the *in-situ* forming scaffold exhibited enhanced wound healing efficacy in terms of wound closure rate, collagen content, as well as α-SMA and β1-integrin expression.

Biocompatibility is an essential criterion for any wound healing scaffold. In our previous study, we demonstrated the CH-CS PEC to be highly hemocompatible [3]. As wound healing scaffolds directly come in contact with cells, one of the major toxicities is due to cell membrane destabilization. RBC has one of the weakest plasma membranes among all types of body cells. We have demonstrated that the CH-CS PEC does not cause hemolysis. In the current study, we have observed significantly increased proliferation and migration of both keratinocyte and fibroblast cells when grown on the CH-CS PEC, better than cells grown on Petri plates,

indicating high compatibility of the scaffold to the skin cells. Furthermore, in the *in-vivo* study, the groups treated with CH-CS PEC (both lyophilized and *in-situ* forming) showed no redness or other complications after treatment. Altogether, these data indicate the high biocompatibility of the CH-CS PEC.

Altogether, this study demonstrated that mixing CH and CS solution made a highly viscoelastic, porous scaffold that can support epidermal and dermal cell proliferation and bio-function with an enhanced *in-vivo* wound healing efficacy. This scaffold's simplistic design strategy and easy preparation have substantial significance for possible clinical translation.

References

1. Wojtowicz, A.M., et al., *The importance of both fibroblasts and keratinocytes in a bilayered living cellular construct used in wound healing.* Wound Repair Regen, 2014. **22**(2): p. 246-55.

2. Stunova, A. and L. Vistejnova, *Dermal fibroblasts—A heterogeneous population with regulatory function in wound healing.* Cytokine & Growth Factor Reviews, 2018. **39**: p. 137-150.

3. Sharma, S., K.L. Swetha, and A. Roy, *Chitosan-Chondroitin sulfate based polyelectrolyte complex for effective management of chronic wounds.* Int J Biol Macromol, 2019. **132**: p. 97-108.

4. Coelho, P.G.B., et al., *Evaluation of dermal collagen stained with picrosirius red and examined under polarized light microscopy.* An Bras Dermatol, 2018. **93**(3): p. 415-418.

5. Crowe, A.R. and W. Yue, *Semi-quantitative Determination of Protein Expression using Immunohistochemistry Staining and Analysis: An Integrated Protocol.* Bio Protoc, 2019. **9**(24).

6. Tchemtchoua, V.T., et al., *Development of a chitosan nanofibrillar scaffold for skin repair and regeneration.* Biomacromolecules, 2011. **12**(9): p. 3194-204.

7. Nezhad-Mokhtari, P., M. Akrami-Hasan-Kohal, and M. Ghorbani, *An injectable chitosan-based hydrogel scaffold containing gold nanoparticles for tissue engineering applications.* Int J Biol Macromol, 2020. **154**: p. 198-205.

8. Barra, A., et al., *Biocompatible chitosan-based composites with properties suitable for hyperthermia therapy.* J Mater Chem B, 2020. **8**(6): p. 1256-1265.

9. Cheung, R.C., et al., *Chitosan: An Update on Potential Biomedical and Pharmaceutical Applications.* Mar Drugs, 2015. **13**(8): p. 5156-86.

10. Chaudhuri, O., et al., *Effects of extra-cellular matrix viscoelasticity on cellular behaviour.* Nature, 2020. **584**(7822): p. 535-546.

11. Hosseini, M.S. and A.A. Katbab, *Effects of surface viscoelasticity on cellular responses of endothelial cells.* Rep Biochem Mol Biol, 2014. **3**(1): p. 20-8.

12. Roether, J., et al., *Microstructure, local viscoelasticity and cell culture suitability of 3D hybrid HA/collagen scaffolds.* PLoS One, 2018. **13**(12): p. e0207397.

13. Livak, K.J. and T.D. Schmittgen, *Analysis of relative gene expression data using real-time quantitative PCR and the 2(-Delta Delta C(T)) Method.* Methods, 2001. **25**(4): p. 402-8.

14. Tracy, L.E., R.A. Minasian, and E.J. Caterson, *Extra-cellular Matrix and Dermal Fibroblast Function in the Healing Wound.* Adv Wound Care (New Rochelle), 2016. **5**(3): p. 119-136.

15. Myllyharju, J. and K.I. Kivirikko, *Collagens and collagen-related diseases.* Ann Med, 2001. **33**(1): p. 7-21.

16. Kadler, K.E., et al., *Collagen fibril formation.* Biochem J, 1996. **316 (Pt 1)**: p. 1-11.

17. Xue, M. and C.J. Jackson, *Extra-cellular Matrix Reorganization During Wound Healing and Its Impact on Abnormal Scarring.* Adv Wound Care (New Rochelle), 2015. **4**(3): p. 119-136.

18. Volk, S.W., et al., *Diminished type III collagen promotes myofibroblast differentiation and increases scar deposition in cutaneous wound healing.* Cells Tissues Organs, 2011. **194**(1): p. 25-37.

19. Lovvorn, H.N., 3rd, et al., *Relative distribution and crosslinking of collagen distinguish fetal from adult sheep wound repair.* J Pediatr Surg, 1999. **34**(1): p. 218-23.

20. Hallock, G.G., et al., *Analysis of collagen content in the fetal wound.* Ann Plast Surg, 1988. **21**(4): p. 310-5.

21. Verhaegen, P.D., et al., *Differences in collagen architecture between keloid, hypertrophic scar, normotrophic scar, and normal skin: An objective histopathological analysis.* Wound Repair Regen, 2009. **17**(5): p. 649-56.

22. Jester, J.V., et al., *TGFbeta induced myofibroblast differentiation of rabbit keratocytes requires synergistic TGFbeta, PDGF and integrin signaling.* Exp Eye Res, 2002. **75**(6): p. 645-57.

23. Serini, G., et al., *The fibronectin domain ED-A is crucial for myofibroblastic phenotype induction by transforming growth factor-beta1.* J Cell Biol, 1998. **142**(3): p. 873-81.

24. Hinz, B., et al., *Alpha-smooth muscle actin expression upregulates fibroblast contractile activity.* Mol Biol Cell, 2001. **12**(9): p. 2730-41.

25. Chitturi, R.T., et al., *The role of myofibroblasts in wound healing, contraction and its clinical implications in cleft palate repair.* J Int Oral Health, 2015. **7**(3): p. 75-80.

26. Ghahary, A., et al., *Keratinocyte differentiation inversely regulates the expression of involucrin and transforming growth factor beta1.* J Cell Biochem, 2001. **83**(2): p. 239-48.

27. Mohammadzadeh, L., et al., *A novel egg-shell membrane based hybrid nanofibrous scaffold for cutaneous tissue engineering.* J Biol Eng, 2019. **13**: p. 79.

28. Meng, E., et al., *Bioapplications of Bacterial Cellulose Polymers Conjugated with Resveratrol for Epithelial Defect Regeneration.* Polymers (Basel), 2019. **11**(6).

29. Dally, J., et al., *Hepatocyte Growth Factor Mediates Enhanced Wound Healing Responses and Resistance to Transforming Growth Factor-beta(1)-Driven Myofibroblast Differentiation in Oral Mucosal Fibroblasts.* Int J Mol Sci, 2017. **18**(9).

30. Chmielowiec, J., et al., *c-Met is essential for wound healing in the skin.* J Cell Biol, 2007. **177**(1): p. 151-62.

31. Werner, S., T. Krieg, and H. Smola, *Keratinocyte-fibroblast interactions in wound healing.* J Invest Dermatol, 2007. **127**(5): p. 998-1008.

32. Seeger, M.A. and A.S. Paller, *The Roles of Growth Factors in Keratinocyte Migration.* Adv Wound Care (New Rochelle), 2015. **4**(4): p. 213-224.

33. Vecino, E., et al., *Influence of extra-cellular matrix components on the expression of integrins and regeneration of adult retinal ganglion cells.* PLoS One, 2015. **10**(5): p. e0125250.

34. Delcommenne, M. and C.H. Streuli, *Control of integrin expression by extra-cellular matrix.* J Biol Chem, 1995. **270**(45): p. 26794-801.

35. Chen, X., et al., *Peptide-Modified Chitosan Hydrogels Accelerate Skin Wound Healing by Promoting Fibroblast Proliferation, Migration, and Secretion.* Cell Transplant, 2017. **26**(8): p. 1331-1340.

36. Liu, H., et al., *A functional chitosan-based hydrogel as a wound dressing and drug delivery system in the treatment of wound healing.* RSC Advances, 2018. **8**(14): p. 7533-7549.

37. Katayama, Y., et al., *Chondroitin Sulfate Promotes the Proliferation of Keloid Fibroblasts Through Activation of the Integrin and Protein Kinase B Pathways.* Int J Mol Sci, 2020. **21**(6).

38. Jin, J., et al., *Effect of chondroitin sulfate proteoglycans on neuronal cell adhesion, spreading and neurite growth in culture.* Neural Regen Res, 2018. **13**(2): p. 289-297.

39. Zeltz, C. and D. Gullberg, *The integrin-collagen connection--a glue for tissue repair?* J Cell Sci, 2016. **129**(4): p. 653-64.

40. Martinelli-Klay, C.P., et al., *Modulation of MCP-1, TGF-beta1, and alpha-SMA Expressions in Granulation Tissue of Cutaneous Wounds Treated with Local Vitamin B Complex: An Experimental Study.* Dermatopathology (Basel), 2014. **1**(2): p. 98-107.

41. Yeh, Y.C., et al., *Mechanotransduction of matrix stiffness in regulation of focal adhesion size and number: reciprocal regulation of caveolin-1 and beta1 integrin.* Sci Rep, 2017. **7**(1): p. 15008.

42. Sun, Z., S.S. Guo, and R. Fassler, *Integrin-mediated mechanotransduction.* J Cell Biol, 2016. **215**(4): p. 445-456.

43. Tsang, V.L. and S.N. Bhatia, *Three-dimensional tissue fabrication.* Adv Drug Deliv Rev, 2004. **56**(11): p. 1635-47.

44. Wang, P., et al., *In situ formed anti-inflammatory hydrogel loading plasmid DNA encoding VEGF for burn wound healing.* Acta Biomater, 2019. **100**: p. 191-201.

45. Griffin, D.R., et al., *Accelerated wound healing by injectable microporous gel scaffolds assembled from annealed building blocks.* Nat Mater, 2015. **14**(7): p. 737-44.

46. Ryan, C.N.M., M.N. Doulgkeroglou, and D.I. Zeugolis, *Electric field stimulation for tissue engineering applications.* BMC Biomed Eng, 2021. **3**(1): p. 1.

Chapter 5

In-vitro and *in-vivo* evaluation of anti-bacterial and anti-inflammatory efficacy

5.1 Backg0round

Wound infections and inflammation is the primary cause of the development of wound chronicity. They harbor diverse microbiota species like *Staphylococcus aureus*, *Pseudomonas aeruginosa*, *Corynebacterium* spp., *Streptococcus* spp., *Enterococcus* spp., and *Enterococcus* spp., along with numerous low-abundance species [1]. Various antibiotics are used for the treatment of wound infections. However, continuous use of antibiotics causes antibiotic resistance [2]. Hence, there is a need to develop antibiotic-free wound dressing that has antibacterial efficacy and can control inflammation post-bacterial clearance. The biophysical and biochemical characteristics of the ECM are known to alter macrophage behavior [3]. However, due to the loss of ECM in chronic wounds, modulation of macrophage activity becomes dysregulated. Alternatively, ECM-mimetic biopolymeric scaffolds can be designed with macrophage modulatory function. It has been demonstrated that macrophages grown on soft and medium-stiff gels showed an antiinflammatory phenotype, while stiff hydrogel showed a pro-inflammatory phenotype [4]. The substrate stiffness impacts the cell morphology and area, demonstrating the change in the macrophage phenotype.

After evaluating the effect of CH-CS PEC on the dermal and epidermal cells, we evaluated the efficacy of CH-CS PEC on macrophages. Using a polyelectrolyte complexation technique, we developed an ECM-mimetic, in-situ forming biopolymeric scaffold. This chapter underlined the CH-CS scaffold's antimicrobial activity and mode of action. The hydrogel-based scaffold acts as a local niche for macrophage immunomodulation. The physicochemical properties of the hydrogels alter the cellular behavior and macrophage plasticity. The hydrogel stiffness has a direct impact on macrophage function. Sridharan *et al*. reported the effect of material stiffness on the macrophage behavior and phagocytic potential of the macrophages. The viscoelasticity and self-healing properties of CH-CS PEC provide an environment conducive for the macrophages to turn into M2 phenotype. The stiffness and viscoelasticity of the substrate affect macrophage plasticity and phagocytic activity. Further, the inflammation levels were studied by evaluating the mRNA level expressions of TNF-α and IL-10, post 3h and 6h of bacterial exposure, and were confirmed by studying the NF-kβ expression at the protein level. Lastly, the antibacterial and controlled inflammatory potential was confirmed by studying the in-vivo rat wound infection model.

5.2 Materials and methods

High molecular weight chitosan (MW≈700kDa, DD: more than 90%) was purchased from Sisco Research Laboratories (SRL) Pvt. Ltd. (India). Chondroitin sulfate monosodium salt (MW 475.39 Da) was procured from Tokyo Chemical Industry Co. Ltd. RAW 264.7 murine macrophage cell line, and *GFP E.coli* was a kind gift from Dr. Sandhya Marathe (Department of Biological Sciences, BITS Pilani, Pilani Campus). *P. aeruginosa* bacteria was a kind gift from Prof. Prabhat Nath Jha (Department of Biological Sciences, BITS Pilani, Pilani Campus). Dulbecco modified Eagle medium, 10% fetal bovine serum was obtained from HiMedia Laboratories Ltd., India. α-smooth muscle actin antibody, β1-integrin antibody, NF-κβ, VE-Cadherin antibody, GAPDH antibody, and Alexaflur secondary anti-rabbit antibody were procured from Cell Signaling Technology (USA). Phalloidin-iFluor 532 Reagent (ab176755) was a gift from Prof. Syamantak Majumder (Department of Biological Sciences, BITS Pilani, Pilani Campus). All the primers were procured from Imperial Life sciences, India. SYBR green qPCR kit and cDNA synthesis kit were procured from Biorad. All other chemicals used were of A.R grade.

5.2.1 Preparation of Chitosan- chondroitin sulfate polyelectrolyte complex

CH-CS PEC was fabricated using the process reported in our previous work [5]. Briefly, 5% w/v of CH solution was prepared in 1% v/ v of glacial acetic acid and further dialyzed to remove the glacial acetic acid until the pH of the solution became ~7. 5% w/v chondroitin sulfate was prepared in Milli-Q water. CH-CS PEC was prepared by mixing CH and CS solution in a 1:1 v/v ratio using a custom-made double-barreled syringe

5.2.2 Antibacterial efficacy study

1. Determination of bacterial cell viability

The study was performed using the micro-broth dilution method using tetraphenyl tetrazolium chloride (TTC) dye. The experiment was performed *Pseudomonas aeruginosa* and *Bacillus subtilus.* The study used CH-CS PEC, CH, and CS as treatment groups. Microbial inoculums were prepared by subculturing microorganisms into Luria Bretani (LB) broth at 28 °C for 18 h and were diluted to approximately 10^5 to 10^6 colony-forming units per ml (CFU/ml) in LB broth. Briefly,

96 well plates were coated with 50 µl of CH, 50ul of CHCS scaffold, and 50 µl of 5 % CS solution was added as treatment. A 150 µl of test microorganism was added to these coated 96 wells microplates. The microplates were then incubated at 28°C for 24 h. After incubation, 40 µl of Triphenyl tetrazolium chloride (1.0 mg/ml, TTC) was added to each well and was incubated for 3 h. Color changes of TTC in the microplate from colorless to red were accepted as microbial cell viability, and intensity was observed at 470 nm [6]. Further, the treated test organism was also plated on the fresh LB agar plate to count the no. of CFU/ml after 24 h treatment.

2. Determination of reactive oxygen species

The study was performed on *Pseudomonas aeruiginosa.* The microbial inoculum was prepared by subculturing microorganisms into Luria Bretani (LB) broth at 28 °C for 18 h and was diluted to approximately 10^5 to 10^6 colony-forming units per ml (CFU/ml) in LB broth. Briefly, 96 well plates were coated with 50µl of CH, 50µl of CH-CS scaffold, and 50µl of 5 % CS solution was added as treatment. A 150 µl of test microorganism was added to these coated 96 wells microplates.

The bacteria were exposed to the treatment for 24h. After 24h of treatment, test microbes were washed with PBS by centrifuging at 1500 RPM for 5 minutes. To determine ROS, the treated bacterial cells were incubated with DCFDA (20 µM) for 1h. Fluorescence was measured using a microplate reader (Fluoroskan Ascent) at 485 nm excitation and 530 nm emission. Relative change in DCFDA fluorescence was calculated with respect to bacterial cell viability [7]. Bacterial cell viability was studied by the protocol discussed above by using TTC dye.

3. Determination of bacterial cell membrane integrity

The study was performed on *Pseudomonas aeruiginosa.* Zeta potential is a marker for the determination of bacterial membrane integrity. Zeta potential and size distribution curves can determine the bacterial cell aggregation and change in membrane depolarization of the bacteria. The zeta potential of the bacteria treated with CH, CS, and CH-CS PEC was analyzed using the Malvern zeta sizer instrument. The treatment condition for the experiment was similar to that of the above experiment. After 24h of treatment incubation, the bacterial cells were washed with PBS, and further, the bacterial cell suspension was used to determine zeta potential and size distribution [8].

4. SEM analysis

Further, FESEM analysis was performed for CH, CS, and CH-CS treated and untreated bacterial cells to confirm changes in the membrane permeability of the bacterial cells after treatment. The study was performed on *Pseudomonas aeruginosa.* The FESEM analysis was performed on FEI APREO-S scanning electron microscope.

5.2.3 *In-vitro* Cell culture studies

1. Cytocompatibility study

RAW 264.7 murine macrophage cell line was used for the study. Cytocompatibility was confirmed by staining the live and dead cells using Hoesct/propidium iodide stain and by MTT assay. Cells were grown on the coverslips coated with CH and CH-CS scaffold. CS solution was added after seeding. After 24h, the cells were stained with 5 μg/ml of Hoesct and 1 μg/ml of propidium iodide for 10 minutes. The Live and dead cells were then observed under a fluorescent microscope (Zeiss) [9]. For the MTT assay, RAW 264.7 cells were cultured in 96-well plates pre-coated with CH and CH-CS scaffold at 2 x 103 cells/well density. CS solution was added directly at the time of seeding. After 72h of incubation, cytotoxicity was analyzed using MTT. Formazan crystals formed by live cells were dissolved in DMSO, and readings were captured at 570 nm with a differential filter of 630 nm by a Multiskan SKY microplate spectrophotometer [18]. Untreated samples served as the control.

2. Macrophage morphometric analysis

For morphology evaluation, the cells were grown on the coverslip at a density of 0.4×10^5. Post 24h of incubation, cells were fixed in 4% formaldehyde for 15 mins. After fixation, the cells were stained with Phalloidin-iFluor 532 reagent (ab176755) for 40 mins. The images were taken at 63x using a confocal microscope (Zeiss). The images were further quantified for cell spreading, Circularity and aspect ratio using Image J software. SEM images of the cells grown on the coverslip were performed by dehydrating the macrophages to the gradient ethanol concentration and further processing the samples in FESEM (Apreo).

3. Development of *In-vitro* macrophage infection model

The *in-vitro* macrophage infection model was developed using *Pseudomonas aeruginosa* and RAW 264.7 murine macrophages. The macrophages were grown on CH and CH-CS scaffold and treated with CS solution. After 24h the cells were exposed to the bacterial strain in the multiplicity index of 1:10. The macrophages were exposed to bacteria for 3h and 6h.

4. Determination of extracellular bacteria

The macrophages were grown on CH and CH-CS scaffold and treated with CS solution for 24 h. After 24h, cells were exposed to the bacterial strain in the multiplicity index of 1:10. The macrophages were exposed to bacteria for 3h and 6h. At the respective time point, the extracellular bacteria were removed. The bacteria were washed with PBS twice and further plated on the fresh LB agar plates for CFU count. To determine intracellular bacteria, macrophages exposed to bacteria were lysed using 0.2% triton-X 100 for 5 minutes. The cells were further collected and centrifuged at 1500 RPM for 10 minutes. The pellet was suspended in PBS and plated for the determination of intracellular bacterial count. The bacteria were incubated for 12h at 28°C.

5. Determination of Phagocytic index

Bacterial internalization of GFP *E.coli* into the macrophages was performed to check its phagocytic ability. GFP *E.Coli* was grown in LB agar containing 50µg/ml of ampicillin. The bacteria were grown at 37°C for 8h to reach the optical density of 0.4. For phagocytic index determination, the macrophages were grown on a coverslip precoated with CH and CH-CS scaffold and treated with CS solution for 24 h. After 24h the cells were exposed to the bacterial strain in the macrophage-to-bacteria ratio of 1:10. The macrophages were exposed to bacteria for 3h. After bacterial exposure, the macrophages were washed with PBS twice. Cells were further fixed with 4% paraformaldehyde for 10 minutes and stained with Phalloidin iflur for the f-actin staining. The coverslips were mounted with 70% glycerol and observed under a confocal microscope at 63x magnification. The number of GFP bacteria internalized per macrophage was counted for the determination of the phagocytic index, excluding the extracellular bacteria [10].

6. qPCR analysis

All the qPCR studies were performed on CFX Thermocycler (BioRad). Total RNA was isolated using the TRI reagent. The final RNA concentration was analyzed using Nanodrop (SimpliNano-Biochrom). Next, the isolated RNA samples were synthesized using a RevertAid cDNA synthesis kit (BioRad). The transcript levels of the gene of interest were measured by quantitative PCR (qPCR). The q-PCR reactions were performed using the SYBR Green chemistry. The data were normalized against GAPDH as the housekeeping gene. The study was performed to check the change in the mRNA expression of TNF-αand IL-10 in both uninfected and infected macrophages. The primers used for qPCR are mentioned in **Table 5.1**. The studies were performed in five groups, CH-CS PEC, CH, CS, Untreated cells infected with bacteria, and untreated cells. For the mRNA expression of uninfected cells study was performed in four groups CH-CS PEC, CH, CS, and untreated cells.

Table 5.1 List of primers used in the study.

	Forward (5'-3')	Reverse (5'-3')
GAPDH	ACCCAGAAGACTGTGGATGG	TCTAGACGGCAGGTCAGGTC
TNF-α	GCCTCTTCTCATTCCTGCTTG	CTGATGAGAGGGAGGCCATT
IL-10	CCCTGGGTGAGAAGCTGAAG	CACTGCCTTGCTCTTATTTTCACA

7. Immunoblotting Studies

An immunoblotting study was performed for the estimation of β1 integrin and NF-κβprotein. β1 integrin was performed on the uninfected macrophages treated with CH, CS, and CH-CS PEC to determine the effect of viscoelasticity on the macrophage behavior. NF-κβ levels were evaluated to study the inflammation state of the macrophages exposed to bacteria post 3h and 6h. $1x10^6$ cells were grown on the 6.0 cm dishes pre-coated with 200μl of CH and 200μl CH-CS PEC. CS was added to the solution at the time of seeding. After 24h of treatment, the protein was isolated from the cells using RIPA lysis buffer containing 1% of protease inhibitor for the estimation of β1 integrin and NF-κβ. The concentration of protein was normalized by taking CH and CH-CS PEC as blank for the respective samples, as CH is sensitive to the Bradford reagent.

To check the inflammation status, we exposed the CH, CH-CS PEC, and CS-treated cells to the bacteria for 3h and 6h. The protein was isolated with the same process. The protein concentration was estimated using the Bradford reagent. As CH interacts with the Bradford reagent, all the samples CH and CH-CS PEC without cells were taken as blank for the estimation of the protein concentration. The protein was denatured in 5× loading buffer by heating (100°C for 10 min) and cooling on ice. Equal concentrations of the total protein were resolved using denaturing polyacrylamide gels (5% stacking and 10% resolving). The resolved protein was then transferred to a PVDF membrane (BioRad). It was then blocked with a 5% bovine serum albumin (HiMedia). The blot was probed with antibodies against β1 integrin, NF-κβ, and loading control GAPDH (Cell Signaling Technologies, USA). The secondary antibodies used were horseradish peroxide-conjugated goat anti-rabbit IgG (Cell Signaling Technologies, USA). The protein intensity was detected using Chemidoc (BioRad). The band intensities were quantified using ImageJ software. The fold change protein expression was quantified with respect to the loading control, i.e., GAPDH band intensity.

5.2.4 *In-vivo* studies

1. *In-vivo* infection wound model

The *in vivo* wound healing study was performed in the Wistar rats with a full-thickness excisional wound of 1×1 cm^2 area. Three groups were included in the study: i) control (untreated), ii) in-situ CH-CS PEC, and iv) a market-available CH-based pre-formed scaffold. *In-situ* CH-CS PEC treatment was given through a custom-made double-barreled syringe, with CH solution in one chamber and CS solution in the other chamber. For application, both the pistons of the double-barreled syringe were compressed simultaneously, leading to the ejection of both solutions at the same rate. The solutions were mixed in the wound bed itself, leading to the formation of the *in-situ* scaffold. After the creation of the wound, the wound bed was infected with 10^8 CFU/ml of *Pseudomonas aeruginosa.* The bacterial colonies were counted by collecting the bacteria swab every alternate day of the treatment. Further, the wound healing efficacy was evaluated by analyzing the wound closure. The area of wound closure was quantified using ImageJ software.

2. Histology study

Representative animals from each group were sacrificed on day 5 and day 10. Their skin from the wound area was fixed, paraffin-embedded, sectioned, and stained with H&E dye. H&E staining was used to determine the cellular morphology and skin integrity. The stained sections were examined under brightfield microscopy. The images were taken at the 4x and 10x magnification.

3. Immunofluorescence staining

Immunohistochemical analysis of NF-κβ and VE-Cadherin was performed in the skin sections. The sections were dewaxed and rehydrated. Antigen unmasking was performed by heating the sections in the citrate buffer (pH 6.0) in a water bath at 80°C for 15 min. The samples were treated with 0.1% trion-X100 for 5 minutes. For IHC staining, sections were washed and blocked with 5% w/v of bovine serum albumin in Tris Buffered Saline with Tween 20 for 1h. Further, the sections were incubated with anti-rabbit NF-κβ and anti-mouse VE-Cadherin antibody (1:500 dilutions, CST) at 4°C overnight. The sections were washed and incubated with secondary fluorescent antibody (1:1000 dilution, CST) for 3h at room temperature. The sections were counterstained with DAPI for nuclear staining and mounted. The images were taken at 20x magnification for the evaluation of the protein expression.

5.2.5 Statistical analysis

The data were analyzed using GraphPad Prism software version 8. Comparison among data sets was statistically determined using one-way or two-way ANOVA; post hoc Tukey's test was performed to compare each group's means with every other group. Data were represented as mean ± SD.

5.3 Results and discussion

Controlling wound infection and inflammation is of primary interest to clinicians for improved wound healing. Persistent infection and sustained inflammation are two of the major causes for transitioning from a normal wound to a chronic wound [11]. The development of bioactive wound dressings which can modulate these is an active area of research. Many different materials have been evaluated for this purpose; among them CH is one of the most studied due to its favorable

characteristics, including biocompatibility, biodegradability, and hemostatic property [12]. CH is also reported to have antibacterial and macrophage stimulatory activity [13, 14]. CS is also a glycosaminoglycan. It is a component of the human extracellular matrix and has been reported to promote cell proliferation. CS can down-regulate COX-2 and iNOS pathways and show antiinflammatory activity [15].

5.3.1 Development of *in-situ* CH-CS PEC

The cross-linked scaffold formation between positively charged CH and negatively charged CS was done based on electrostatic interaction by mixing 5% w/v CH and 5% w/v CS in a 1:1 v/v ratio. A high molecular weight CH (MW ≈ 700 kDa) and low molecular weight CS (disaccharide form; MW 475 Da) were used to increase spontaneous mixing between them. Low molecular weight CS can penetrate easily in the viscous CH gel, leading to electrostatic cross-linking and fabrication of the CH-CS PEC.

5.3.2 Antibacterial efficacy of CH-CS PEC against *Pseudomonas aeruginosa* and *Bacillus subtilus*.

Bacterial growth at the wound site activates the immune responses, which prolongs the inflammation-causing disturbance in the wound healing process. The major bacterial species involved in skin infection are *Staphylococcus aureus* and *Pseudomonas aeruginosa*. Hence controlling bacterial growth is one of the critical parameters for improved wound healing. In the present study, we have examined the antibacterial efficacy of CH-CS PEC against *Pseudomonas aeruginosa*. The antibacterial activity of the CH-CS PEC was studied by the micro broth dilution method by analyzing the number of viable bacterial cells using TTC dye. With CH-CS PEC treatment, bacterial viability was 7.05±0.01%, compared to 40.19±0.52% observed with CH, and 72.19±0.02% with CS (**Fig. 5.1B**). The study was also performed on a gram-positive strain, *Bacillus subtilus,* to evaluate the effect of CH-CS PEC on the gram-positive bacteria. The data demonstrated 41% of bacterial cell viability when treated with CH-CS PEC, where CH and CS exhibited cell viability of 59% and 88% (**(Fig. 5.1A**).CH has previously been reported to have good antibacterial activity [16, 17]. We have observed a significantly increased bacterial cell death with CH-CS PEC compared to CH. A scaffold's wettability, stiffness, and roughness have been demonstrated to affect bacterial growth [18]. The substrate viscosity also modulates bacterial cell

adhesion by creating resistance to shear stress [19]. The enhanced cell death observed with CH-CS PEC could be because of the lower bacterial cell adhesion on the material surface and stiffness of the CH-CS PEC (as demonstrated in the rheological data, Chapter 3).

Further evaluation of anti-bacterial efficacy was performed on *P. aeruginosa.* It has been reported that the generation of reactive oxygen species (ROS) is one of the major mechanisms for bacterial cell death with CH treatment.[20] In order to find out whether ROS was involved in the antibacterial activity of CH-CS PEC, we evaluated ROS generation by quantifying DCFDA staining of CH-CS PEC-treated *P aeruginosa*. The data demonstrated a high level of DCFDA fluorescence in *P aeruginosa* cells treated with CH-CS PEC (68.93± 4.23), compared to CH (10.13±2.35), CS (7.90±2.11) and untreated cells (5±0.45) (**Fig. 5.2A**). This high level of ROS with CH-CS PEC treatment could be one of the reasons for the increased bacterial cell death.
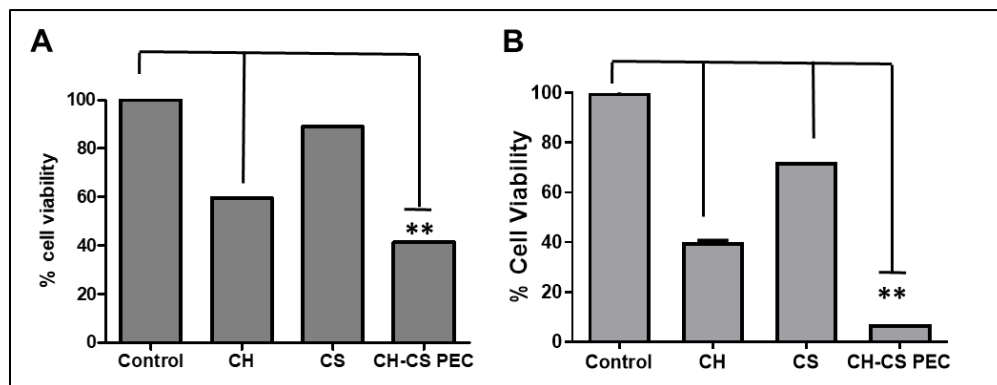
Fig. 5.1 Antibacterial efficacy analysis in *Bacillus subtilus* and *Pseudomonas aeruginosa* treated with different polymers for 24h. **A**: The % bacterial cell viability (*Bacillus subtilus)* after 24h of CH, CS, and CH-CS PEC and its comparison with control bacteria. **B**: The % bacterial cell viability (*Pseudomonas aeruginosa)* after 24h of CH, CS, and CH-CS PEC and its comparison with control bacteria. Statistical analysis was done using One-way ANOVA with Tukey multiple comparison test. ** denotes p-value < 0.05 compared to Control.

Furthermore, CH is reported to kill bacteria by altering bacterial membrane permeability [21]. In order to find out the membrane permeability of *P aeruginosa* cells treated with CH-CS PEC, the change in the membrane potential was studied by evaluating the zeta potential of the treated bacteria using Malvern Zetasizer (**Fig. 5.2B**). It was observed that the zeta potential of untreated bacteria was −5.71±0.62 mV, whereas it increased with CH (−4.36±0.35), CS (−4.0±0.68), and

CH-CS (-3.5 ± 0.55) treated bacteria, indicating destabilization of the outer membrane with those treatments. Additionally, scanning electron microscopic (SEM) analysis was done with control (untreated), CH, CS, and CH-CS-treated bacteria to evaluate the outer membrane of the treated bacteria directly. As shown in **Fig. 5.2C**, the outer membrane of untreated bacteria was found to be smooth, without any abnormality, whereas with CH and CH-CS PEC treatment, prominent outer membrane destabilization was observed in terms of the formation of cavities. More number of cavities was observed in the CH-CS PEC-treated bacteria than CH. These data indicated CH-CS PEC treatment would lead to the formation of membrane cavities in the bacteria, resulting in alteration of membrane potential, causing increased ROS generation and, ultimately, death of the bacteria.
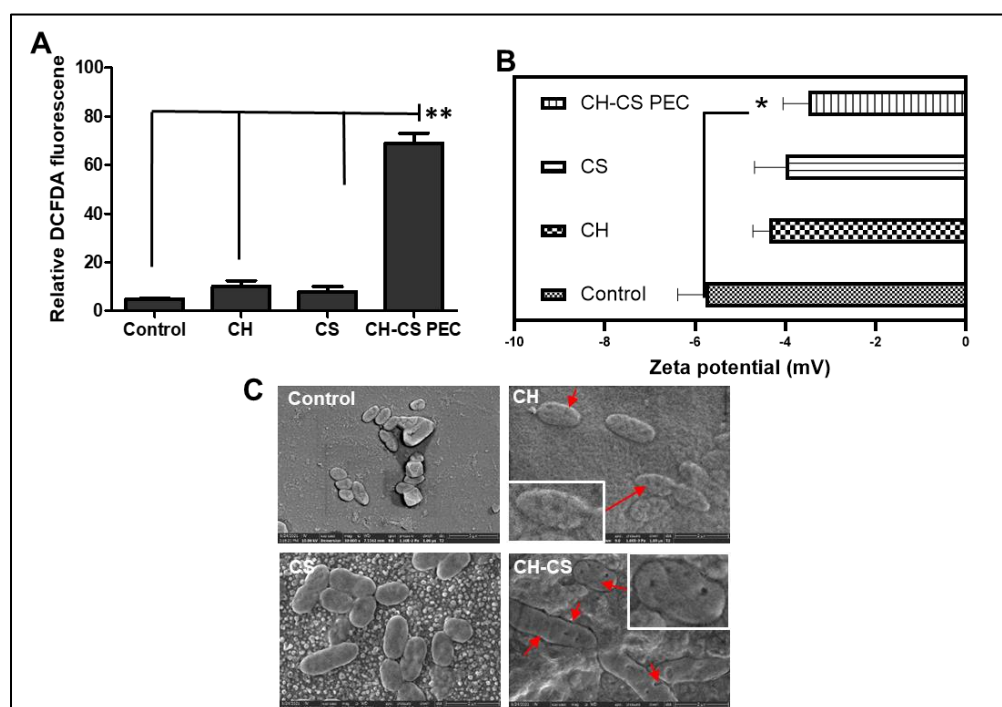
Fig. 5.2 Evaluation of ROS generation and bacterial membrane integrity on *P. aeruginosa*. **A)** Relative DCFDA fluorescence intensity for the evaluation of ROS generation in the bacteria treated with different polymers and its comparison with control bacteria. **B)** Zeta potential analysis of the bacteria with different treatment groups for 24h for the evaluation of bacterial cell membrane integrity, C: FESEM images of the control bacteria and bacteria treated with CH, CS, and CH-CS PEC post 24h. The red arrows demonstrate the disruption of the bacterial cell membrane. Statistical analysis was done using One-way ANOVA with Tukey multiple comparison test. ** denotes p-value < 0.05 compared to Control
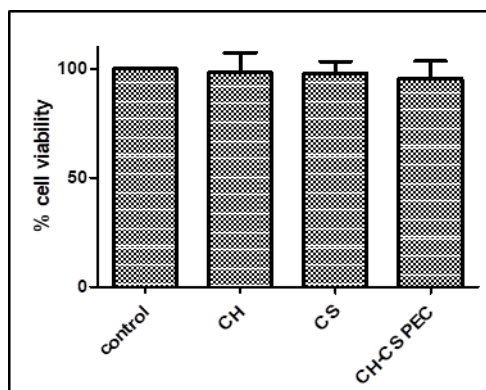
Fig. 5.3 Cytocompatibility of macrophages treated with CH, CS, and CH-CS PEC by performing MTT assay post 72h of incubation.

5.3.3 Effect of CH-CS PEC on macrophage survival

Before studying the effect of CH-CS PEC on the macrophages, Cytocompatibility of CH-CS PEC was performed by live/dead and MTT assays on macrophages (RAW264.7 cell line). The live/dead staining was performed using Hoescht/PI staining for labeling the live and dead cells. The data depicted almost no cell death in the cells treated with CH, CS, and CH-CS PEC (**Fig. 5.4**). Further, the Cytocompatibility was confirmed by the MTT assay. Cell viability was found to be more than 90% in CH (98.2±9.09%), CS (97.77±5.57%), and CH-CS PEC (95.3±8.2%) (**Fig. 5.3**), demonstrating high macrophage compatibility.
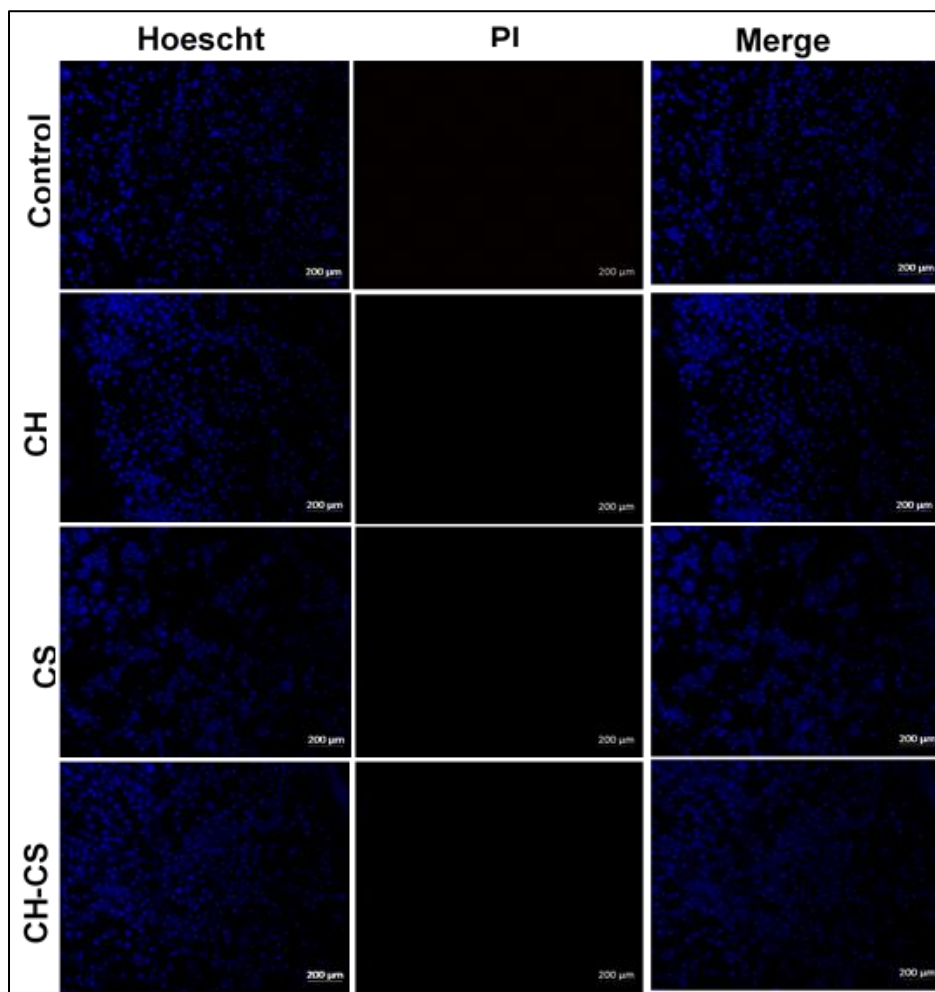
Fig. 5.4 Live/dead staining of the macrophages treated with CH, CS, and CH-CS PEC and compared with untreated cells.

5.3.4 Effect of CH-CS PEC on macrophage morphology

Next, we wanted to evaluate CH-CS PEC's effect on the macrophages to decipher the inflammatory potential of this scaffold. The impact of hydrogel-based scaffold on macrophage functionality is very well documented [22, 23]. Viscoelasticity of the material alters the macrophage morphology and polarity [24, 25]. Macrophages undergo antiinflammatory M2 polarization when seeded on a soft to medium-stiff surface; however, with increased stiffness, the macrophage turns into a pro-inflammatory M1 phenotype [4, 26]. We have observed a storage modulus (G`) of ~21000 Pa with CH-CS PEC, which can be considered as a medium stiff surface.

To understand the effect of this scaffold on the macrophages, first we evaluated the effect of CH-CS PEC on macrophage morphology. Macrophage cells (RAW264.7 cell line) were seeded on the coverslips precoated with CH and CH-CS PEC. For CS treatment, cells were incubated with CS solution. The cells were incubated for 24h and subsequently treated with Phalloidin-red to stain the actin filaments of the macrophage cells to visualize their morphology. Fluorescent microscopic analysis revealed a change in cell shape and cytoskeletal matrix in the cells treated with CH-CS PEC (**Fig. 5.5 A**). The change in morphology was studied by analyzing the cell spreading, circularity, and aspect ratio of the treated cells. All the parameters were quantified using ImageJ software and compared with that of the untreated cells. The untreated cells were found to have a cell area of 164.83 ± 14.29 μm^2, whereas, with CH treatment, it was 307.73 ± 80.74 μm^2, with CS treatment 254.52 ± 29.88 μm^2, and with CH-CS PEC treatment 271.19 ± 37.86 μm^2. A decrease in cell area was observed with CH-CS PEC treated cells, compared to CH treatment. Reduction in the cell area indicates the antiinflammatory behavior of the macrophages [27]. To further confirm the change in morphology, we evaluated the circularity value and aspect ratio of macrophages. The circularity value determines the roundness of the cell with respect to its area and perimeter. The aspect ratio decreases with the deformation of the perfect circle. The circularity and aspect ratio of untreated macrophages was found to be 0.79 ± 0.02 and 1.28 ± 0.09, respectively, whereas, with CH treatment, it was 0.74 ± 0.02 and 1.26 ± 0.05, with CS 0.59 ± 0.17 and 1.56 ± 0.36, respectively. Macrophages treated with CH-CS PEC showed a circularity of 0.34 ± 0.07 and an aspect ratio of 2.47 ± 0.11, indicating a non-circular, elongated phenotype (**Fig. 5.5B**). This observation was also corroborated by SEM analysis of the macrophages. Control and CH-treated cells were found to be mostly round in shape, whereas, with CS, some elongation was observed. CH-CS PEC-treated macrophages were found to have more elongated morphology (**Fig. 5.5C**). It has been reported that macrophages got elongated to increase their phagocytic activity [28, 29]
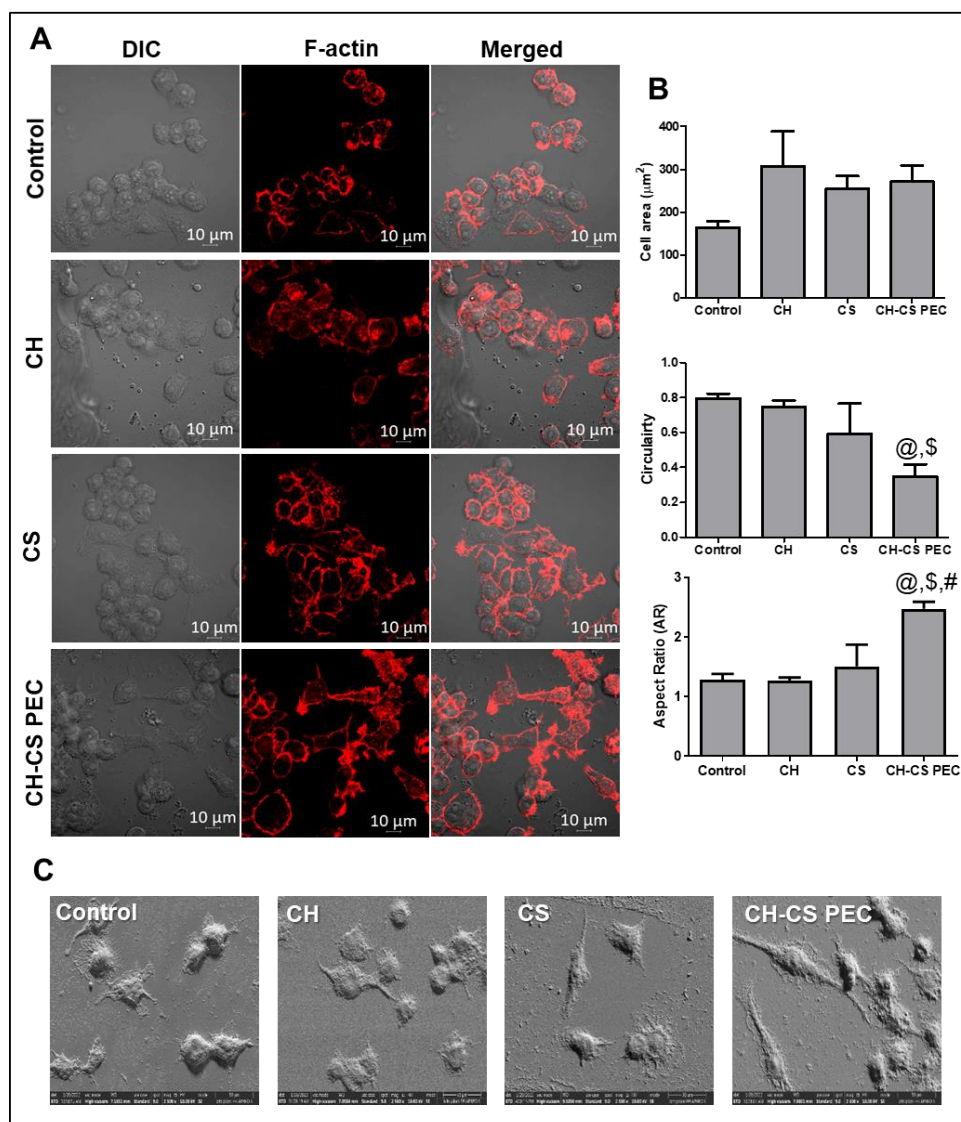
Fig. 5.5 Determination of the change in the macrophage morphology in the different treatment conditions. **A:** Representation of the change in the actin cytoskeleton in the macrophage treated with CH, CS, and CH-CS PEC. The elongated morphology was observed in the CH-CS PEC, depicting the sign of the M2 phenotype. **B:** Evaluation of cell area, circularity, and aspect ratio to quantify macrophage morphology. **C:** FESEM images of the macrophages treated with CH, CS, and CH-CS PEC. Statistical evaluation was performed by applying using one-way ANOVA with Tukey multiple comparison test. @, \$, # denotes p-value < 0.05 compared to Control, CH, and CS.

Based on the change in actin cytoskeleton and macrophage morphology in the presence of the viscoelastic CH-CS PEC, we hypothesized the involvement of β1-integrin. β1-integrin plays an important role in sensing the microenvironment's physical change and the macrophage polarity induction [30]. We evaluated the β1-integrin protein expression by Western blot analysis in the

macrophages treated with CH, CS, and CH-CS PEC. The expression level was normalized against control (untreated) cells. A 6.98±0.46-fold increase in β1-integrin expression was observed with CH-CS PEC treated macrophages, while with CH and CS treatment, a moderate increase was observed (2.74±0.2-fold and 1.86±0.17-fold, respectively (**Fig. 5.6A-B**). Increased β1-integrin expression has been associated with the increased phagocytic activity of the macrophages through an immunomodulatory M2 phenotype [30, 31]. To confirm the change in macrophage phenotype, we evaluated the mRNA expression of pro-inflammatory cytokine (TNF-α) and antiinflammatory cytokine (IL-10). The mRNA expression was normalized against untreated macrophages, and GAPDH was used as the housekeeping gene. The macrophages treated with CH showed 0.43±0.25 and 9.64±0.10 fold increase in TNF-αand IL-10 in comparison to CS (0.93±0.76 and 1.2±0.46) and CH (2.66±1.2 and 0.3±0.07) (**Fig. 5.6C**).
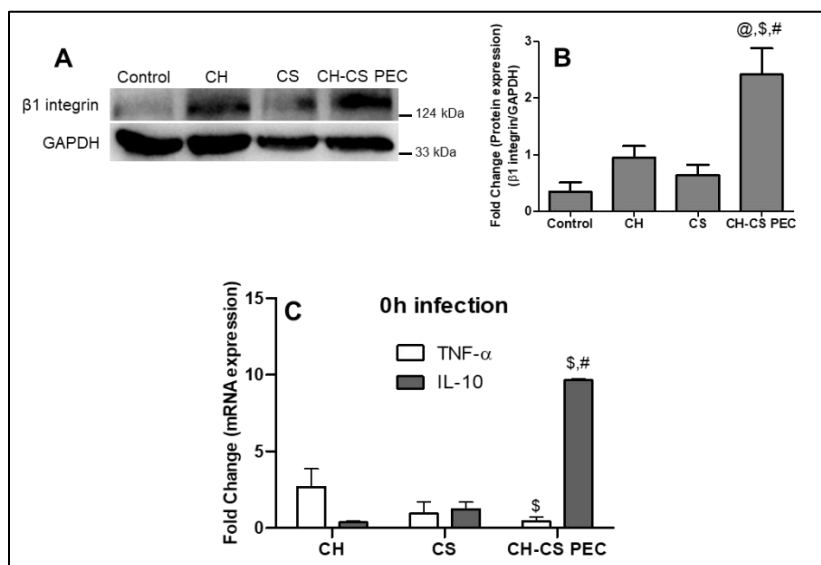
Fig. 5.6 Immunomodulation of macrophages treated with different polymers for 24 h. A) Immunoblotting of β1 integrin in macrophages treated with CH, CS, and CH-CS PEC and its comparison with the untreated macrophages. B) mRNA expression of TNF-α and IL-10 on the macrophages treated with CH, CS and CH-CS PEC. Gene expression normalized with untreated cells and GAPDH as housekeeping. Statistical analysis was done using One-way ANOVA with Tukey multiple comparison test. # and $ denotes p value < 0.05 compared to CS and CH

5.3.5 Evaluation of macrophage bacterial uptake and change in cytokine expression

After demonstrating a change in the macrophage morphology indicating an increase in the phagocytic capability, we next evaluated the direct phagocytic activity of the CH-CS PEC-treated

macrophages. For this, **an *in-vitro* macrophage infection model** was developed with the multiplicity of 1:10. Macrophages were plated on different scaffolds (CH, CS, and CH-CS PEC), incubated for 24h, and exposed to *P. aeruginosa* infection for 3h. After that, the culture supernatant was isolated and cultured on LB agar plate to find out the number of extracellular bacteria, as well as the macrophage cells were collected, homogenized, and plated to find out the number of phagocytosed bacteria. The data (**Fig. 5.7**) demonstrated increased intracellular bacterial count in CH-CS PEC [$(396\pm19.1)\times10^6$], compared to CH [$(220\pm27.6)\times10^6$], CS [$(231\pm44.54)\times10^6$], and untreated [$(47\pm8.4)\times10^6$]. Correspondingly, the extracellular bacterial count with CH-CS PEC was significantly lower [$(43\pm7.7)\times10^6$], compared to CH [$(245\pm25.45)\times10^6$], CS [$(94\pm21.92)\times10^6$], and untreated cells [$(400\pm127)\times10^6$]. The data demonstrated increased bacterial uptake by the macrophages treated with CH-CS PEC, resulting in reduced extracellular bacterial count and increased intracellular bacterial count.
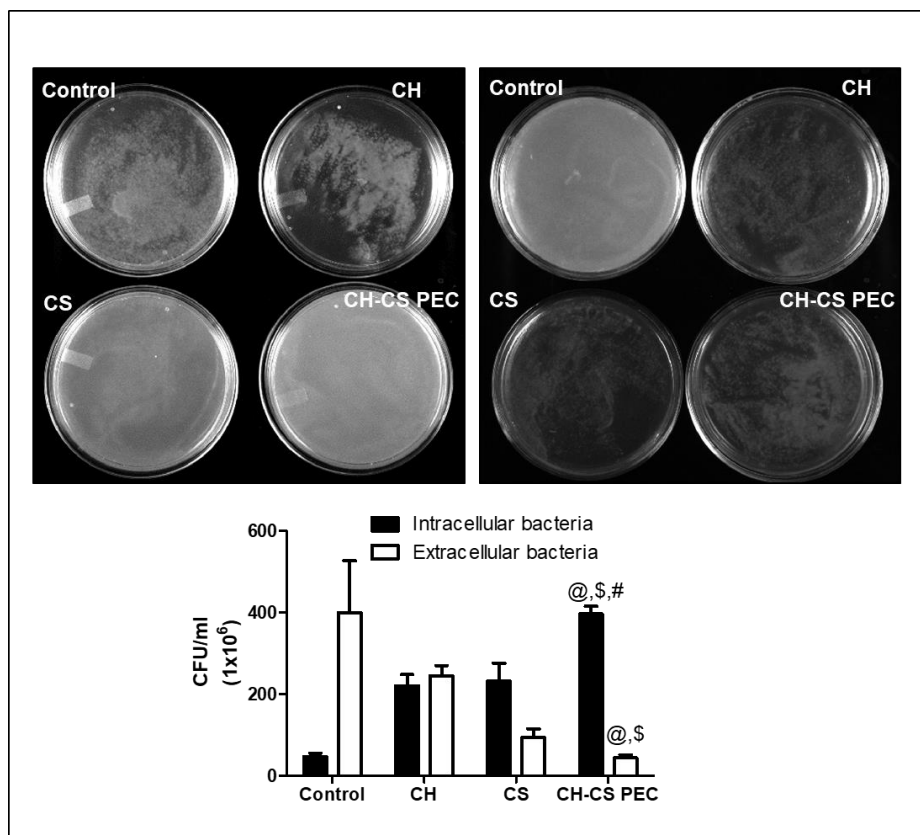
Fig. 5.7 Evaluation of intracellular and extracellular bacteria content in the macrophages treated with different treatments post 3h of infection. Statistical analysis was done using two-way ANOVA with Tukey multiple comparison test. @, $, # denotes p-value < 0.05 compared to Control, CH, and CS, respectively.

To confirm the increased phagocytic activity of the CH-CS PEC treated macrophages, macrophages were treated as previously and infected with GFP-tagged *E. Coli*. Post 3h of bacterial exposure, the cells were washed thoroughly with PBS and stained with phalloidin. Internalization of the GFP tagged *E. Coli* was evaluated by imaging the slides using confocal microscopy at 63x magnification (**Fig. 5.8**). Significant increase in phagocytosis was observed in the CH-CS PEC treated macrophages, compared to other treatments. The phagocytic index was computed by counting the total number of bacterial cells internalized per macrophage using ImageJ software to quantify the extent of phagocytosis. Both CH (phagocytic index: 2.27 ± 1.14) and CS (phagocytic index: 3.1 ± 0.08) exhibited a moderate increase in phagocytosis than untreated macrophages (phagocytic index: 1.45 ± 0.34). Corroborating the previous data, treatment with CH-CS PEC resulted in a significant increase in the phagocytic index (4.2 ± 0.32) compared to all other groups (**Fig. 5.9**).
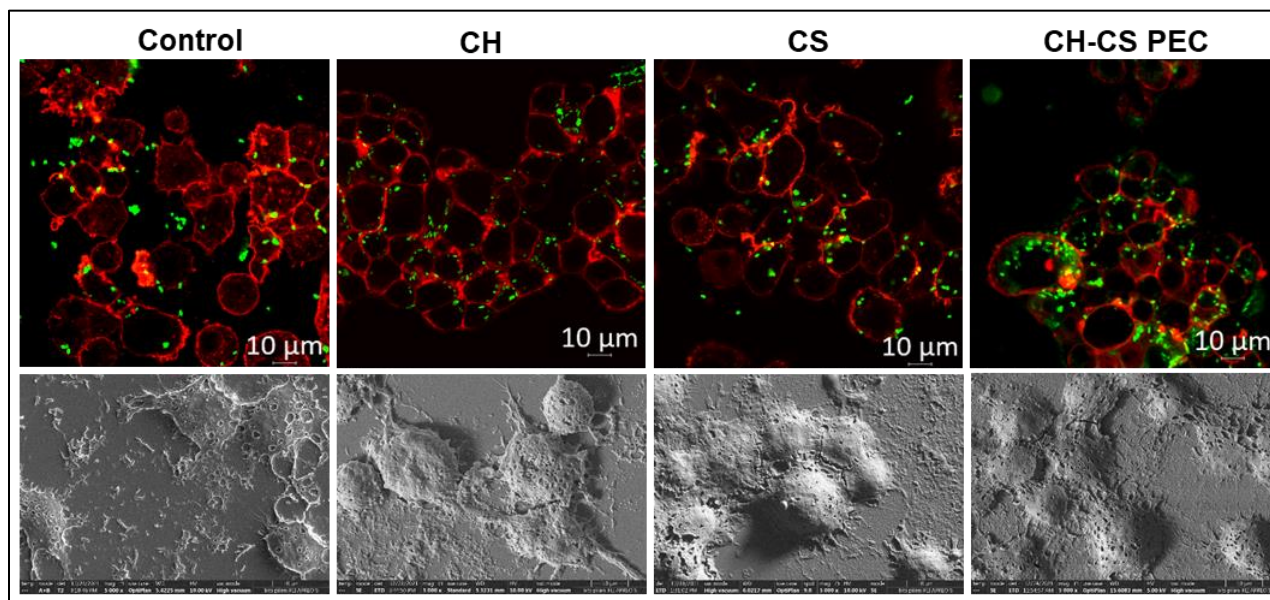
Fig. 5.8 Determination of macrophage activation in *in-vitro* infection model. Fluorescent images and FESEM images of internalization of *GFP E. Coli* to the macrophages (stained with phalloidin)
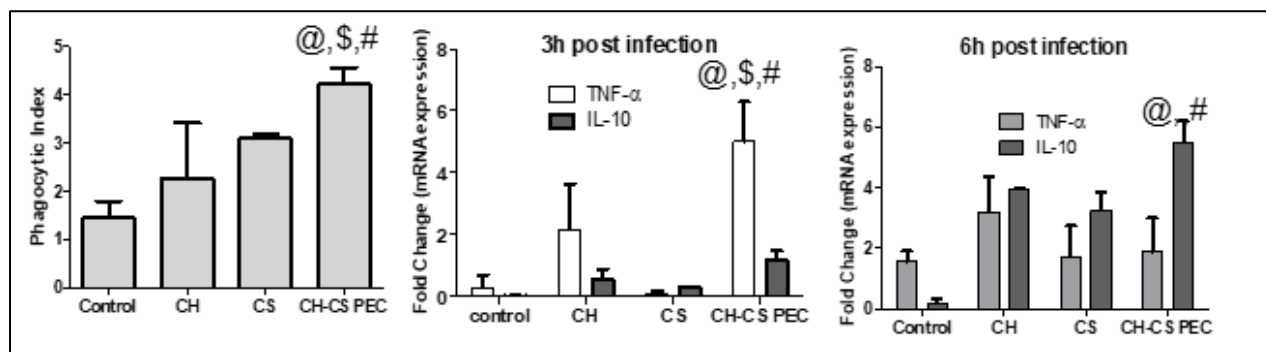
Fig. 5.9 Evaluation of macrophage efficacy in an infected condition. A: Evaluation of Phagocytic index of macrophages post 3h of bacterial exposure. B & C: Evaluation of fold change in mRNA expression of TNF-α and IL-10 in macrophages treated with CH, CS, and CH-CS PEC at 3h and 6h post-infection. Statistical analysis was done using two-way ANOVA with Tukey multiple comparison test. @,$,# denotes p-value < 0.05 compared to Control, CH, and CS.

After observing enhanced phagocytosis, we next wanted to evaluate these macrophages' cytokine profiles to understand their activation and polarization status. Two representative cytokines were selected, TNF-α and IL-10, characterizing M1 and M2 phenotypes. Expressions of these cytokines were evaluated by qRT-PCR analysis after 3h and 6h post-infection with *P. aeruginosa*. The expression was normalized against untreated macrophages not exposed to bacteria. 3h post-infection, a substantial increase in TNF-α was observed with CH-CS PEC treatment (5.0±1.17-fold), compared to CH (2.13±0.56-fold) and CS (0.1±0.07-fold) (**Fig. 5.9**). This data was in agreement with the bacterial internalization data, and indicated macrophage polarization to the M1 phenotype. Surprisingly, there was also a slight increase in the M2 macrophage marker IL10 expression with the CH-CS PEC treatment (1.17±0.30-fold), compared to CH (0.56±0.30-fold), and CS (0.29±0.01-fold) treated macrophages. It has been previously reported that *P. aeruginosa* infection could activate a mixed M1/M2 macrophage phenotype; however, a more robust and prolonged M1 polarization was observed, indicating chronic inflammation [32]. We wanted to determine whether CH-CS PEC treatment can modulate the M1/M2 dynamics with *P. aeruginosa* infection. When expression of M1 (TNF-α) and M2 (IL10) markers was analyzed 6h post-infection, a shift in the cytokine pattern was observed. With CH-CS PEC treatment, expression of M2 marker IL10 increased significantly (5.47±1.15-fold) compared to 3h post-infection (1.17±0.30-fold), whereas TNF-α expression decreased (3h: 5.0±1.2-fold; 6h: 1.87±1.69-fold). This reversal was observed with CH (TNF-α: 3.11±1.363-fold; IL10: 3.78±1.76-fold) and CS (TNF-α: 1.70 ± 1.03-fold; IL10: 3.23±0.61 and) treatments as well; however, the conversion was

milder. This data indicated that CH-CS PEC was better at controlling macrophage-mediated inflammation and could induce the M2 phenotype.
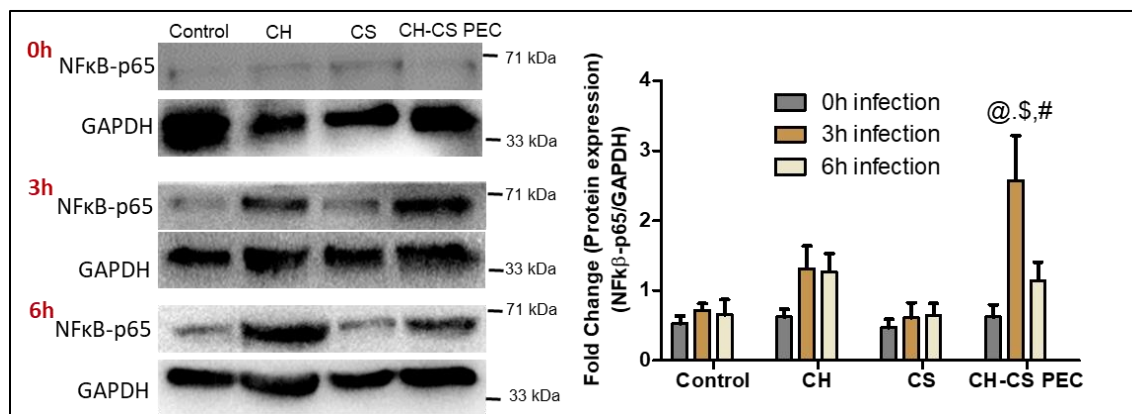
Fig. 5.10 Immunoblotting of NF-κβ-p65 in the macrophages in untreated and treated with CH, CS and CH-CS PEC at 0h(a) and post 3h(b) and 6h(c) of bacterial exposure. Statistical analysis was done using two-way ANOVA with Tukey multiple comparison test. @,$,# denotes p-value < 0.05 compared to Control, CH, and CS.

Further, we performed immunoblotting for NF-κB to confirm the M1/M2 dynamics in the macrophages (**Fig. 5.10**). The NF-κB signaling pathway is associated with M1 polarization [33]. Corroborating with TNF-α/IL10 data, NF-κB expression was found to be highest at 3h post-infection in the CH-CS PEC treated cells (4.5± 1.91) compared to CH (1.71±0.2), CS (1.52±0.45), and untreated macrophages (0.38±0.23). However, at 6h post-infection, it reduced significantly in the CH-CS PEC treated cells (0.84±0.23), whereas, with CH (1.02±0.25) and CS (0.41±0.16), it remained at the same level.

Macrophages help bacterial clearance during infections; however, this could trigger uncontrolled inflammation, leading to impaired healing. Hence, it is important to control inflammation. It has previously been demonstrated that viscoelastic hydrogels can polarize macrophages to an antiinflammatory M2 phenotype with a high phagocytic capacity [4]. Our observation was in agreement with this previous report.

5.3.6 *In-vivo* infection wound model

After demonstrating the antibacterial and antiinflammatory efficacy of CH-CS PEC on macrophages in-vitro, we next studied the effect of CH-CS PEC on the in-vivo infection wound model. The study was performed in Wistar rats with a full-thickness excisional wound of 1×1 cm^2 area. After the wound creation, the wound bed was infected with 10^8 CFU/ml of *Pseudomonas aeruginosa.* The study included three groups: control (untreated), CH-CS PEC, and a marketed chitosan dressing. *In-situ* CH-CS PEC treatment was given through a custom-made double-barreled syringe, with CH solution in one chamber and CS solution in the other chamber. For application, both the pistons of the double-barreled syringe were compressed simultaneously, leading to the ejection of both solutions at the same rate. The solutions were mixed in the wound bed itself, leading to the formation of the *in-situ* scaffold. The wound healing was analyzed by taking images of treated wounds every second day. The bacterial swab was collected every second day before the treatment and was grown on the agar plates to check the bacterial load at the wound bed.

Treatment with CH-CS PEC exhibited faster wound closer. At day 10, the percentage wound closure was calculated to be 96.09±1.63% with in-situ CH-CS PEC, compared to 86.93±0.65% with the marketed product and 83.08±5.96% in the untreated control (**Fig. 5.11 B**). No significant difference was observed between the marketed product and the control, whereas significantly ($p<0.05$) increased wound closure was observed with the CH-CS PEC treatment. This improved wound healing also reduced the bacterial colony count with CH-CS PEC. A consistent decrease in the CFU count was observed with the CH-CS PEC treatment (46.0±23.23), compared to CH marketed dressing (117±72.5) and untreated animal (120±35.21) **(Fig. 5.11C)**. No bacterial colonies were observed post day-6. This could be because after day 6, 50% of the wounds were closed.
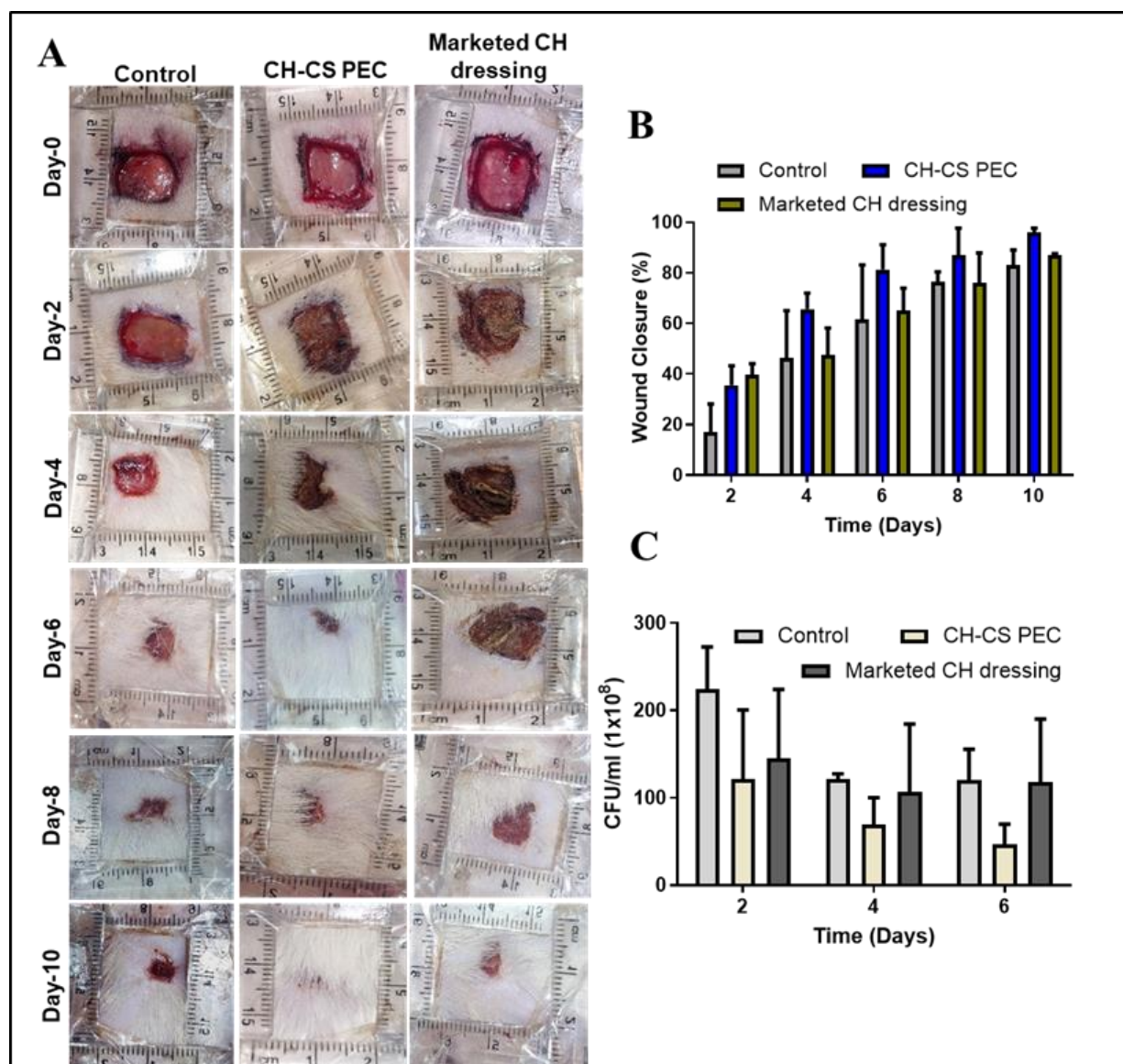
Fig. 5.11 *In-vivo* infection rat wound model. A: *In-vivo* wound healing efficacy in rat infected excisional wound model. B: % Wound closer rate, C: In-vivo bacterial count of the wound exudate at days 2, 4, and 6 post-infection. Statistical analysis was done using 2-way ANOVA with Tukey multiple comparison test. @ denotes p value < 0.05 compared to control, # denotes p value < 0.05 compared to marketed. ns: not significant compared to control.

5.3.7 Histology studies

After confirming efficient wound closure and in-vivo antibacterial efficacy with the CH-CS PEC, histological evaluation of the wounds was performed 5th and 10th-day post-treatment in all the three groups (**Fig. 5.12**). On the 5th day post-treatment, considerable granulation tissue was observed in the CH-CS PEC and marketed CH dressing. The red inflammatory cells (marked as a star) were

observed in high numbers post 5th day of animal sacrifice. However, epidermal tissue was completely absent in the untreated control determining the initial healing progression (Epidermal region marked as an arrow). Reduction in the inflammatory cells was observed in CH-CS PEC in comparison to the marketed dressing and untreated control. The presence of epidermal region (broken epidermis, marked as an arrow) and granulation tissue was observed in untreated and CH-based marketed dressing with the presence of inflammatory cells. However, significantly improved re-epithelization was observed in the animals treated with the CH-CS PEC compared to others.
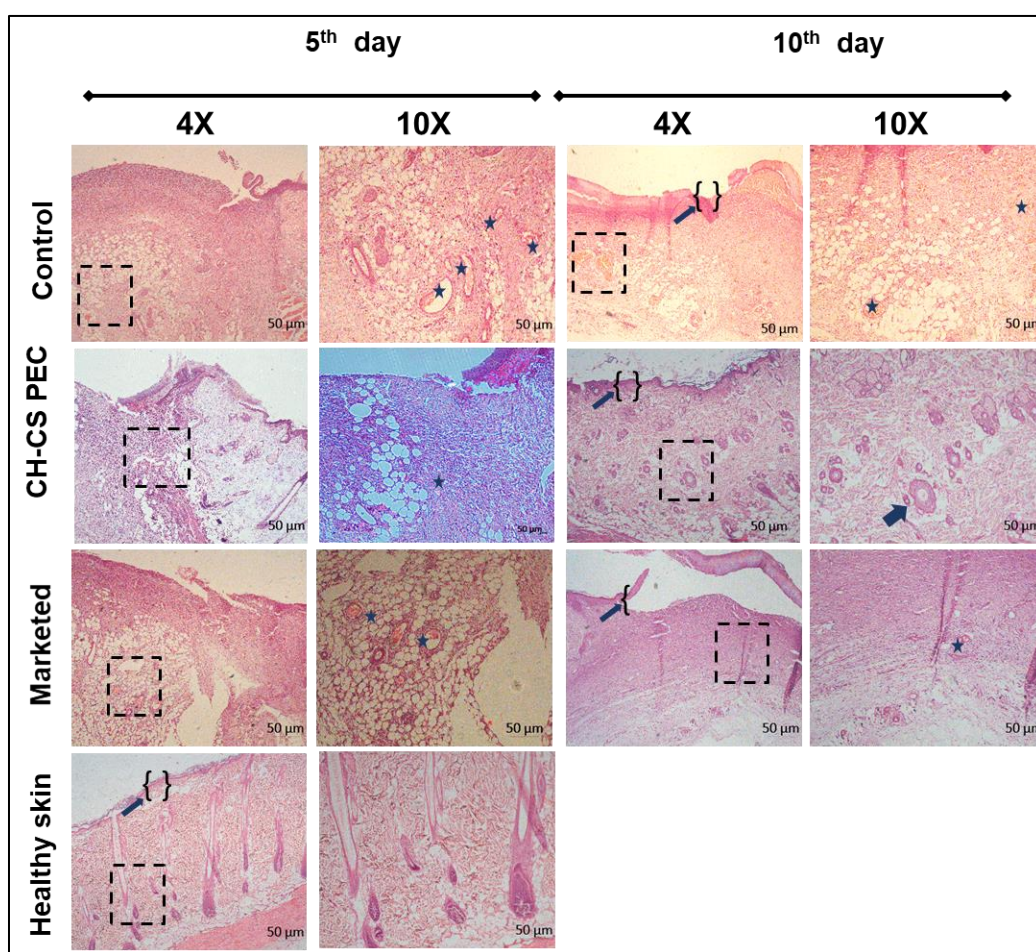
Fig. 5.12 Histopathological evaluation of the skin at 4× and 10× magnification at 5th day and 10th day after the treatment. Star mark depicts the presence of inflammatory cells, and the arrow with a bracket represents the epidermis formation. Arrow depicts the blood vessel, Scale bar 50 μm.

5.3.8 Evaluation of NF-κB expression

The histology analysis depicted effective wound repair with CH-CS PEC compared to marketed CH-based dressing in an infected wound model. As previous experiments indicated modulation of the inflammatory response with CH-CS PEC, *in-vivo* inflammation at the wound site was evaluated by analyzing NF-κB expression by fluorescent microscopy. NF-κB expression was assayed on 5th and 10th day post-infection in all three groups. As depicted in **fig.5.13**, CH-CS PEC-treated group exhibited reduced NF-κB expression at both 5th and 10th-day post-infection compared to other groups. This data indicated that in the *in-vivo* dermal infection model, treatment with CH-CS PEC could reduce inflammation and improve wound healing.
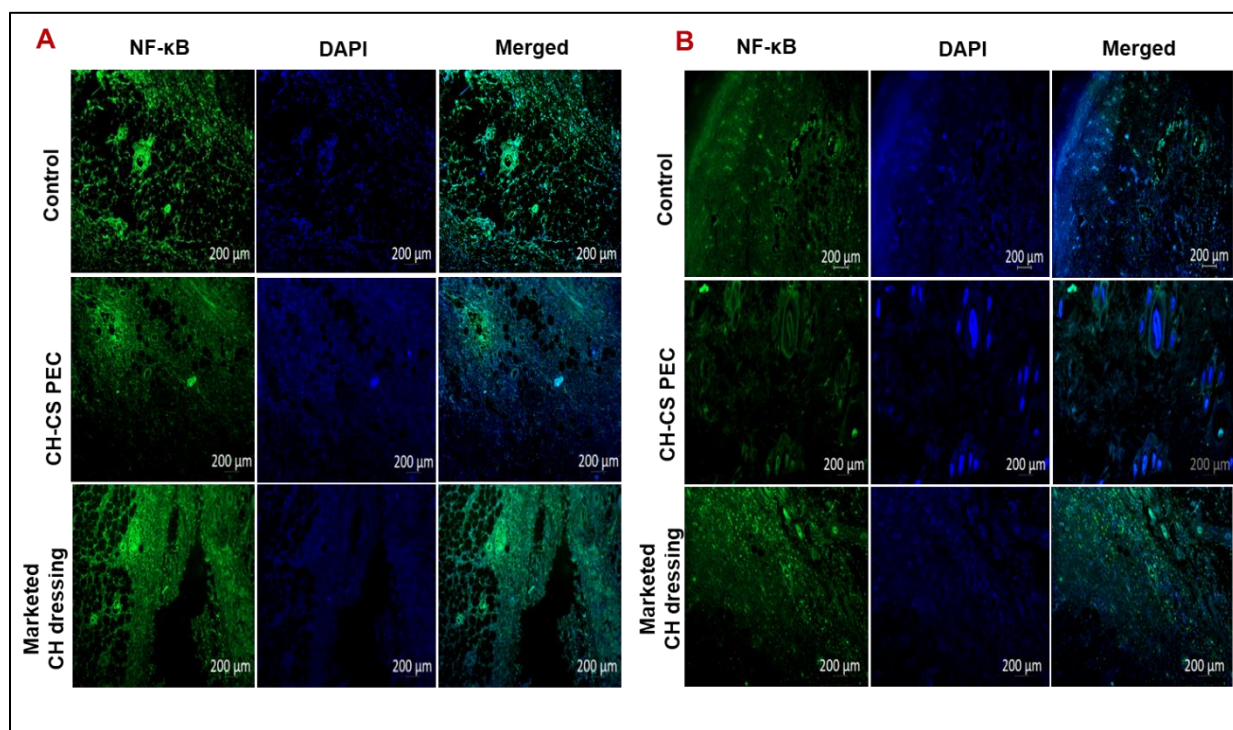
Fig. 5.13 Immunofluorescence imaging in in-vivo skin section at 5th and 10th day of the study foir the evaluation of NF-κβ expression.

5.3.9 Evaluation of VE-cadherin

Endothelial cell adhesion molecules can be the initial sign of the angiogenesis and wound repair process. Vascular endothelial (VE) cadherin is an endothelial cell-specific adhesion molecule located at the junction of the endothelial cells [34]. It maintains the integrity of the endothelial

cells. We evaluated the VE-cadherin expression to mark the formation of the blood vessel 10th day of the wound healing. The data demonstrated significantly higher angiogenesis in CH-CS PEC-treated animals than in the other groups **(fig.5.14)**.
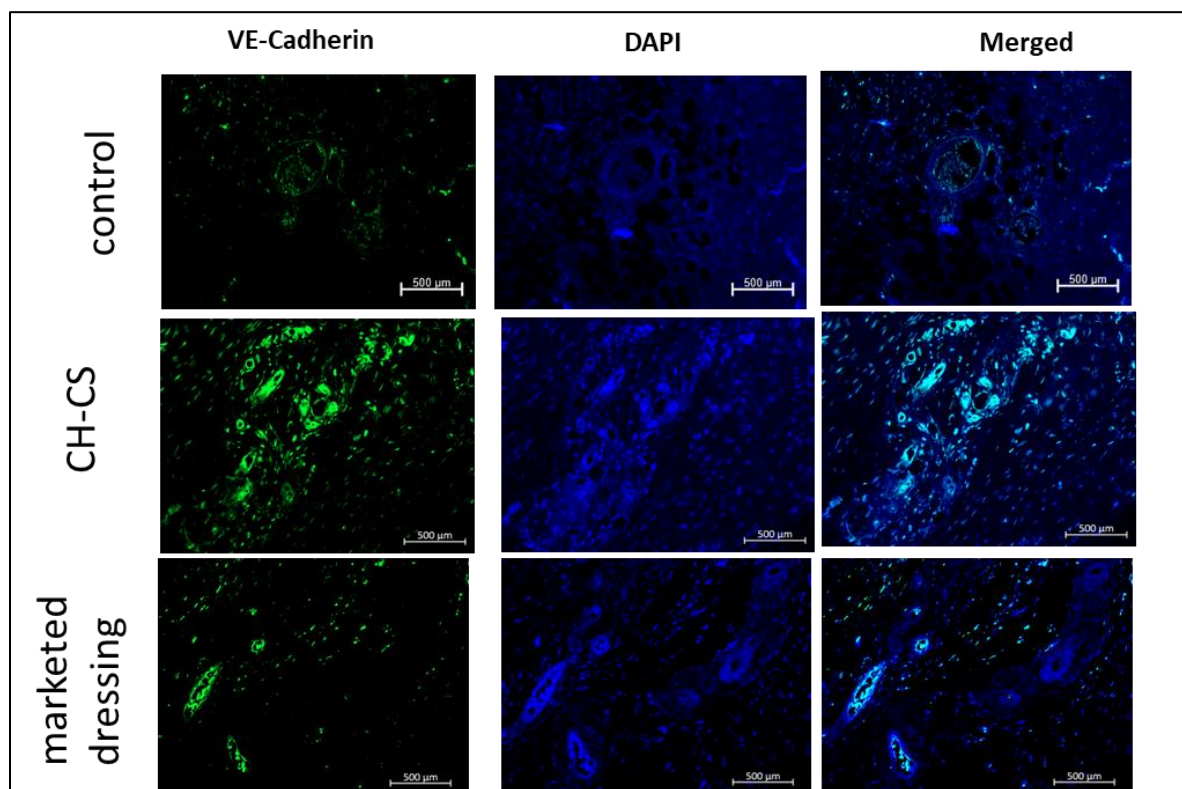
Fig. 5.14 Immunofluorescence imaging in *in-vivo* skin section at10th day of the study for the evaluation of VE-Cadherin.

5.4 Conclusion

Developing a wound dressing that can protect from opportunistic infections, as well as produce a conducive environment for the modulation of macrophage function would be highly advantageous. For both functionalities, direct contact with the respective cells is essential. We have developed an *in-situ* forming, porous, viscoelastic scaffold (CH-CS PEC) that can be directly applied at the wound site, improving its interaction with the wound bed cells. The present study indicated a potent antibacterial activity of CH-CS PEC through membrane pore formation and increased ROS generation in the bacterial cells. Moreover, the scaffold could alter macrophage polarization to an M2-phenotype due to its unique material properties, leading to increased phagocytic activity and

reduced inflammation. Macrophages grown on the CH-CS PEC were less prone to pyroptosis induction, which reduced death when treated with heat-killed bacteria and LPS. Further, considerable improvement in the wound healing rate was observed in the *in-vivo* excision-infection wound model. In histological studies, fewer inflammatory cells were observed in the CH-CS PEC-treated animals compared to a commercially available CH-based dressing and untreated control. The reduced expression of NF-κB at the wound bed substantiated the immunomodulatory effect of CH-CS PEC. Also, significant improvement in vascularization was observed in the CH-CS PEC-treated animals. Altogether, the current study exhibited the influence of the material properties of a scaffold on antibacterial activity and macrophage behavior. This study established that CH-CS PEC has substantial antibacterial activity on its own, as well as it can modulate macrophages to an anti-inflammatory phenotype with enhanced *in-vivo* wound healing efficacy.

References

1. Verbanic, S., et al., *Microbial predictors of healing and short-term effect of debridement on the microbiome of chronic wounds.* NPJ Biofilms Microbiomes, 2020. **6**(1): p. 21.
2. Yang, W.T., et al., *Antimicrobial and anti-inflammatory potential of Angelica dahurica and Rheum officinale extract accelerates wound healing in Staphylococcus aureus-infected wounds.* Sci Rep, 2020. **10**(1): p. 5596.
3. Friedemann, M., et al., *Instructing Human Macrophage Polarization by Stiffness and Glycosaminoglycan Functionalization in 3D Collagen Networks.* Adv Healthc Mater, 2017. **6**(7).
4. Sridharan, R., et al., *Material stiffness influences the polarization state, function and migration mode of macrophages.* Acta Biomater, 2019. **89**: p. 47-59.
5. Sharma, S., K.L. Swetha, and A. Roy, *Chitosan-Chondroitin sulfate based polyelectrolyte complex for effective management of chronic wounds.* Int J Biol Macromol, 2019. **132**: p. 97-108.
6. Yasa, I., et al., *Assessment of antimicrobial activity of nanosized Ag doped TiO(2) colloids.* World J Microbiol Biotechnol, 2012. **28**(7): p. 2531-9.
7. Ong, K.S., Y.L. Cheow, and S.M. Lee, *The role of reactive oxygen species in the antimicrobial activity of pyochelin.* J Adv Res, 2017. **8**(4): p. 393-398.
8. Halder, S., et al., *Alteration of Zeta potential and membrane permeability in bacteria: a study with cationic agents.* Springerplus, 2015. **4**: p. 672.
9. Lema, C., A. Varela-Ramirez, and R.J. Aguilera, *Differential nuclear staining assay for high-throughput screening to identify cytotoxic compounds.* Curr Cell Biochem, 2011. **1**(1): p. 1-14.
10. Chen, H.Y., et al., *Examination of galectins in phagocytosis.* Methods Mol Biol, 2015. **1207**: p. 201-13.
11. Kadam, S., et al., *Bioengineered Platforms for Chronic Wound Infection Studies: How Can We Make Them More Human-Relevant?* Frontiers in Bioengineering and Biotechnology, 2019. **7**.
12. Dai, T., et al., *Chitosan preparations for wounds and burns: antimicrobial and wound-healing effects.* Expert Rev Anti Infect Ther, 2011. **9**(7): p. 857-79.
13. Abedian, Z., et al., *Antibacterial activity of high-molecular-weight and low-molecular-weight chitosan upon oral pathogens.* J Conserv Dent, 2019. **22**(2): p. 169-174.
14. Mori, T., et al., *Mechanism of macrophage activation by chitin derivatives.* J Vet Med Sci, 2005. **67**(1): p. 51-6.
15. Burge, K.Y., et al., *The Protective Influence of Chondroitin Sulfate, a Component of Human Milk, on Intestinal Bacterial Invasion and Translocation.* J Hum Lact, 2019. **35**(3): p. 538-549.
16. Ong, T.H., et al., *Chitosan-propolis nanoparticle formulation demonstrates anti-bacterial activity against Enterococcus faecalis biofilms.* PLoS One, 2017. **12**(3): p. e0174888.
17. Ardila, N., et al., *Antibacterial Activity of Neat Chitosan Powder and Flakes.* Molecules, 2017. **22**(1).
18. Zheng, S., et al., *Implication of Surface Properties, Bacterial Motility, and Hydrodynamic Conditions on Bacterial Surface Sensing and Their Initial Adhesion.* Front Bioeng Biotechnol, 2021. **9**: p. 643722.
19. Valentin, J.D.P., et al., *Substrate viscosity plays an important role in bacterial adhesion under fluid flow.* J Colloid Interface Sci, 2019. **552**: p. 247-257.
20. Sreelatha, S., et al., *Evaluating the Antibacterial Activity and Mode of Action of Thymol-Loaded Chitosan Nanoparticles Against Plant Bacterial Pathogen Xanthomonas campestris pv. campestris.* Front Microbiol, 2021. **12**: p. 792737.

21.   Xia, J., et al., *Superclear, Porous Cellulose Membranes with Chitosan-Coated Nanofibers for Visualized Cutaneous Wound Healing Dressing.* ACS Appl Mater Interfaces, 2020. **12**(21): p. 24370-24379.

22.   Zhu, Y., et al., *Modulation of macrophages by bioactive glass/sodium alginate hydrogel is crucial in skin regeneration enhancement.* Biomaterials, 2020. **256**: p. 120216.

23.   Kumar, M., et al., *Immunomodulatory injectable silk hydrogels maintaining functional islets and promoting anti-inflammatory M2 macrophage polarization.* Biomaterials, 2018. **187**: p. 1-17.

24.   McWhorter, F.Y., C.T. Davis, and W.F. Liu, *Physical and mechanical regulation of macrophage phenotype and function.* Cell Mol Life Sci, 2015. **72**(7): p. 1303-16.

25.   Li, J., et al., *Engineering mechanical microenvironment of macrophage and its biomedical applications.* Nanomedicine (Lond), 2018. **13**(5): p. 555-576.

26.   Chen, M., et al., *Substrate stiffness modulates bone marrow-derived macrophage polarization through NF-kappaB signaling pathway.* Bioact Mater, 2020. **5**(4): p. 880-890.

27.   Jain, N., J. Moeller, and V. Vogel, *Mechanobiology of Macrophages: How Physical Factors Coregulate Macrophage Plasticity and Phagocytosis.* Annu Rev Biomed Eng, 2019. **21**: p. 267-297.

28.   van Furth, R., et al., *Morphological, cytochemical, functional, and proliferative characteristics of four murine macrophage-like cell lines.* Cell Immunol, 1985. **90**(2): p. 339-57.

29.   Mayhew, T.M. and M.A. Williams, *A quantitative morphological analysis of macrophage stimulation. I. A study of subcellular compartments and of the cell surface.* Z Zellforsch Mikrosk Anat, 1974. **147**(4): p. 567-88.

30.   Cha, B.H., et al., *Integrin-Mediated Interactions Control Macrophage Polarization in 3D Hydrogels.* Adv Healthc Mater, 2017. **6**(21).

31.   Bhalla, S., et al., *beta(1)-integrin mediates pressure-stimulated phagocytosis.* Am J Surg, 2009. **198**(5): p. 611-6.

32.   Chen, S., et al., *Pseudomonas aeruginosa infection alters the macrophage phenotype switching process during wound healing in diabetic mice.* Cell Biol Int, 2018. **42**(7): p. 877-889.

33.   Liu, C.P., et al., *NF-kappaB pathways are involved in M1 polarization of RAW 264.7 macrophage by polyporus polysaccharide in the tumor microenvironment.* PLoS One, 2017. **12**(11): p. e0188317.

34.   Vestweber, D., *VE-cadherin: the major endothelial adhesion molecule controlling cellular junctions and blood vessel formation.* Arterioscler Thromb Vasc Biol, 2008. **28**(2): p. 223-32.

Chapter 6

Development and evaluation of simvastatin-loaded CH-CS PEC

6.1 Background

Polymeric hydrogels are suitable carriers for drug delivery because of their high water uptake capacity, porous network, and tunable physicochemical properties [1]. These hydrogels allow the localized release of the therapeutic load at the target site. Many of these hydrogels are formed by covalent cross-links to increase their elasticity. However, this limits its application due to its irreversible nature [2]. Therefore, developing a hydrogel-based carrier with good mechanical strength and viscoelasticity is needed. Hydrogels with self-healing properties could be a potential candidate for topical drug delivery as they can reform their shape at different strains [3].

CH-CS PEC illustrated high water absorption capacity, good viscoelasticity, and self-healing properties (**discussed in Chapter 3**). All these properties mark CH-CS PEC as ideal for drug delivery. In the previous chapters, we estimated CH-CS PEC's functional efficacy on the significant players of wound healing (fibroblasts, keratinocytes, and macrophages) in acute and infected wound models. However, its efficacy on endothelial cells remains unexplored. Therefore, in this chapter, we studied the efficacy of CH-CS PEC and drug-loaded CH-CS PEC on endothelial cells. Angiogenesis is crucial for proper wound healing. The newly formed blood vessels participate in the granulation tissue formation and support the growing tissue by providing nutrition and oxygen [5]. However, in diseased conditions like diabetes, angiogenesis is impaired due to ischemic and hypoxic conditions. Hence, developing an angiogenesis-potentiating therapeutic strategy is a prime need for treating diabetic ulcers. Considering the importance of angiogenesis, we chose Simvastatin (SIM) as a model drug for loading into CH-CS PEC. Statins are well-recognized as lipid-lowering drugs; however, recent reports demonstrated their role as a pro-angiogenic molecule in ischemic injury [7] and wound healing [6]. Statins enhance angiogenesis by activating ENOS/AKT pathway, resulting in increased expression of vascular endothelial growth factor (VEGF) [8]. Multiple studies suggested that SIM's pleiotropic wound healing effect, including anti-inflammatory activity, improved endothelial function and the healing process [9].

In the present study, in order to incorporate the hydrophobic drug SIM in the hydrophilic CH-CS PEC, we developed SIM-loaded Soluplus-vitamin E TPGS micelles. Simvastatin is a BCS class-II drug having a log P of 4.8. Few studies have demonstrated the application of SIM topically for wound healing [10, 11]. However, these studies used a single amphiphilic polymer to make the

micelle. Single polymer-based polymeric micelles lack stability due to a limited number of building blocks, leading to low drug loading. The development of mixed micelles can address this issue. Mixed micelles are nano-carrier composed of a combination of block copolymers, or copolymers and surfactants, to significantly improve drug loading [12]. In the current study, we have developed Soluplus (S)-Vitamin E TPGS (TPGS) based mixed micelles for SIM delivery. Similar mixed-micelles have previously been reported for loading other poorly water-soluble drugs [13, 14].

6.2 Materials and Methods

Simvastatin was procured from Carbosynth and Soluplus from BASF, Mumbai, India. CH and CS were purchased from SRL Pvt Ltd and Tokyo Chemicals Industry. HPLC-grade acetonitrile and acetone were purchased from SD Fine-Chem Limited, Mumbai, India. All other chemicals, solvents, and reagents used for HPLC analysis were either of HPLC grade or analytical grade. HPLC analysis was performed on a Shimadzu liquid chromatography system (Kyoto, Japan) consisting of LC10AT binary pump, SPD-M20A Photo Diode Array detector, CTO-10ASP column oven, and SIL-HT autosampler. Zodiac RP-18 column was used for the HPLC. Matrigel was procured from Merck. Penicillin-Streptomycin (10,000 U/mL) (#15140122), Prolong™ Gold Antifade Mounted with DAPI (4′,6-diamidino-2-phenylindole) (#P36935), were purchased from ThermoFisher Scientific, USA.

6.2.1 Determination of critical micelle concentration

The formation of mixed micelles was confirmed by determining the CMC of S-TPGS conjugate in an aqueous solution by fluorescence spectroscopy using pyrene as a probe. Mixed micelles of S-TPGS in different ratios (4:0, 4:1,3:2,2:3,1:4,0:4) at concentrations ranging from 0.00125 mg/mL to 3.2 mg/mL were mixed with pyrene solution (6×10^{-7} M) and incubated for 24h at with shaking at RT. The fluorescence intensity of the solution was recorded using a spectrofluorimeter (RF-5301 Shimadzu, Japan) at excitation and emission wavelengths of 300–400 nm and 390 nm, respectively. Plot was constructed between I_1/I_3 *versus* the logarithm of S-TPGS micelles concentration wherein the I_1, and I_3 values were determined from the shifting of peak intensities at the wavelengths of 375 and 392 nm [19].

6.2.2 Development of SIM micelles and SIM micelles loaded CH-CS gel

Simvastatin micelles were prepared by the thin film hydration method. SIM, TPGS, and Soluplus were solubilized in acetone in different weight ratios. The micelles were prepared by using Soluplus (S) and Vitamin E TPGS (TPGS). The polymers were taken in different ratios of 4:1, 1:4, 2:3, and 3:2 of S to TPGS. The polymer solution of different ratios was mixed in a SIM-to-polymer ratio of 1:10 ratio (**50mg batch**). The mixture of polymers and SIM was solubilized in acetone (10 ml), and the solution was dried under a vacuum using a rotary vacuum evaporator. Further, the SIM-polymer film was re-suspended in water (10 ml) under magnetic stirring for 2h, and size reduction was performed using the ultrasonication process (1 min at 30% amplitude).

6.2.3 Fabrication of CH-CS polyelectrolyte complex (PEC) and loading of Simvastatin micelles to CH-CS scaffold

CH-CS PEC was prepared using polyelectrolyte complexation technology. Briefly, 5% w/v of CH solution was prepared in 1% v/v of glacial acetic acid. The CH gel was further dialyzed against Milli-Q for 12h. 5% w/v solution of CS was prepared in Milli-Q water. SIM micelles loaded CH-CS PEC was prepared by mixing CH and SIM micelles initially. The 5% w/v CS solution was mixed with CH-SIM micelles to develop SIM micelles loaded CH-CS PEC.

6.2.4 Measurement of Simvastatin by HPLC method

HPLC analytical method for measuring the Simvastatin entrapment efficiency and release profile of the CH-CS loaded micelles. A reverse phase isocratic analytical method was developed for the estimation of SIM. Zodiac RP C-18 column was used as the stationary phase, while the mobile phase was 85:15 acetonitrile to Potassium dihydrogen phosphate buffer (pH 4.2). A flow rate of 1ml/min and sample injection volume of 20 µl with a run time of 10 minutes provided a sharp drug peak at 238nm with a retention time of 7.8 minutes. The linearity was observed from 0.5-16 µg/ml.

6.2.5 Physicochemical characterization of the SIM micelles

Particle size and Polydispersibility index were analyzed by dynamic light scattering (DLS) using Malvern Nano ZS (Malvern's instrument Ltd., UK) at 25 °C. The morphology of the micelle was analyzed by Scanning Electron Microscopy (SEM). Micelle suspension was placed on a glass

coverslip and air-dried. The sample was further sputter coated with gold, and the morphology was examined using SEM.

The entrapment efficiency was evaluated by centrifuging 1ml of the prepared micelles at 17500 RPM for 30 minutes. After centrifugation, the supernatant was removed and the micellar pellet was solubilized in 1ml of acetonitrile. The sample was vortexed for 10 minutes and was analyzed using the developed HPLC method.

%EE = (weight of the drug in the micelles / initial weight of drug) $\times$ 100

6.2.6 *In vitro* drug release profile

The in-vitro drug release was performed using the Franz diffusion cell apparatus. Briefly, 200 μl of the SIM-loaded CH-CS PEC was kept in the donor compartment. The dialysis membrane (snake skin-HiMedia) was used for separating the donor and the receptor compartment. The phosphate buffer pH 7.4 containing 1% tween 80 was used as dissolution media in the study. A total 20 ml volume of the dissolution media was used for the study. Samples of 1 ml volume were collected at respective time points from 0.25, 0.5, 1, 3, 6, 12, 24, and 48h. Further, the dissolution release model fit was performed using DD solver software.

6.2.7 Rat aortic ring assay for the determination of angiogenesis

The aortic ring assay demonstrates the formulation's angiogenic potential by observing endothelial cells sprouting from the isolated rat aorta embedded in the formulation. The protocol was performed to study the Simvastatin-loaded CH-CS gel's angiogenesis potential. The experiment was studied in three groups, CH-CS scaffold, SIM-loaded CH-CS scaffold, and Matrigel- ECM matrix gel as a positive control. Endothelial cell sprouting demands the presence of a 3D environment for growth. SIM as a treatment group alone was excluded due to this reason. Initially, 100μl of CH-CS and 0.5μM Simvastatin loaded CH-CS gel was prepared in a 24-well plate (dose was optimized from the experiments 0.5-1 and 2 μM SIM concentration). Matrigel was used as a positive control for the study. Following euthanasia, the rat's thoracic aorta was isolated, separating the heart, lungs, and other organs. Further, the excess fat layer was removed with the blade and cut into fine sections of 1-2mm in width. The sections were then placed in the CH-CS gel SIM-loaded CH-CS gel and Matrigel. The embedded aortic rings were incubated for 1h. After 1h incubation, the rings were suspended with 500 μl of the endothelial cell-specific media. The media

change was given every alternate day, supplementing SIM (0.5 µM) to the media. The study was continued for seven days. The gel-embedded aortic rings were observed microscopically to evaluate the endothelial cell sprouting.

6.2.8 Development of *in-vivo* diabetic wound model

All the animal studies were performed in accordance with the Animal ethics committee. Streptozotocin (STZ) was used for inducing diabetes. STZ was solubilized in 10 mM sodium citrate buffer pH 4.5. Briefly, Wistar rats weighing 180-200 gms were given a single intraperitoneal dose of STZ (40 mg/kg). The blood glucose level was monitored after the 4th day of the STZ injection using an AccuChek-Active glucometer (AccuChek). Animals showing fasting blood glucose of >250 mg/dl were considered for the development of the excision wound model. The wound was created on the animals after 7th day of STZ dose. Four wounds of 0.8x0.8 cm^2 area were created on each animal. The study was executed with four treatment controls, Untreated, SIM-treated, CH-CS PEC, and CH-CS (SIM) PEC. Before the wound creation, the fasting blood glucose level of the animals was monitored. The treatment was changed every alternate day, and data was recorded by taking an image of the wound bed. The animals were sacrificed on day 5th and day 10th for Histology and immunostaining studies.

6.2.9 Histology study

Representative animals from each group were sacrificed on day 5 and day 10; their skin from the wound area was fixed, paraffin-embedded, sectioned, and stained with H&E dye. H&E staining was used to determine the cellular morphology and skin integrity. The stained sections were examined under brightfield microscopy. The images were taken at 4× magnification.

6.2.10 Estimation of total collagen

Representative animals from each group were sacrificed on day 5 and day 10. Their skin from the wound area was fixed, paraffin-embedded, sectioned, and stained for total collagen content evaluation. Masson trichrome staining was performed to determine the mechanical integrity of the newly formed skin. The stained sections were examined under bright field microscopy. The images were taken at 4× magnification.

6.2.11 Immunostaining of VEGF protein

Immunohistochemically analysis of VEGF was performed in the skin sections. The sections were dewaxed and rehydrated. Antigen unmasking was performed by heating the sections in the citrate buffer (pH 6.0) in a water bath at 80°C for 15 min. Further, the samples were incubated with 3% hydrogen peroxide to quench endogenous peroxidase for 10 minutes. For IHC staining, the samples were washed and blocked with 5% w/v of bovine serum albumin in Tris Buffered Saline with Tween 20 for 2h. Further, the sections were incubated with VEGF primary antibody (1:500) at 4°C overnight. The sections were washed and incubated with HRP-conjugated secondary antibody (1:1000) for 2h at room temperature. The color was developed using the DAB substrate (CST). Further, the sections were counterstained with hematoxylin and mounted. The image quantification was done using the method reported by Crowe et al., using the image J color deconvolution method [20]. The area fraction of the healthy skin was considered as the standard for the % estimation.

6.2.12 Statistical analysis

The data were analyzed using GraphPad Prism software version 8. Comparison among data sets was statistically determined using one-way or two-way ANOVA; post hoc Tukey's test was performed to compare each group's means with every other group. Data were represented as mean ± SD.

6.3 Results and discussion

The SIM micelles were developed to incorporate hydrophobic SIM in a hydrophilic matrix. Polymeric micelles as a drug carrier is very well documented [21, 22]. However, simple micelles exhibit stability issues and show burst release of the drug. Various strategies are studied to increase the stability of the polymeric micelles [23]. One such strategy is by reducing its critical micelle concentration (CMC) value [24]. One of the strategies to reduce CMC is the development of mixed micelles. W developed mixed micelles of Soluplus and Vitamin E TPGS in different ratios. Soluplus is polyvinyl caprolactam–polyvinyl acetate–polyethylene glycol graft copolymer. It improves the solubility of poorly water-soluble drugs [25]. On the other hand, TPGS is an amphiphilic polymer having the ability to improve the absorption of the drug. Along with its

efficacy as an efficient absorption enhancer [26], it has also shown its biological effect in the skin wound healing.

6.3.1 Determination of CMC

In the present study, we explored the development of SIM-loaded mixed micelles made up of Soluplus and Vitamin E TPGS. TPGS is an amphiphilic polymer having enhanced skin penetration and application in topical drug delivery [27, 28]. On the other hand, Soluplus is a block copolymer having low critical micelle concentration. Soluplus is well-documented as a carrier for topical drug delivery [29]. Both Soluplus and TPGS were used to develop mixed micelles loaded with SIM. Mixed micelles are developed by a combination of an amphiphilic surfactant and graft copolymer or two graft polymers [30]. **Fig. 6.1** demonstrates the CMC determination of S-TPGS micelles in different ratios. Amongst all the ratios, S-TPGS micelles (4:1) depicted the lowest CMC value (0.05mg/ml). Fig. **6.1 (A & B)** illustrates the spectra for pyrene-loaded S-TPGS micelles (4:1) and the plot of I1/I3 vs. logarithmic concentration of S-TPGS (4:1) micelles. The CMC values of the uni polymers and the other S-TPGS combination are illustrated in **Fig 6.1(C)**.
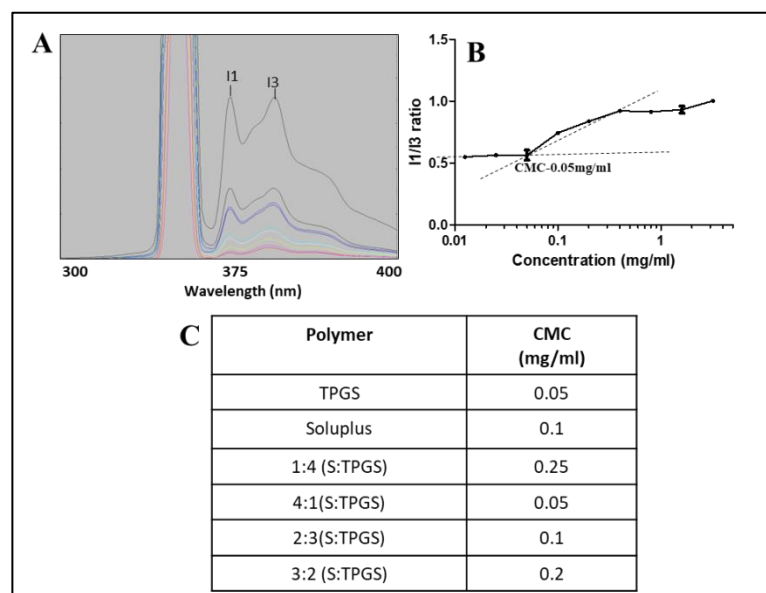

Polymer	CMC (mg/ml)
TPGS	0.05
Soluplus	0.1
1:4 (S:TPGS)	0.25
4:1(S:TPGS)	0.05
2:3(S:TPGS)	0.1
3:2 (S:TPGS)	0.2

Fig. 6.1 CMC determination of S-TPGS mixed micelles

6.3.2 Development of Simvastatin polymeric micelles

Simvastatin-based mixed micelles were developed using Soluplus and vitamin E TPGS for loading Simvastatin, a poorly water-soluble drug. Soluplus is recognized for the solubility enhancement of BCS Class-II drugs [34]. Hence we developed Simvastatin-loaded Soluplus-TPGS mixed micelles to enhance the drug's aqueous solubility. The different ratios (4:0, 3:2, 2:3,1:4,0:4) of Soluplus-TPGS micelles loaded with SIM were prepared using the thin film hydration method, and the ratio of Soluplus to TPGS was selected based on its particle size and entrapment efficiency. Further, the optimized micelles were loaded into the CH-CS PEC for the controlled and prolonged release of SIM.

6.3.3 Determination of particle size and Polydispersibility index

Particle size and distribution of the drug-loaded nano-carriers is the crucial parameter that may affect the biological efficacy of the drug. In the current study, the particle size distribution and polydispersity index (PDI) were evaluated to study the impact of the Soluplus to TPGS ratio on the stability of the nanoformulation. The particle size (Z_{avg}) and PDI were evaluated using a Malvern zeta sizer. **Table 6.1** demonstrates the particle size and PDI of the SIM micelles prepared in different ratios. The size of the pure Soluplus and the pure TPGS showed a small size. However, the PDI was too high, depicting the low stability of the micellar system. However, the combination of the micellar system with an increased proportion of Soluplus gave the smallest size with the low PDI, demonstrating the acceptable formation of micelles. A similar kind of micellar system was applied for paclitaxel loading, and Similar behavior was observed in a previous study [14]. Further, the size and morphology of the stable micellar system (4:1) were evaluated by FESEM. The FESEM depicted the average particle size of 89.53 nm (**Fig. 6.2**), corroborated with the dynamic light scattering data.

Table. 6.1 Particle size, polydisperisbility index and encapsulation efficiency of the SIM micelles prepared from different ratios of S-TPGS.

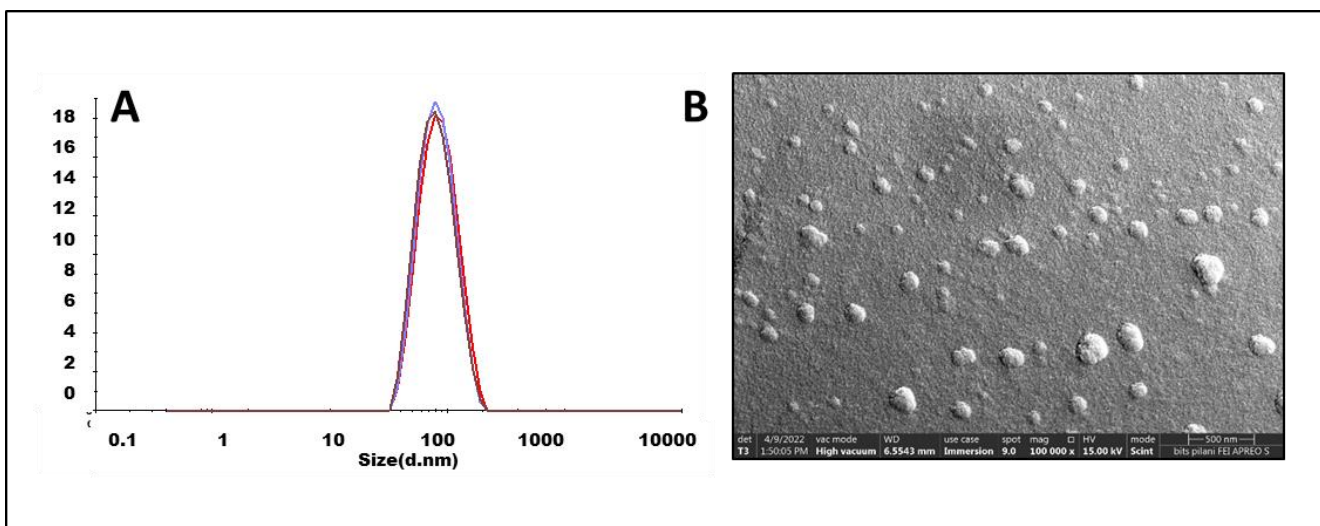| Sr. No.	S-TPGS ratio	Particle size (nm)	Polydispersibility Index	Encapsulation efficiency (%)
1.	4:0	198± 9.03	0.345±0.03	53.02± 2.74
2.	4:1	76.63±2.33	0.105±0.09	86.66±2.55
3.	3:2	93.25±1.44	0.18±0.01	42.89±8.48
4.	2:3	231±9.44	0.352±0.12	32.63±8.44
5.	1:4	293±15.7	0.44±0.02	31.27±1.96
6.	0:4	45.5±4.35	0.435±0.03	47.03±2.55

Fig. 6.2 A) Particle size distribution graph of S: TPGS (4:1) mixed micelles, B) FESEM image of 4:1 S: TPGS micelles.

6.3.4 Determination of Simvastatin encapsulation efficiency

Next, drug encapsulation efficiency was evaluated to select the optimum ratio of Soluplus to TPGS. Simvastatin was detected using the HPLC method. The mobile phase used was 85:15 of acetonitrile-10mM dihydrogen potassium phosphate buffer pH 4. The retention time was 7.4 minutes with a 1 ml/min flow rate. The linearity range was obtained between 0.5 and 16 μg/ml.

The encapsulation efficiency of different Soluplus-TPGS mixed micelles was compared with that of the pure Soluplus and TPGS micelles (**Table 6.1**). The mono-polymeric micelles showed better entrapment efficiency compared to all other ratios except 4:1. The S-TPGS (4:1) micelles exhibited 86.66±2.55 % drug encapsulation. The increased drug entrapment and reduction in the CMC value with the micelles prepared with 4:1 S-TPGS ratio depicted the optimum stability of the micellar system [14, 35].

6.3.5. *In-vitro* drug release kinetics

Polysaccharide-based gels are efficient carriers for the controlled release of nanoformulations. In our study, we have developed SIM-loaded mixed micelles. After determining the physiochemical parameters of the mixed micelles, we wanted to check the in-vitro drug release of SIM from these micelles and micelle-loaded CH-CS PEC. The micelle-loaded CH-CS PEC was prepared by mixing it with CH, which was then mixed with CS solution to make the CH-CS (SIM) PEC. The

release study was performed with four experimental groups, SIM solution, SIM micelles, and SIM loaded in CH-CS PEC and CH-CS (SIM) PEC. The release study was performed in a Franz diffusion cell and was conducted for 48h with 20 ml of dissolution media volume (1% Tween 80 in PBS). SIM showed 96.47% cumulative release in 3h, whereas, with SIM-loaded micelles, the drug release rate decreased to 72.15 % in 3h. Directly loading SIM solution in the CH-CS PEC also resulted in a quick release: in 3h, 98% cumulative release was observed. The slowest and controlled release of SIM was observed with the CH-CS (SIM) PEC (**Fig. 6.3**). In 3h, it exhibited ~40% drug release and followed a uniform release kinetics till 48h (**Fig. 6.3**). At 48h, the cumulative release was found out to be 87.29 %. Further, the release kinetics model was analyzed using the DD solver. The release of SIM from CH-CS (SIM) PEC was found to follow the Koremeyer-Peppas model (R2- 0.9541 and n=0.24), illustrating diffusion-controlled release. Self-healing hydrogels have previously been used as a carrier for drug delivery. These gels prolong the release because of the interpenetrating networks and their 3D structure. The extensive porous network observed in CH-CS PEC could be a reason for the slow release of micelles from the CH-CS PEC (**Fig. 6.3**).
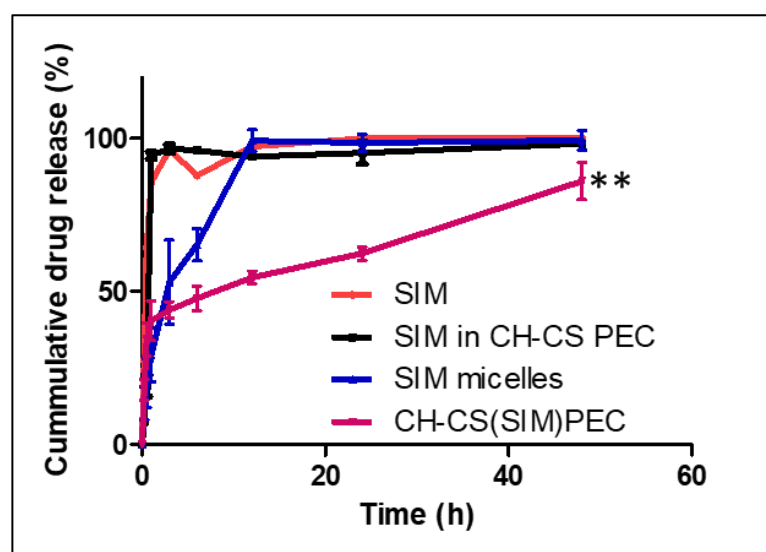
Fig. 6.3 In-vitro Simvastatin release when loaded in CH-CS PEC and its comparison with SIM, SIM loaded CH-CS PEC, and SIM micelles.

6.3.6 *Ex-vivo* angiogenesis study: Evaluation of the angiogenic potential of Simvastatin in the SIM-loaded CH-CS PEC

Angiogenesis is one of the crucial steps involved in the wound-healing process. Developing new blood vessels helps form microvascular networks surrounding the granulation tissue. However,

reduced angiogenesis and damaged microvasculature are observed in the diabetic wound and pressure ulcers [36]. The role of Simvastatin in the angiogenesis process has been reported earlier [37]. Simvastatin synthesizes and releases VEGF, which supports angiogenesis and microvascular network formation [38]. The rat aortic ring assay was performed to evaluate the pro-angiogenic potential of CH-CS (SIM) PEC. The rat aortic ring is an *ex-vivo* angiogenesis model that allows for the easy determination of the sprouted blood vessels. The critical criterion for the assay is the presence of ECM which could provide the 3D environment for developing the new endothelial cells.
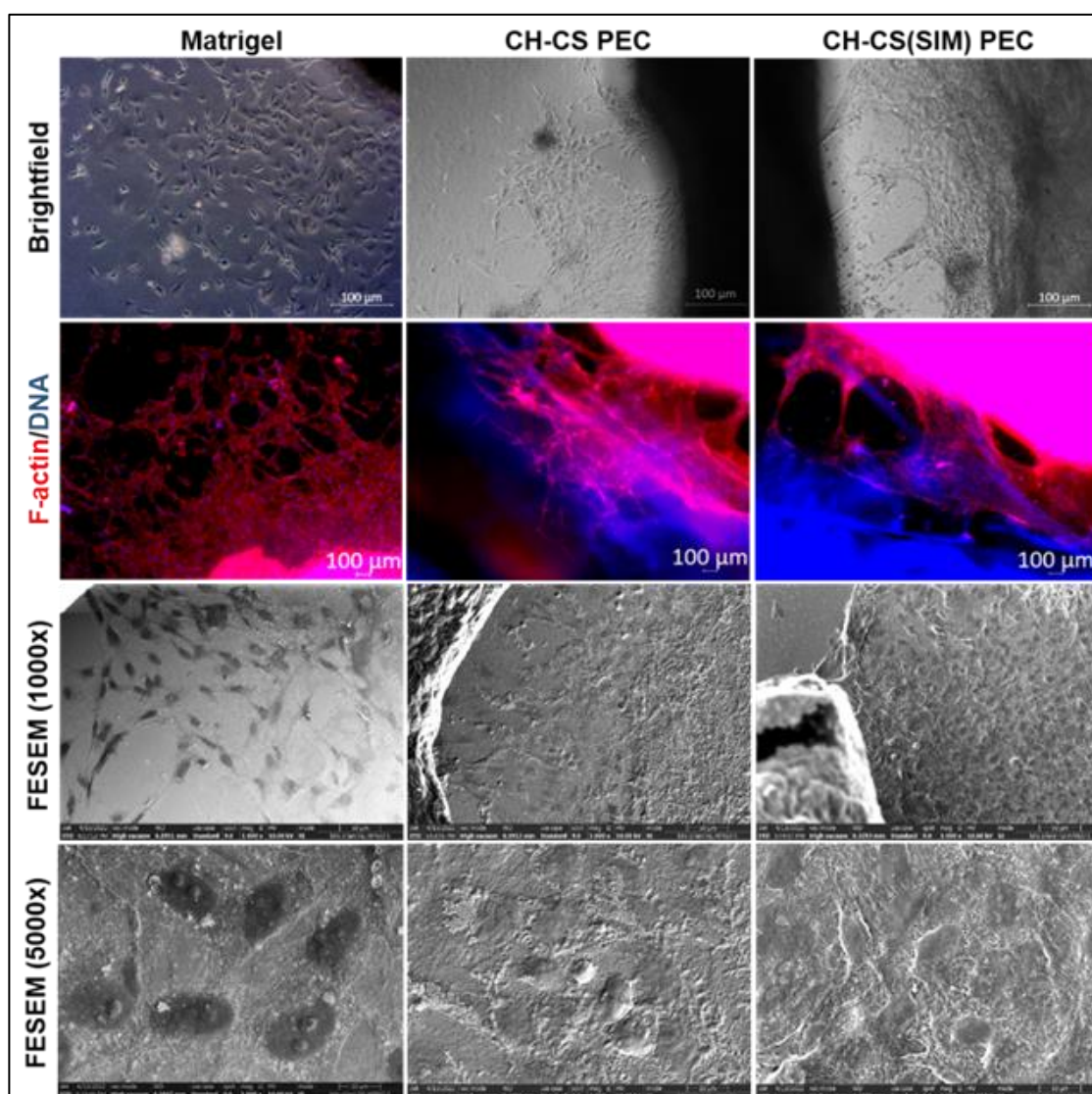

Fig. 6.4 *Ex-vivo* rat aortic ring assay for determination of the angiogenic potential of Simvastatin. Brightfield, F-actin, and FESEM images of the sprouted endothelial cells after seven days of culture in Matrigel CH-CS PEC and CH-CS (SIM)PEC.

We evaluated the angiogenic potential of SIM by embedding the rat aortic ring in the CH-CS (SIM) PEC scaffold (**Fig. 6.4**). In the previous chapter, we reported the viscoelastic property of the CH-CS PEC, which could provide the conducive environment for the sprouting of the rat aorta. SIM was given in 0.5μg/ml dose as reported in the literature [39]. The aortas were observed for 7 days. The brig field images demonstrated enhanced sprouting in the ring embedded in CH-CS (SIM) PEC, demonstrating its angiogenic potential. Surprisingly, the aortic ring embedded in the simple CH-CS PEC also showed enhanced sprouting, showing the angiogenic capability of the CH-CS PEC alone. Aorta embedded in the Matrigel, which was taken as a positive control in this study, exhibited lower sprouting. The blood vessel sprouting was further confirmed by staining the cells with Phalloidin. Further, the morphology was confirmed by the FESEM microscopy (**Fig. 6.4**). Phalloidin staining and SEM analysis corroborated the microscopic data that CH-CS (SIM) PEC had the highest angiogenic potency among all the groups.

6.3.7 *In-vivo* chronic diabetic model development

Understanding the angiogenic potential of CH-CS (SIM) PEC from the *ex-vivo* rat aortic ring assay, we evaluated the wound healing efficacy and angiogenic potential of the CH-CS (SIM) PEC in a diabetic rat excision wound model. Diabetes was induced by giving a one-time dose of streptozotocin (40 mg/kg) intra-peritoneally to the Wistar rats. After seven days of STZ dose, the animals' glucose levels were between 300-450mg/dl. After the 7th day of STZ, a wound of 1×1 cm^2 area was created on the animal. Total of 4 wounds were created on each animal, and were treated with saline, SIM solution (50 μg/ml), CH-CS PEC, and CH-CS (SIM) PEC on each wound on the same animal. This was done to minimize the biological variation in diabetic rats. The wound healing was analyzed by taking images of the wounds every second day. Significantly faster wound closure was observed in the CH-CS (SIM) PEC compared to others (**Fig. 6.5**). The percent wound closure was evaluated using ImageJ software. On day 10, the percent wound closure was found to be 97.43 ±0.36% with CH-CS (SIM) PEC, compared to 91.94±2.35% with CH-CS PEC, 80.99±4.49% with native SIM solution, and 77.46±6.75% with saline treatment. More than 50% wound closure was observed on day 4 with the CH-CS (SIM) PEC compared to other treatment controls.
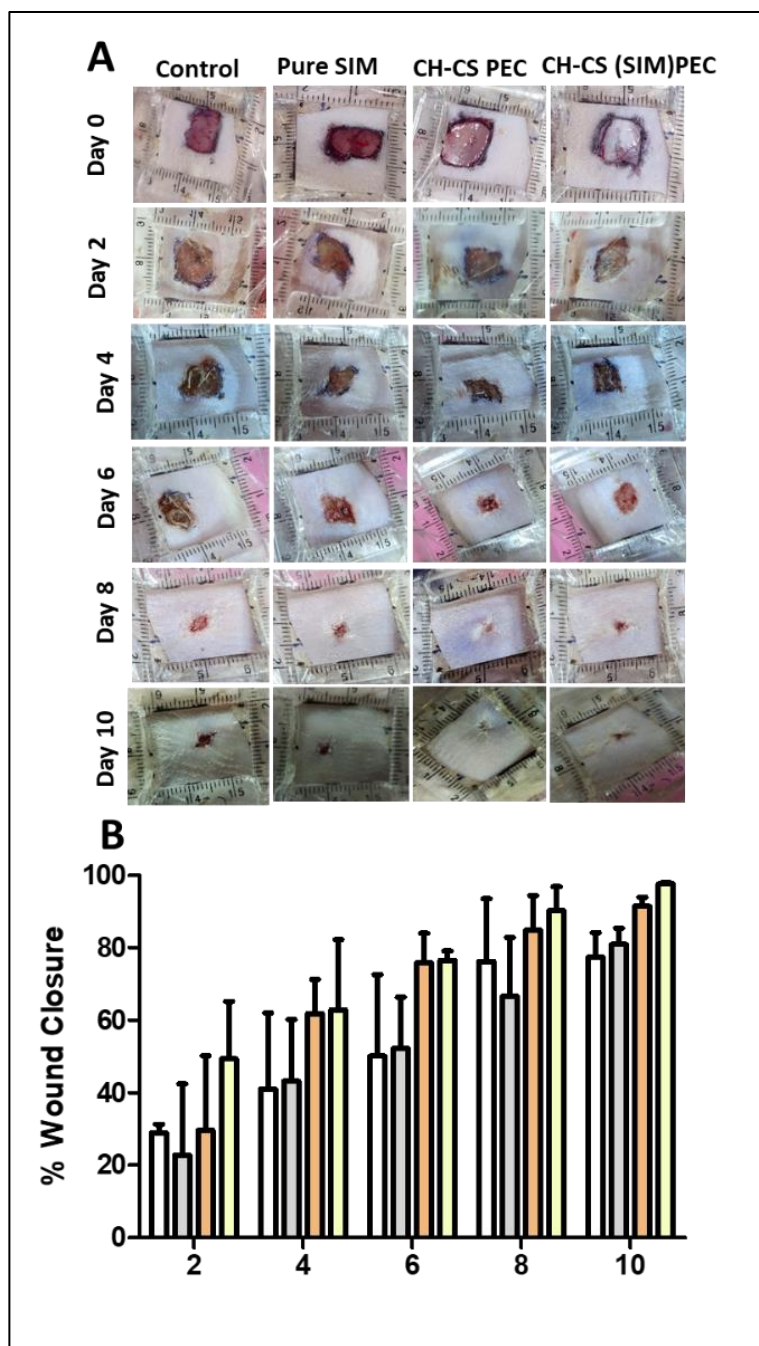
Fig. 6.5 A: *In-vivo* wound healing efficacy in chronic rat excisional wound model. B: % wound closer rate with different treatments.

6.3.8. Histology study

After confirming efficient wound closure with the CH-CS (SIM) PEC, histological evaluation of the wounds was performed 5 days and 10 days post-treatment in the four groups. On the 5th day post-treatment, a considerable amount of granulation tissue was observed in all the groups except the control, suggesting initiation of healing in the three groups. The control group exhibited the

presence of granulation tissue as late as day 10, while the other three groups showed the presence of neo-epidermis formation and a healed dermal layer on the 10th day. Significantly improved re-epithelization was observed in the animals treated with the CH-CS PEC scaffold and CH-CS (SIM) PEC group compared to the SIM-treated group. Blood vessels were observed in CH-CS PEC and CH-CS(SIM) PEC highlighting the angiogenic potential of the treatment (blood vessels marked with star) (**Fig. 6.6**).

Fig. 6.6 Histopathological evaluation of the skin at 4× and 10× magnification at 5th day and 10th day after the treatment. Scale bar 50 μm. Scale bar 200 μm.

6.3.9 Determination of total collagen content

We examined the total collagen concentration by performing the Masson trichome staining in the animal skin collected on day 10 post-treatment (**Fig. 6.7**). The collagen fibr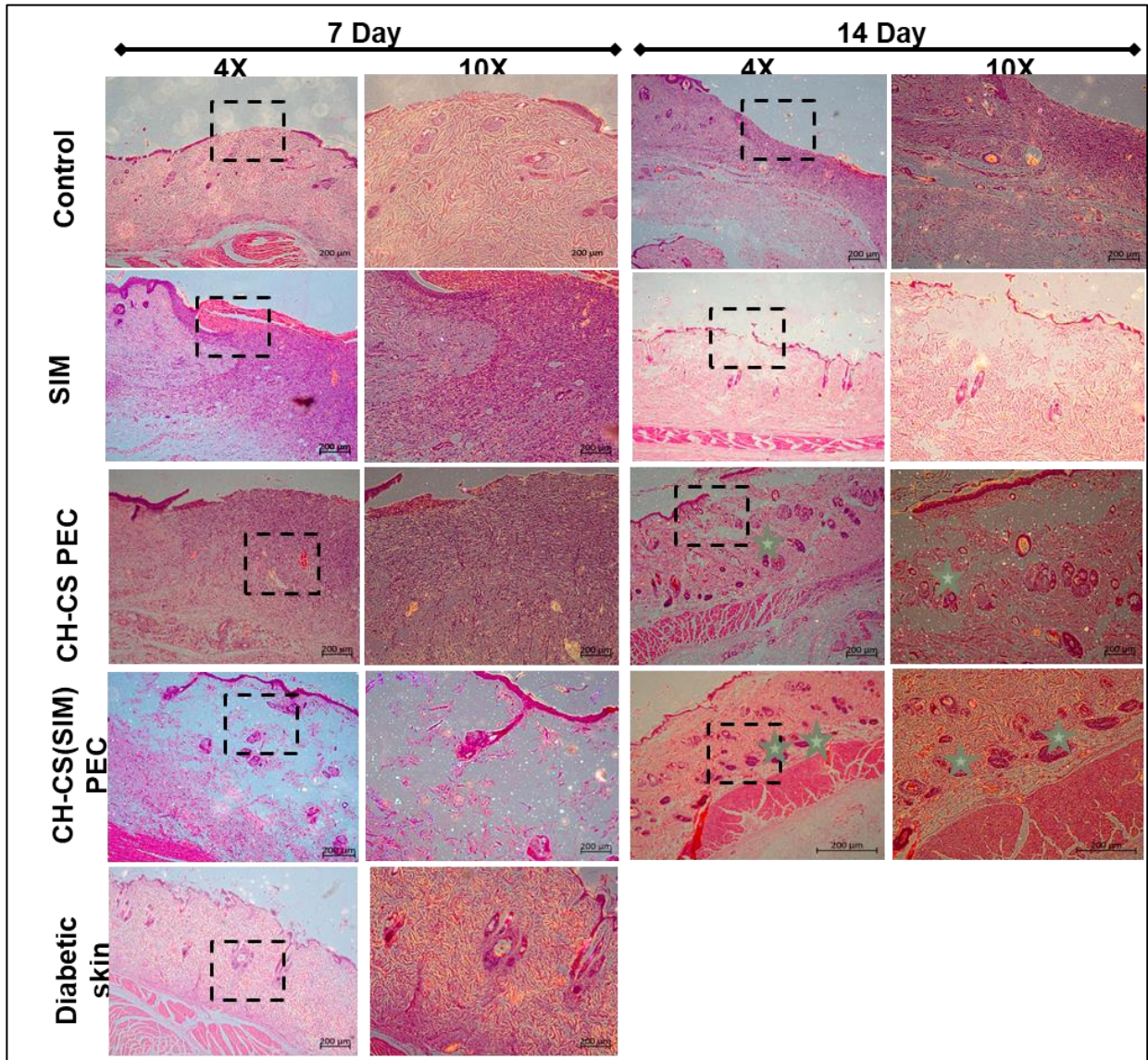ils were stained with aniline blue. The control group exhibited uneven collagen fibrils. The CH-CS (SIM) PEC exhibited a higher collagen content depicting the ECM deposition. Collagen is one of the essential components of the extracellular matrix, which provides mechanical support to the tissue and aids cell adhesion and tissue repair [40]. Animals treated with CH-CS(SIM) PEC exhibited increased total collagen compared to the other treatment groups. The total collagen deposition was estimated by the Image J software deconvolution tool. After adjusting the image scale, the image was separated into different stacks. The green color channel were further quantified for the collagen deposition. As shown in **Fig. 6.7**, CH-CS(SIM)PEC demonstrated the highest deposition (81.85±1.65) of collagen compared to CH-CS PEC (47.09±1.36), SIM (39.92±1.05) and untreated control (26.70±2.00) animals. Treatment with CH-CS PEC showed uneven deposition of the collagen fibrils compared to the CH-CS (SIM) PEC. The results demonstrated enhanced collagen deposition, and faster ECM remodeling, supporting improved re-epithelialization and wound closure rate, with CH-CS(SIM) PEC.
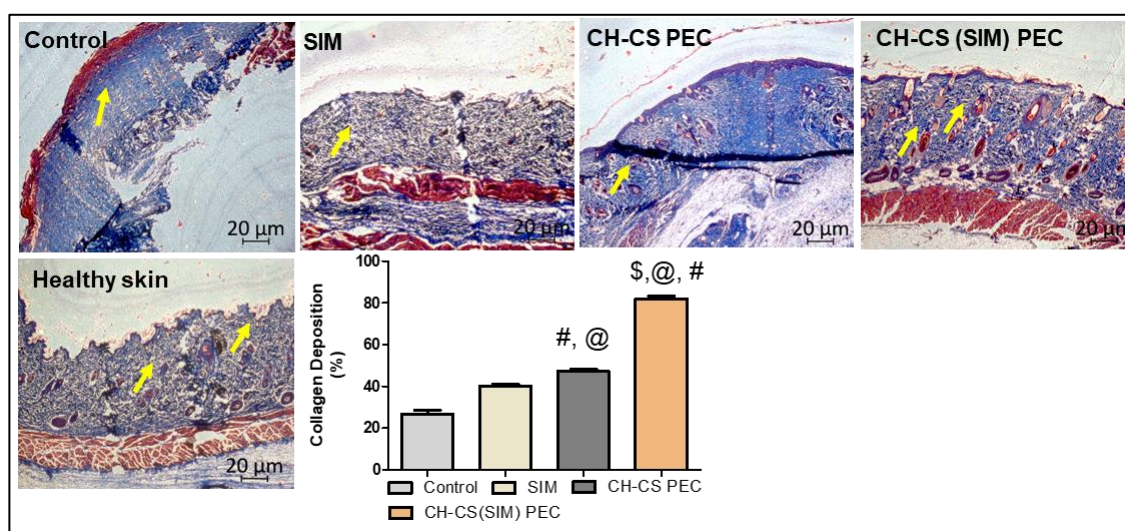

Fig. 6.7 Collagen deposition of the skin sections collected post 10th day of the treatment. Images were taken at 4x and 10x magnification. Scale bar 20μm.

6.3.10 Immunostaining study

After analyzing the efficient wound closure and confirming the enhanced collagen content in the CH-CS (SIM) PEC-treated group, we wanted to analyze the angiogenic potential of the treatment.

Immunohistochemical analysis of VEGF was evaluated to determine angiogenic ability. As depicted in **Fig. 6.8**, the expression of VEGF was minimal in the control group (0.47 ± 0.11) compared to SIM (0.7 ± 0.06) and CH-CS PEC (1.32 ± 0.09) treatments. The CH-CS (SIM) PEC-treated group exhibited the highest amount of VEGF (1.94 ± 0.22) in comparison to all other treatment groups. The results corroborated with the *ex-vivo* rat aortic ring assay confirming the angiogenic potential of CH-CS (SIM) PEC. The high expression of VEGF in CH-CS PEC depicts that CH-CS PEC provides a conducive environment for vascularization.
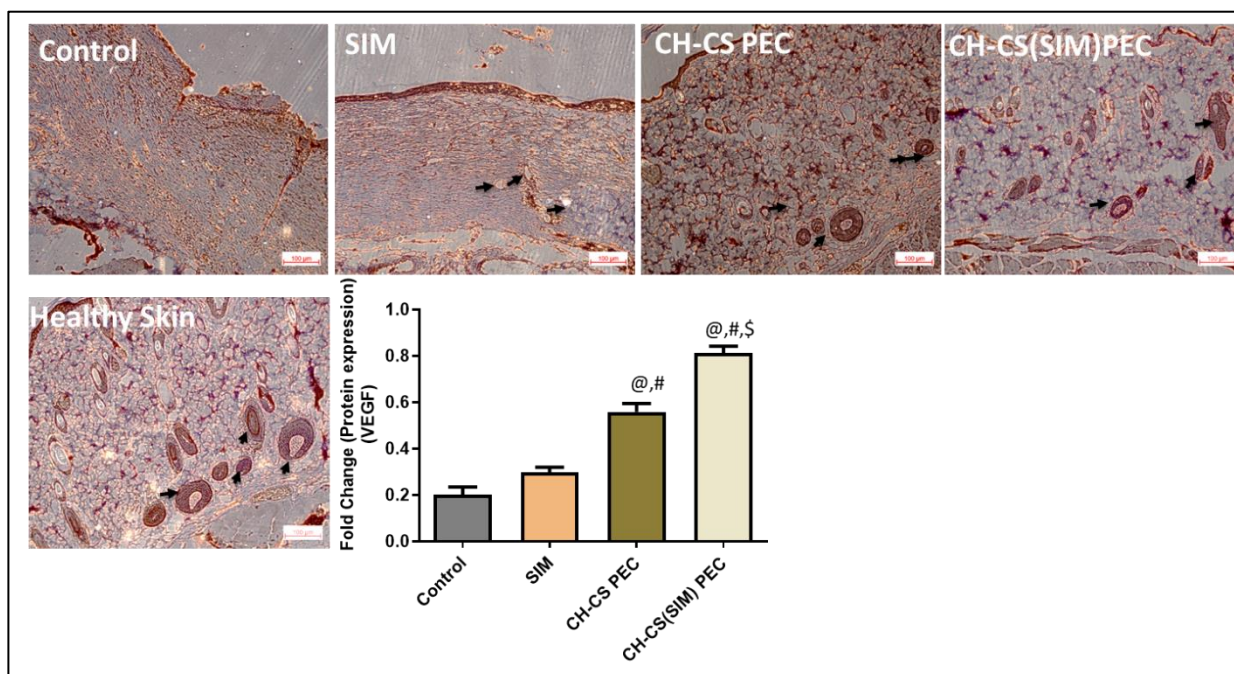
Fig. 6.8 Immunohistochemical staining of VEGF in the skin tissue sections. The expression of the marker was compared with the skin section of the healthy skin, untreated, SIM, and CH-CS PEC alone. Scale bar 100 μm. Statistical analysis was done using one-way ANOVA with Tukey multiple comparison test. @ denotes p-value < 0.05 compared to control, # denotes p-value < 0.5 compared to SIM and $ denotes p-value <0.05 compared to CH-CS PEC.

6.4 Conclusion

The functional efficacy of CH-CS PEC on the different cell types involved in wound healing was discussed in the previous sections. Understanding these findings, we aimed to check the utilization of CH-CS PEC as a carrier for drug delivery. The self-healing property of CH-CS PEC makes it a suitable candidate for drug loading. In the present study, we developed SIM-loaded Soluplus-TPGS mixed micelles. The micelles showed better stability and % dug encapsulation in the Soluplus-TPGS ratio of 4:1. These micelles were further loaded into the CH-CS PEC. The *in-vitro*

drug release kinetics of the SIM from the CH-CS PEC showed a controlled release demonstrating the CH-CS PEC as a suitable candidate for the nano-carrier loading. The slow and controlled drug release from the CH-CS PEC could be because of its porous interconnected networks. As SIM is a pro-angiogenic molecule, we evaluated its angiogenic potential both in the *ex-vivo* rat aortic ring assay and the *in-vivo* diabetic excision wound model. The *ex-vivo* rat aortic ring displayed enhanced sprouting of the endothelial cells in the SIM-loaded CH-CS PEC. Surprisingly, the CH-CS PEC alone also showed high angiogenic potential. The *in-vivo* chronic wound healing data corroborated the *ex-vivo* data depicting the enhanced wound healing potential in both CH-CS PEC and SIM-loaded CH-CS PEC.

References

1. Oh, J.K., D.I. Lee, and J.M. Park, *Biopolymer-based microgels/nanogels for drug delivery applications.* Progress in Polymer Science, 2009. **34**(12): p. 1261-1282.

2. Parhi, R., *Cross-Linked Hydrogel for Pharmaceutical Applications: A Review.* Adv Pharm Bull, 2017. **7**(4): p. 515-530.

3. Liu, Y. and S.-h. Hsu, *Synthesis and Biomedical Applications of Self-healing Hydrogels.* 2018. **6**.

4. Liu, Y. and S.-h. Hsu, *Synthesis and Biomedical Applications of Self-healing Hydrogels.* Frontiers in Chemistry, 2018. **6**.

5. Li, J., Y.P. Zhang, and R.S. Kirsner, *Angiogenesis in wound repair: angiogenic growth factors and the extracellular matrix.* Microsc Res Tech, 2003. **60**(1): p. 107-14.

6. Abu El Hawa, A.A., et al., *The impact of statins on wound healing: an ally in treating the highly comorbid patient.* J Wound Care, 2022. **31**(Sup2): p. S36-S41.

7. Veith, A.P., et al., *Therapeutic strategies for enhancing angiogenesis in wound healing.* Adv Drug Deliv Rev, 2019. **146**: p. 97-125.

8. Yu, M., et al., *Exosomes derived from atorvastatin-pretreated MSC accelerate diabetic wound repair by enhancing angiogenesis via AKT/eNOS pathway.* Stem Cell Res Ther, 2020. **11**(1): p. 350.

9. Sawaya, A.P., et al., *Topical mevastatin promotes wound healing by inhibiting the transcription factor c-Myc via the glucocorticoid receptor and the long non-coding RNA Gas5.* J Biol Chem, 2018. **293**(4): p. 1439-1449.

10. Rego, A.C., et al., *SIMvastatin improves the healing of infected skin wounds of rats.* Acta Cir Bras, 2007. **22 Suppl 1**: p. 57-63.

11. Asai, J., et al., *Topical SIMvastatin accelerates wound healing in diabetes by enhancing angiogenesis and lymphangiogenesis.* Am J Pathol, 2012. **181**(6): p. 2217-24.

12. Sobczyński, J. and B. Chudzik-Rząd, *Chapter 9 - Mixed micelles as drug delivery nanocarriers*, in *Design and Development of New Nanocarriers*, A.M. Grumezescu, Editor. 2018, William Andrew Publishing. p. 331-364.

13. Wang, Y., et al., *Mixed micelles of TPGS and Soluplus® for co-delivery of paclitaxel and fenretinide: in vitro and in vivo anticancer study.* Pharmaceutical Development and Technology, 2020. **25**(7): p. 865-873.

14. Bernabeu, E., et al., *Novel Soluplus(®)-TPGS mixed micelles for encapsulation of paclitaxel with enhanced in vitro cytotoxicity on breast and ovarian cancer cell lines.* Colloids Surf B Biointerfaces, 2016. **140**: p. 403-411.

15. Feng, P., et al., *Chitosan-Based Functional Materials for Skin Wound Repair: Mechanisms and Applications.* Front Bioeng Biotechnol, 2021. **9**: p. 650598.

16. Ou, Y. and M. Tian, *Advances in multifunctional chitosan-based self-healing hydrogels for biomedical applications.* J Mater Chem B, 2021. **9**(38): p. 7955-7971.

17.   Wu, G., et al., *Chondroitin sulfate zinc with antibacterial properties and anti-inflammatory effects for skin wound healing.* Carbohydr Polym, 2022. **278**: p. 118996.

18.   Sharma, S., K.L. Swetha, and A. Roy, *Chitosan-Chondroitin sulfate based polyelectrolyte complex for effective management of chronic wounds.* Int J Biol Macromol, 2019. **132**: p. 97-108.

19.   Italiya, K.S., et al., *Self-assembling lisofylline-fatty acid conjugate for effective treatment of diabetes mellitus.* Nanomedicine: Nanotechnology, Biology and Medicine, 2019. **15**(1): p. 175-187.

20.   Crowe, A.R. and W. Yue, *Semi-quantitative Determination of Protein Expression using Immunohistochemistry Staining and Analysis: An Integrated Protocol.* Bio Protoc, 2019. **9**(24).

21.   Mu, D., et al., *Hyaluronic acid-coated polymeric micelles with hydrogen peroxide scavenging to encapsulate statins for alleviating atherosclerosis.* Journal of Nanobiotechnology, 2020. **18**(1): p. 179.

22.   Hide, D., et al., *SIMvastatin-loaded polymeric micelles are more effective and less toxic than conventional statins in a pre-clinical model of advanced chronic liver disease.* Nanomedicine, 2020. **29**: p. 102267.

23.   Soleymani Abyaneh, H., et al., *Rational design of block copolymer micelles to control burst drug release at a nanoscale dimension.* Acta Biomater, 2015. **24**: p. 127-39.

24.   Zhou, W., et al., *Factors affecting the stability of drug-loaded polymeric micelles and strategies for improvement.* Journal of Nanoparticle Research, 2016. **18**(9): p. 275.

25.   Linn, M., et al., *Soluplus(R) as an effective absorption enhancer of poorly soluble drugs in vitro and in vivo.* Eur J Pharm Sci, 2012. **45**(3): p. 336-43.

26.   Ghezzi, M., et al., *Improvement of Imiquimod Solubilization and Skin Retention via TPGS Micelles: Exploiting the Co-Solubilizing Effect of Oleic Acid.* Pharmaceutics, 2021. **13**(9).

27.   Chong, W.T., et al., *In-vitro and in-vivo evaluations of tocotrienol-rich nanoemulsified system on skin wound healing.* PLoS One, 2022. **17**(5): p. e0267381.

28.   Yang, C., et al., *Recent Advances in the Application of Vitamin E TPGS for Drug Delivery.* Theranostics, 2018. **8**(2): p. 464-485.

29.   Paaver, U., et al., *Soluplus graft copolymer: potential novel carrier polymer in electrospinning of nanofibrous drug delivery systems for wound therapy.* Biomed Res Int, 2014. **2014**: p. 789765.

30.   Cagel, M., et al., *Polymeric mixed micelles as nanomedicines: Achievements and perspectives.* European Journal of Pharmaceutics and Biopharmaceutics, 2017. **113**: p. 211-228.

31.   Singh, V., et al., *Micelles, mixed micelles, and applications of polyoxypropylene (PPO)-polyoxyethylene (PEO)-polyoxypropylene (PPO) triblock polymers.* International Journal of Industrial Chemistry, 2013. **4**(1): p. 12.

32. Saxena, V. and M.D. Hussain, *Poloxamer 407/TPGS mixed micelles for delivery of gambogic acid to breast and multidrug-resistant cancer.* Int J Nanomedicine, 2012. **7**: p. 713-21.

33. Bernabeu, E., et al., *Novel Soluplus((R))-TPGS mixed micelles for encapsulation of paclitaxel with enhanced in vitro cytotoxicity on breast and ovarian cancer cell lines.* Colloids Surf B Biointerfaces, 2016. **140**: p. 403-411.

34. Jin, X., et al., *Soluplus(®) micelles as a potential drug delivery system for reversal of resistant tumor.* Biomed Pharmacother, 2015. **69**: p. 388-95.

35. Piazzini, V., et al., *Enhanced dissolution, permeation and oral bioavailability of aripiprazole mixed micelles: In vitro and in vivo evaluation.* Int J Pharm, 2020. **583**: p. 119361.

36. Sorg, H., et al., *Panta Rhei: Neovascularization, Angiogenesis and Nutritive Perfusion in Wound Healing.* European Surgical Research, 2018. **59**(3-4): p. 232-241.

37. Farsaei, S., H. Khalili, and E.S. Farboud, *Potential role of statins on wound healing: review of the literature.* Int Wound J, 2012. **9**(3): p. 238-47.

38. Bao, P., et al., *The role of vascular endothelial growth factor in wound healing.* J Surg Res, 2009. **153**(2): p. 347-58.

39. Weis, M., et al., *Statins have biphasic effects on angiogenesis.* Circulation, 2002. **105**(6): p. 739-45.

40. Zeltz, C. and D. Gullberg, *The integrin-collagen connection--a glue for tissue repair?* J Cell Sci, 2016. **129**(4): p. 653-64.

Chapter 7

Summary and Conclusion

7. Summary and Conclusion:

The current state of the art for wound dressing primarily focuses on protecting the wound from the external environment and preventing infection. However, these dressings have minimal efficacy on the overall cellular mechanism involved in the healing process. We aimed to develop an easy-to-fabricate biopolymer-based dressing that could mimic the ECM property and contribute to the overall healing process by supporting all types of skin cells, including fibroblasts, keratinocytes, dermal macrophages, and endothelial cells. We have developed a viscoelastic, self-healing, *in-situ* forming scaffold with a porous architecture. The scaffold was fabricated using high molecular weight chitosan (CH) and low molecular weight chondroitin sulfate (CS), using a polyelectrolyte complexation strategy by mixing 1:1 v/v of CH and CS. CH is a well-established polymer in wound healing, while CS is a glycosaminoglycan, a component of ECM. These polymers form an ionic complex *in-situ* due to their opposite charges. The design of CH-CS PEC was optimized using the Design of Experiment (DoE). Additionally, a custom-made double-barrel syringe was designed to deliver these polymer solutions directly at the wound site to make the scaffold *in-situ*, at the wound site.

Physicochemical characterization of the CH-CS PEC was done in terms of FT-IR, DSC, TGA, and solid-state 13C NMR. All the analyses pointed to ionic interaction between CH and CS for the formation of the CH-CS PEC. The surface characteristics of the scaffold were evaluated by XRD and EDS. A significant reduction in the amount of free nitrogen was observed on the surface of the scaffold, indicating the interaction of the $-NH_2$ group of CH for the formation of the CH-CS ionic complex. The %-swelling and %-porosity analyses indicated a substantial increase in porosity in the CH-CS PEC compared to the scaffold prepared with CH alone. It was hypothesized that as CS was cross-linking with the CH gel, it could make a highly porous architecture, while CH alone could not make any cross-linked structure, forming a non-porous film-like architecture. This was supported by the SEM analysis of both scaffolds. CH exhibited an uneven structure without distinct pore formation, while CH-CS PEC showed a highly porous, spongy structure.

Further, the rheological property of the CH-CS PEC was evaluated with respect to the storage modulus (G`) and loss modulus (G``) to analyze the viscoelastic nature of the scaffold. CH-CS PEC exhibited a significantly higher G` (~17000 Pa) compared to G`` (~7800 Pa), which indicated better cross-linking and mechanical strength, whereas CH exhibited a significantly lower value of

G' (~60 Pa), than that of G`` (~90 Pa), indicating the fluidic nature of CH. The increase in the G`
in CH-CS PEC indicated that the electrostatic cross-linking within the polymer matrix acted like
fixed network junctions, increasing the ability of the cross-linked scaffold to store the applied
energy, leading to elastic-like characteristics. The high elasticity of a matrix can act as a
biophysical cue, improving cell proliferation and migration. The CH-CS PEC also showed good
self-healing potential supporting another biophysical feature of ECM. All these characterizations
indicated the high wound-healing potential of the CH-CS PEC. RBCs are the first biological cells
that come in contact with any wound dressing; therefore, we performed a blood compatibility study
on the isolated RBCs. The CH-CS PEC was found to be hemocompatible with good blood cell
adhesion and protein adsorption, demonstrating its effective potential as a hemostatic.

The main players involved in wound healing are fibroblasts, keratinocytes, macrophages, and
endothelial cells. To have an overall effect covering all the stages of wound healing, we need to
confirm the biological efficacy of CH-CS PEC on these cells. First, we checked the cell
proliferation and functional efficacy of fibroblasts and keratinocytes. Fibroblasts participate in cell
proliferation and help in ECM synthesis, while the keratinocytes participate in re-epithelialization.
Due to its site-specific delivery, the developed in-situ CH-CS PEC goes into the wound's deep
crevices, leading to good cell adhesion and cell-substrate contact. The functional efficacy of CH-
CS PEC was evaluated on primary human dermal fibroblasts (HDF) and human keratinocyte
(HaCaT) cell lines. The results depicted enhanced cell migration and cell proliferation in both
fibroblasts and keratinocytes when treated with CH-CS PEC. The average distance migrated by
the HaCaT cells was found to be 0.53 ± 0.05 mm when grown on the CH-CS PEC, compared to
0.40 ± 0.04 mm with CH, 0.34 ± 0.02 mm with CS, and 0.40 ± 0.03 mm in the control cells after
24 h. Similarly, in the case of HDF, after 24 h, the average migration was 1.12 ± 0.06 mm with the
CH-CS PEC, compared to 0.73 ± 0.06 mm with CH, 0.77 ± 0.07 mm with CS, and 0.88 ± 0.05
mm in the control cells. This data suggests that the CH-CS PEC can support and stimulate the
growth of the dermal fibroblasts and epidermal keratinocytes. The proliferation was further
confirmed by immunoblotting analysis of PCNA. PCNA expression increased 1.4 and 1.7-fold in
the HaCaT and HDF cells, respectively, when grown on the CH-CS PEC compared to the control.
The increased expression of PCNA in the cells grown on the CH-CS PEC substantiates the
microscopic observation of higher proliferation in the similarly treated cells. Furthermore, the

expression of different functional markers was analyzed in the keratinocyte and fibroblast cells. Enhanced mRNA expression of α-SMA, collagen-I, and collagen-III was observed in the fibroblasts treated with CH-CS PEC. In keratinocytes, increased expression of functional markers, including involucrin, HGF, and NRG, was observed with CH-CS PEC compared to other groups. The keratinocytes and fibroblasts crosstalk by paracrine signaling. We evaluated the expression of β1-integrin in the conditioned media with both fibroblasts and keratinocytes. The data represented enhanced expression of β1-integrin with CH-CS PEC, indicating improved crosstalk. These data demonstrated that CH-CS PEC could make a healthy environment for the proliferation and function of both the major skin cells involved in wound healing. To validate these *in-vitro* findings, the efficacy of CH-CS PEC was evaluated against an acute rat skin-excisional wound model. Treatment with the *in-situ* forming CH-CS PEC scaffold exhibited enhanced wound healing efficacy in terms of wound closure rate, collagen content, and α-SMA and β1-integrin expression.

Another burden to the healing process is the development of wound infections. It causes a serious problem by altering the wound healing mechanism turning into prolonged inflammation, which causes impaired healing. We hypothesized that as CH and its derivatives were reported to have antibacterial activity, CH-CS PEC also could possess germicidal properties. The CH-CS PEC scaffold's direct antibacterial efficacy was evaluated using *Pseudomonas aeruginosa* as the model microorganism. The results demonstrated instability in the bacterial outer membrane and increased ROS production as the leading cause of bacterial death. Further, CH-CS PEC's influence on macrophage phagocytosis and inflammation was analyzed. The *in-vitro* studies on the macrophage cell line RAW264.7 depicted changes in the actin cytoskeleton arrangement and elongated morphology with an increased β1-integrin expression. When infected with bacteria, CH-CS PEC-treated macrophages exhibited increased phagocytosis with low TNF-α and high IL-10 production, indicating M2-polarization. The in-vivo antibacterial and wound healing efficacy in the P. aeruginosa infected excision wound model supported the in-vitro findings, demonstrating faster wound closure and decreased CFU count in animals treated with CH-CS PEC.

Further, a significant reduction in the NF-κB expression was observed, signifying reduced inflammation. Expression of VE-cadherin was found to be evaluated, representing enhanced angiogenesis. In summary, the results represented the multifunctional efficacy of CH-CS PEC in the healing of the infected wound.

After demonstrating the potential efficacy of CH-CS PEC on different cell types involved in wound healing, we aimed to check the utilization of CH-CS PEC as a carrier for drug delivery. The self-healing property of CH-CS PEC makes it a suitable candidate for drug loading. We developed SIM-loaded Soluplus-TPGS mixed micelles. The micelles showed better stability and % drug encapsulation in the Soluplus-TPGS ratio of 4:1. These micelles were further loaded into the CH-CS PEC. The *in-vitro* drug release kinetics of SIM from the CH-CS PEC showed a controlled release demonstrating the CH-CS PEC as a suitable candidate for nanocarrier loading. The slow and controlled drug release from the CH-CS PEC could be because of its porous interconnected networks. As SIM is a proangiogenic molecule, we evaluated its angiogenic potential both in *ex-vivo* rat aortic ring assay and *in-vivo* diabetes-induced chronic wound model. The *ex-vivo* rat aortic ring displayed enhanced sprouting of the endothelial cells in the SIM-loaded CH-CS PEC. The *in-vivo* chronic wound healing data corroborated the *ex-vivo* data depicting the enhanced wound healing potential in both CH-CS PEC and Sim-loaded CH-CS PEC.

In a nutshell, CH-CS PEC was found to have an overall efficacy on the main players involved in wound healing, viz., keratinocytes, fibroblasts, macrophages, and endothelial cells. The in-situ forming self-healing viscoelastic CH-CS PEC had potential antibacterial activity and showed immunomodulatory behavior. Further, the CH-CS PEC showed enhanced angiogenic potential and wound healing efficacy against the diabetic-induced chronic wound model. Also, the physicochemical property of the scaffold highlights its potential in the loading of cells for cell grafting.

Chapter 8

Future scope and limitations of the study

8.1 Future Scope

The current study illustrates the effects of CH-CS PEC on different cell types in wound healing and as drug delivery carriers. The study unfolds the important biophysical cues in tissue engineering. The viscoelasticity, self-healing capability, and porous structure indicated its ECM-mimicking behavior. Understanding these findings, we believe CH-CS PEC's use in drug delivery and biomedical application. Further studies on the effect of the physicochemical properties of the hydrogel on endothelial cell growth could be an interesting study in the development of cardiac patches. The Immunomodulatory behavior of the CH-CS PEC could be suitable for the treatment of inflammatory disorders. The self-healing and porous structure would allow enhanced encapsulation and could support controlled drug release. The growth factor/biomolecule loading in the CH-CS PEC can increase its potential for use in regenerative medicine. It could be suitable for cell encapsulation for use in tissue regeneration. Further, its good self-healing property could be used as a bio-ink for 3D bio-printing.

8.2 Limitations of the study

1. We could not study the effect of this scaffold on melanocytes, one of the major skin cells responsible for skin pigmentation.

2. Though the initial result suggested scar-free wound healing, it could not be explored completely.

3. The detailed mechanism regarding the increase in endothelial cell sprouting with only CH-CS PEC has not been completely explored.

Appendix

List of patents

1. A porous scaffold composition for tissue regeneration and method of preparing the same, Indian Patent Application no. 201911050058, Inventors: Roy A. and Sharma S. Filed on December 04, 2019.

2. Formulation for wound healing, Indian Patent Application no. 201811035517, Inventors: Roy A. and Sharma S. Filed on September 18, 2019.

List of publications

1. Dual antibacterial and anti-inflammatory efficacy of an in-situ forming viscoelastic wound dressing. **Swati Sharma**, Harishkumar Madhyastha, Shrikant Kirwale, Yash katakia, Syamantak Majumder, Aniruddha Roy,, Carbohydrates polymers, 2022, 298:p.120126

2. Development of an in-situ forming, self-healing scaffold for dermal wound healing: in-vitro and in-vivo studies. **Swati Sharma**, Harishkumar madhyastha, K Laxmi Swetha, Kavyasree Marijvala, Radha madhyastha, Yuichi Nakajima, Aniruddha Roy. *Materials Science and Engineering: C* Volume 128, 2021, 112-263

3. Chitosan-Chondroitin sulfate based polyelectrolyte complex for effective management of chronic wounds **Swati Sharma**, K.L. Swetha, A. Roy International Journal of Biological Macromolecules Volume 132, 1, 2019, Pages 97-108

List of publications other than thesis

1. Chitosan, chondroitin sulfate, and hyaluronic acid based in-situ forming scaffold for efficient cell grafting. Shrikant Kirwale, **Swati Sharma**, Aniruddha Roy., International Journal of Biological Macromolecules, volume 225, 2023,938-951.

2. Design and dermatokinetic evaluation of Apremilast loaded nanostructured lipid carriers embedded gel for topical delivery: A potential approach for improved permeation and prolong skin deposition R. Vamshi Krishna, **Swati Sharma**, Aniruddha roy, Gautam singhvi, *Colloids and Surfaces B: Biointerfaces* Volume 206, October 2021, 111945

3. Solid lipid nanocarriers embedded hydrogel for topical delivery of apremilast: In-vitro, ex-vivo, dermatopharmacokinetic and anti-psoriatic evaluation, R. Vamshi Krishna, **Swati Sharma**, Aniruddha roy, Gautam singhvi, *Journal of Drug Delivery Science and Technology* Volume 63, June 2021, 102442

4. A comprehensive review of the strategies to improve oral drug absorption with special emphasis on the cellular and molecular mechanismsTanmay Padhye, Kavyasree Marijvala, K.Laxmi Swetha **Swati Sharma** *Journal of Drug Delivery Science and Technology* Volume 61, February 2021, 102178

5. Development of a tumor extracellular pH-responsive nanocarrier by terminal histidine conjugation in a star shaped poly(lactic-co-glycolic acid), K.L. Swetha, Kavyasree Marijvala, **Swati Sharma** *European Polymer Journal* Volume 147, 15 March 2021, 110337

6. Development of a size-tunable paclitaxel micelle using a microfluidic-based system and evaluation of its in-vitro efficacy and intracellular delivery, K.L. Swetha, Kavyasree Marijvala, **Swati Sharma** *Journal of Drug Delivery Science and Technology* Volume 60, December 2020, 102041

7. Curcumin loaded nanostructured lipid carriers for enhanced skin retained topical delivery: optimization, scale-up, in-vitro characterization and assessment of ex-vivo skin

8. deposition, R. Vamshi Krishna, **Swati Sharma**, Aniruddha roy, Gautam singhvi, *European Journal of Pharmaceutical Sciences* Volume 152, 1 September 2020, 105438

9. Disulfiram potentiates docetaxel cytotoxicity in breast cancer cells through enhanced ROS and autophagy, K.L. Swetha, Kavyasree Marijvala, **Swati Sharma** *Pharmacological Reports* Volume 72,2020, pages1749–1765.

Swati Sharma

BIOGRAPHICAL SKETCH

Name	Current Position
Swati Sharma	PhD research scholar Department of Pharmacy Birla Institute of Technology & Science, Pilani Vidya Vihar, Pilani, Rajasthan 333031

Professional Experience

- Assistant Professor at Indukaka Ipcowala College of Pharmacy, Anand, Gujarat India– Aug,2016-Jun2017
- Junior research Fellow at Nirma University, Gujarat, India- Jun-2017-Sept, 2017.

Education/Training

Institution and Location	Degree	Duration	Field Of Study
Anand Pharmacy College, Anand, India	B. Pharm.	2010-2014	Pharmacy
Anand Pharmacy College, Anand, India	M. Pharm.	2014-2016	Pharmaceutics

Personal Statement

Ms. Swati Sharma is currently a research scholar at the Birla Institute of Technology and Science – Pilani. She is currently working on the use of polymeric scaffolds in skin regeneration. She is focused on designing a biopolymeric-based scaffold and its applications in tissue engineering. She has two Indian patents and 11 research publications. Her Ph.D. work has been technology transferred for scaleup to Alicorn Med. Pvt. Ltd., an Indian start-up company, for possible commercialization.

Dr. Aniruddha Roy

BIOGRAPHICAL SKETCH	
Name Aniruddha Roy	**Current Position** Associate Professor Department of Pharmacy Birla Institute of Technology & Science, Pilani Vidya Vihar, Pilani, Rajasthan 333031

Professional Experience

- Associate Professor, Birla Institute of Technology & Science, Pilani Campus, Nov, 2015 – Present.
- Assistant Professor, Birla Institute of Technology & Science, Pilani Campus, Nov, 2015 – July, 2021.

Education/Training

Institution and Location	Degree	Duration	Field Of Study
Jadavpur University, Kolkata, India	B. Pharm.	1999- 2003	Pharmacy
Jadavpur University, Kolkata, India	M. Pharm.	2004-2006	Pharmacology
National Institute of Immunology, NewDelhi, India	Ph.D.	2006- 2012	Drug delivery
Indian Institute of Technology (IIT), NewDehi, India	Post-doc	2012- 2013	Polymer Chemistry
Ontario Institute for Cancer Research,Toronto, Canada	Post-doc	2013- 2014	Drug delivery
University of British Columbia, Vancouver,Canada	Post-doc	2014- 2015	Drug delivery

Personal Statement

Dr. Aniruddha Roy, Associate Professor at Birla Institute of Technology and Science - Pilani, is an accomplished scientist and has been recognized for his scholarly publications in highly reputed peer-reviewed scientific journals. He has made significant contributions in targeted drug delivery and pharmacokinetics-pharmacodynamics evaluation, especially in cancer therapy, supported by his various publications in highly reputed peer-reviewed scientific journals. His main area of research expertise includes nanomedicine, combination therapeutics and therapy of resistant cancer. He has extensive experience in in-vitro/in-vivo studies of innovative nanoparticle systems including ex-vivo and in-vivo characterization of nanomedicines for cancer therapy. Also, he is recognized for designing modified biopolymers for diverse applications, including wound healing. His research work resulted in the publication of 26 research articles in leading journals. Currently, he has more than 1400 citations from his publications with an h-index of 17. As a lead researcher, he is the inventor of 4 patented platform technologies. One of this technology has been taken up by FACIT (the commercialization agent for Ontario Institute for Cancer Research, Toronto, Canada) and another one by Alicorn Med. Pvt. Ltd., an Indian start-up company, for possible commercialization.